Synthesis of Nanometer-Sized and Multi-Spin Macromolecules and their Magnetic Force Microscopic Images

A Thesis
Presented to
Waseda University

February 2003

Tsuyoshi Michinobu

Preface

In recent years, nanometer-sized magnetic materials have intensively been investigated with a view to large data storage for future information technology. The main approach of recent research has been attributed to inorganic elements with strong magnetic moments. On the other hand, an attempt to synthesize a macromolecular ferromagnet or a purely organic-derived magnetic macromolecule has been continuing for a few decades. They are also suggested to be promising in nanoscale science, because an organic macromolecule can be tuned its property through molecular design and a high molecular-weight macromolecule has its molecular size on a nanometer scale. A π-conjugated but non-Kekulé type high-spin polyradical is a recent candidate for such a magnetic macromolecule. The highest value of spin-alignment (S) in a macromolecule has been increasing year by year and has now reached about 5000 for the highly cross-linked polyradical using a triarylmethine radical as the spin source, which was the first organic macromolecule behaving as a superparamagnet below 10 K as reported by A. Rajca last year. However, the triarylmethine radical can survive only at low temperature, so it is difficult to develop this polyradical for practical use.

This thesis deals with magnetic macromolecules which are stable even under air at room temperature. In particular, macromolecules extended in two- or three-dimensions were noted, because the cylindrical or spherical molecules with a nanometer-size can be easily detectable by scanning probe microscopy (SPM) techniques. The novel preparation of polyradical particles utilizing emulsion or dispersion polymerization is one such example. Nanometer-sized π-conjugated polyradicals were also prepared by polycondensation between two multi-functionalized conjugated subparts under the precise control of the connectivity and terminal structures. Magnetic force microscopy (MFM) as an SPM application to combine the keywords 'nano-scale' and 'magnetism' was for the first time applied to detect the weak magnetic moment derived from the magnetic macromolecules. This thesis reveals that the magnetic information of the nanometer-sized magnetic macromolecules can be expressed as the intensity of the MFM image in different ways.

Tsuyoshi Michinobu

Contents

Chapter 1

Introduction

1.1 Introduction to nano-scale magnetic materials

There has been considerable interest in constructing magnetically active nano-scale materials because the magnetic structure size is a key factor in determining the upper limit of the stored data density in magnetic materials.[1-4]   The major approach has typically been top-down engineering methods of grains or etching bulk materials. However, it is often difficult for the top-down approach to obtain nanoscale structures with a controlled size and shape.   On the other hand, bottom-up procedures from molecules open up the possibility of creating new nano-structured building blocks.   In particular, organic macromolecules are some of the useful candidates in developing micro-electronic and -magnetic devices because they possess a single-molecular size of nanometer order.

Recent advances in organic synthesis have allowed the preparation of well-defined macromolecules with active functions.   For example, the macromolecules bearing a large number of unpaired electrons have been studied, which reveal their fascinating magnetic properties in term of molecular-based magnets.[5,6]   One of the advantages of such chemical bottom-up approaches is that the size and shape of the molecules are easily designed and constructed by conventional macromolecular chemistry to give macromolecules with two- or three-dimensional topologies such as dendritic, ladder, and star structures.   If such nanometer-sized macromolecules themselves become magnetically detectable, they are a potentially new class of magnetic materials.

There is another interest in nanoscale science and technology, that is to observe nanometer-sized structures with scanning probe microscopies (SPMs).   Among the SPMs, several kinds of methods to directly image magnetic structures have been developed and the high performance operations are continuously investigated.[7]   The instrument most widely used now is magnetic force microscopy (MFM), which has a high spatial resolution of 10 nm scales.

This chapter is intended to provide an overview of the recent progress in the magnetically responsible macromolecules bearing unpaired electrons and the basic principles of MFM operations.

1.2 Magnetic macromolecules

It has been considered that organic molecules are magnetically inactive and only transition and lanthanide elements and their related compounds are applicable to magnetic materials. Recently, a variety of organic radical molecules have opened up a new field of magnetic materials, which would offer a tremendous potential in combination with the fine-tunable characteristics of organic molecules. The study of macromolecules bearing the unpaired electrons of radical groups or organic polyradicals is one of the examples of this trend.

The first type of organic polyradicals is composed of an unconjugated backbone bearing highly stable radicals in its side chains.[8-16] Such macromolecules can be synthesized from (i) oxidation or reduction of a precursor macromolecule, (ii) preparation and the subsequent polymerization of a radical monomer containing a vinyl group, and (iii) introduction of a radical unit to a macromolecular backbone through a polymer reaction. The preparation of poly(4-methacryloylamino- or 4-methacryloyloxy-2,2,6,6-tetramethylpiperidine-1-oxyl) **1** is shown as an example (Fig. 1.1). It is generally difficult to achieve a high yield in chemical oxidation reaction of the precursor macromolecule (here piperidine groups as a radical precursor)[17] except for
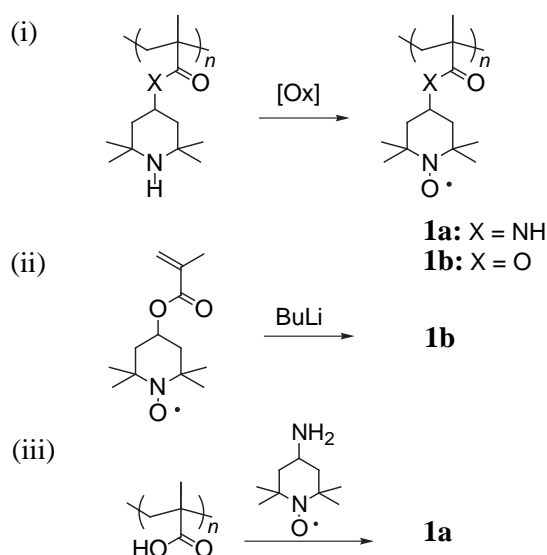

Fig. 1.1. Preparation procedures of poly(4-methacryloylamino- or 4-methacryloyloxy-2,2,6,6-tetramethylpiperidine-1-oxyl).

the recent report of almost quantitative conversion of poly(4-methacryloyloxyl-2,2,6,6-tetramethylpiperidine) to **1b** via the oxidation with *m*-chloroperbenzoic acid.[18]   **1** could be prepared by the anionic polymerization of the corresponding monomer with butyllithium or phenylmagnesium bromide as the initiator, maintaining a high spin concentration.[19-22]   Polymer reaction of precursor macromolecules usually gave the desired polyradicals with reasonalbe yields.[23,24]   The studies concluded that they are chemically stable at ambient conditions and that an electron exchange interaction takes place between the pendant nitroxide radicals.   They also suggested a through-space weak antiferromagnetic interaction between the pendant radicals.   These polyradicals have also been investigated as redox resins and antioxidants.

In order to give a ferromagnetic character to these polyradicals, π-electrons would play a vital role.   Since the first report of an organic macromolecular ferromagnet in 1986 by A. A. Ovchinnikov et al.,[25] a π-conjugated backbone has been used to ferromagnetically connect radical species via the through-bond intramolecular exchange interaction.   The design of a non-Kekulé and non-disjoint type molecule is a prerequisite for the ferromagnetic interaction or high-spin state in a π-conjugated polyradical.[26,27]   Taking into account the non-Kekulé type biphenyl biradicals **2**, they are classified into two groups (Fig. 1.2).   The effective overlap of the two nonbonding molecular orbitals (NBMOs) on the *m,p'*-isomer favors the parallel orientation of the two unpaired electrons according to Hund's rule to stabilize the triplet ground state,
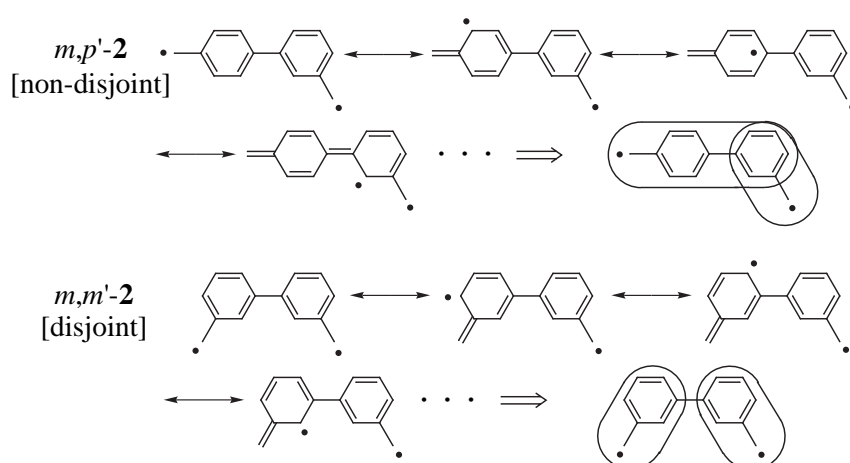
Fig. 1.2.   Non-disjoint and disjoint type connectivities of biphenyl biradicals **2**.

which is called a non-disjoint system. On the other hand, the complete separation of the two NBMOs on the *m,m'*-isomer results in a smaller exchange interaction between the two unpaired electrons, and consequently, the almost total degeneration of the triplet and singlet states, which is called the disjoint system.

π-Conjugated polyradicals precisely prepared according to the non-Kekulé and non-disjoint rules are expected to have a very high spin quantum number (*S*) in proportion to the degree of polymerization.[28-31] A. Rajca synthesized poly(1,3-phenylenephenylmethine)s and extended it to the star-shaped decaradical **3** and dendritic pentadecaradical **4**.[32] These polyradicals displayed a strong through-bond ferromagnetic interaction between adjacent radicals at low temperature but relatively low *S* values, e.g., 3.5 for **4** with 15 radical sites. This is because a small number of radical defects or a failure in generation of a radical interrupts the π-conjugated pathway and consequently suppresses an increase of *S* value. In order to overcome this disadvantage, a calix[4]arene ring as a macrocyclic structure with two pathways for the exchange interaction was newly selected. The defect-insensitive macrocyclic
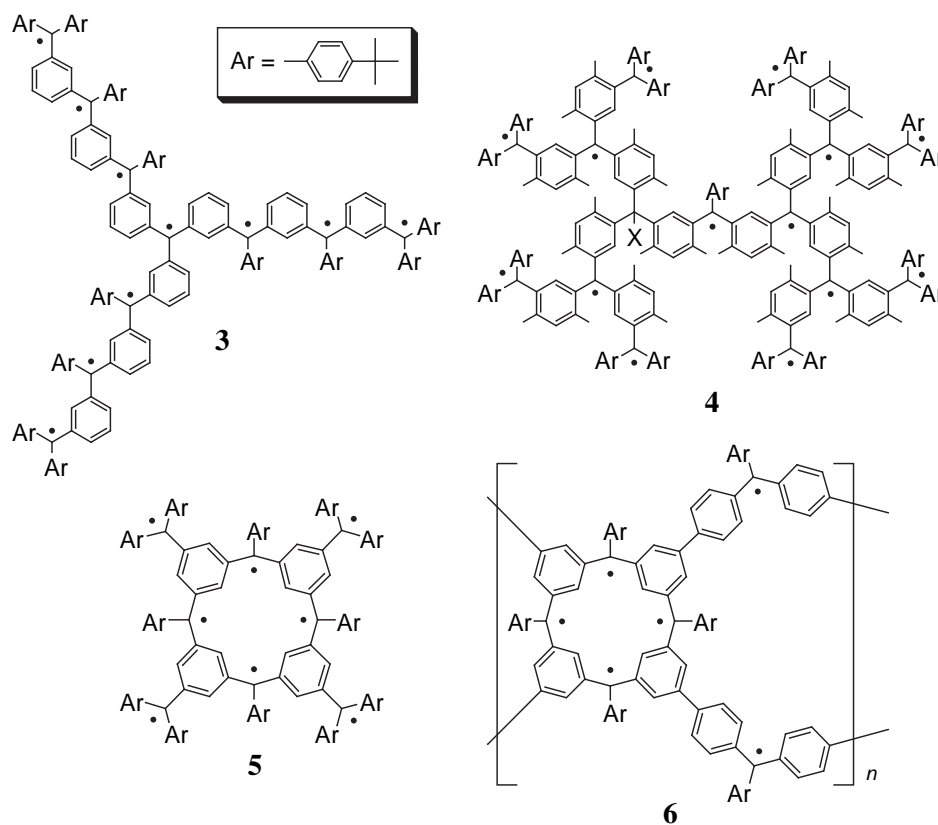
octaradical **5** and the ladder type tetradecaradical showed a high *S* value of 3.8 and 6.2, respectively, as expected.[33,34] Polycondensation of the two tetrafunctionalized calix[4]arene subparts using the Negishi coupling reaction gave a polymacrocyclic network macromolecule. The corresponding polyradical **6** is designed with an alternating connectivity of the macrocyclic subpart (*S* = 2) and linker moiety (*S* = 1/2) in a non-Kekulé and non-disjoint fashion, which induces a high *S* value irrespective of either the ferromagnetic or antiferromagnetic coupling between the subpart and the linker moiety.[35] For the soluble part of **6** with $M_n > 10^5$, a striking increase of *S* > 40 was realized.[36] Remarkably, the insoluble part of **6** exhibited an average *S* value of 5000 and behaved magnetically as insulating spin glasses and blocked superparamagnets at low temperature.[37] This is the first example of the purely organic-derived magnetic macromolecule with magnetic anisotropy.

Another approach to obtain a very high-spin polyradical is a π-conjugated macromolecule pendantly bearing radical groups in a non-Kekulé and non-disjoint fashion. In contrast to Rajca's polyradicals, which lack chemical stability at room temperature, the pendant-type polyradical has the advantages that a chemically stable radical species such as phenoxyl and nitroxide can be introduced as a pendant radical group and that it is insensitive to the radical defects because of a long distance interaction through the π-conjugated backbone to align even remote radicals.[38-40] Poly(phenylenevinylene)-based polyradicals **7** and **8** were synthesized using the Heck reaction of bromostyrene derivatives.[41-44] The backbone has a relatively high coplanarity and radicals can be delocalized over the entire molecule to effectively interact with each other. In addition, these polyradicals are stable enough to be handled even under air at room temperature. Although the *S* value for polynitroxide **8** with the spin concentration of 0.9 remained 1, polyphenoxyl **7** with the spin concentration of 0.7 displayed *S* = 2.5. The star-shaped polyradical **9** as a pseudo-two-dimensionally extension form of **7** demonstrated the cooperative ferromagnetic interaction between the 1,3,5-benzenetriyl core and three branch chains to give *S* = 3.5.[45,46] Further development to achieve a more robust ferromagnetic interaction is based on the extension and coplanarity of the two-dimensional π-conjugated system. Polycondensation of the star-shaped hexamer **9** as a trifunctionalized subpart and 1,3-divinyl-4-phenoxylbenzene as a bifunctionalized subpart using the Pd/P catalyst yielded the starburst-shaped planar macromolecule with $M_n = 3.2 \times 10^4$.[47] The ionization

potential of the macromolecule indicated a highly extended π-conjugation beyond **9**. The corresponding polyradical **10** with the spin concentration of 0.4 reached $S = 5$, which was definitely higher than that of **9**.
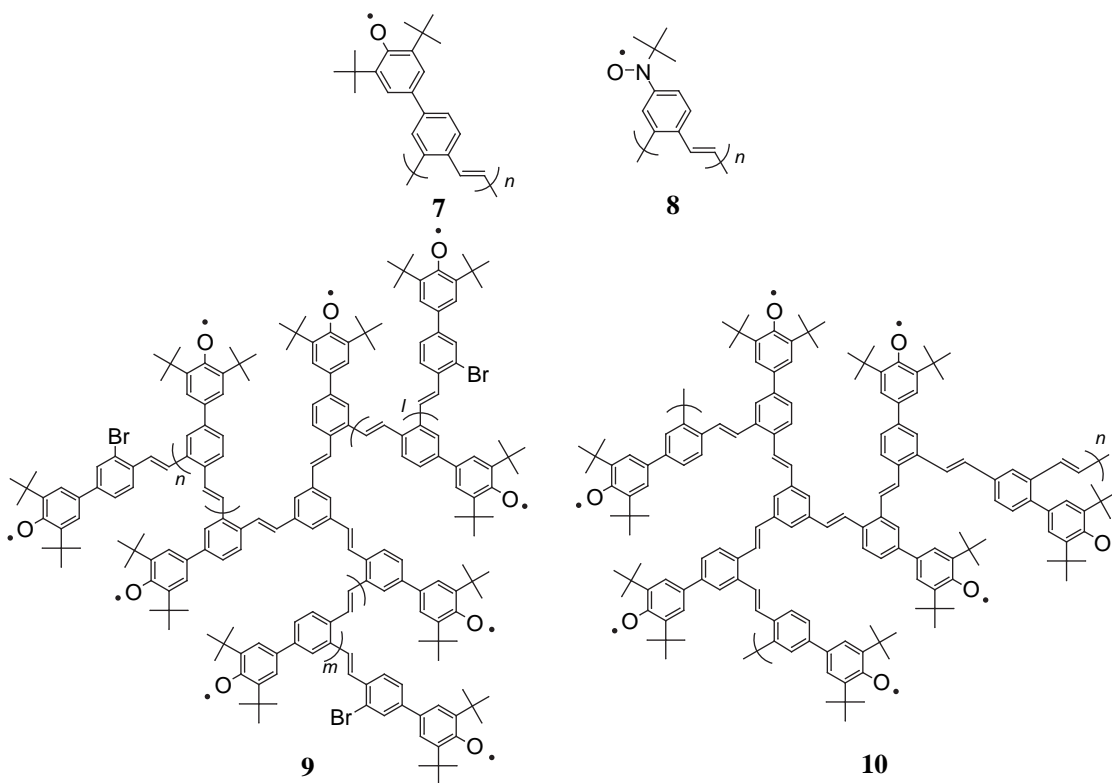
A chemically stable radical species has also been introduced into the main chain of π-conjugated polyradicals. Ionic radicals or certain polarons were often employed as such radical species. D. A. Dougherty et al. synthesized **11** with $M_n = 3.6 \times 10^3$ through Suzuki coupling reaction of 2,6-di-*tert*-butyl fuchsone moiety and *m*-phenylene coupler.[48] The electrochemically generated poly(anionic radical) **11** showed $S = 2$ with the spin concentration of 0.6, which provided the good correlation between spin concentration and S value. Cationic radicals of triarylamine or *p*-phenylenediamine (aminium cationic radicals) are one of the chemically persistent radicals, and their spin density is known to be delocalized into the aromatic groups. J. F. Hartwig et al. applied the palladium-catalyzed amination reaction to the synthesis of linear macromolecules containing the aminium cationic radicals.[49-51] **12** and **13** have a

regiodefined primary structure with M_n = 2.2×10^4 and 3.5×10^4, respectively, which indicated the possibility of a high-spin ground state.   R. J. Bushby et al. synthesized the two-dimensional network structure of the triarylamine-based macromolecule with M_w = 3.4×10^4 via the Suzuki coupling reaction.[52-54]   Exposure of a thin film of the precursor macromolecule to SbCl$_5$ vapor gave the corresponding poly(aminium cationic radical) **14**, which displayed S = 4 with the spin concentration of 0.6.   S. C. Blackstock et al. reported the poly(arylamine) dendrimer **15**, which shows the unique redox behavior with a gradient.[55]   The interior three *p*-phenylenediamine moieties of **15** are classified as a quartet structure judging from the previous report,[56,57] and **15** itself corresponds to a precursor of the high-spin poly(aminium cationic radical).   All of the polyradicals mentioned here have more or less difficulty in optimizing radical generation to form the largest spin cluster.   Therefore, the macrocyclic or pendant type approach is certainly essential to avoid the radical defect in a π-conjugated high-spin polyradical.   Furthermore, as revealed by the successful performance of Rajca's
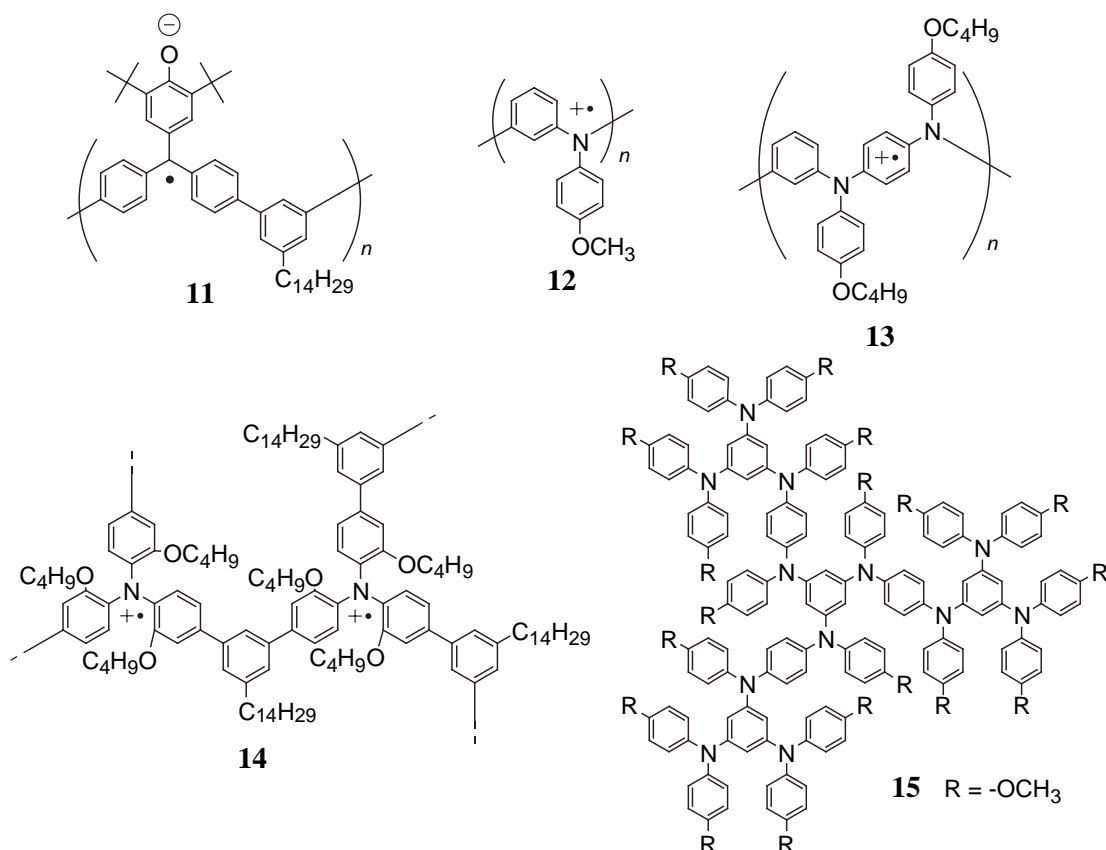
polyradical, the dimensionally extended network polyradical is an effective approach to achieve a magnetic macromolecule with very high S values.   The employment of stable radical species as a spin source in the network polyradicals should become the next trend toward a macromolecular ferromagnet effectively working at room temperature.

1.3 Magnetic force microscopy

Magnetic force microscopy (MFM) has emerged as a type of non-contact operation mode of scanning probe microscopy.[58-64]   The advantages for its magnetic imaging include a fairly high resolution on a 10 nm scale and simple operation under ambient conditions in most cases without any special sample preparation, which made MFM a standard analytical tool and has lead to rapid progress in MFM applications to material science and data storage.   On the other hand, quantitative interpretation of MFM images still remains a challenging topic and many active studies have been undertaken in this area.

MFM is, from an instrumental point of view, very closely related to atomic force microscopy (AFM) except for being equipped with a ferromagnetic probe.   The microscope's cantilever equipped with the ferromagnetic probe achieves a local magnetostatic interaction between the probe and the stray micromagnetic field from a sample on the substrate.   The probe is assumed to effectively behave as a point dipole, which provides the basic idea of the magnetic force acting on the probe: If the effective magnetic moment of the probe is oriented along the vertical direction without inversion induced by the magnetic field of a sample and the magnetic distribution of a sample is not perturbed by the probe's dipole moment, the MFM response is proportional to the second differential with respect to the vertical component of the stray field originating from a sample at the probe location.   The quantitative analysis of the magnetic response is generally difficult, because there is a problem in determining properties of the probe such as spring constant and magnetic moment, which are the important variables in the magnetic force calculation.   Nevertheless, many attempts have been made to calibrate an MFM probe and calculate its magnetic moment, and some of them were successful under certain conditions.[58,65]   They revealed that an MFM image could be reasonably simulated using the parameters.   Magnetic

dissipation microscopy, which monitors the drive power necessary to keep a constant amplitude of cantilever oscillation during MFM imaging, also offered a promising prospect for quantitatively evaluating MFM probe performance.[66,67]

Separation of the surface topography and magnetic contrast is a practically important issue especially when scanning a rough surface. The Lift Mode technique[68] developed by Digital Instruments, Inc., is efficient for the complete image acquisition. The first scan is in the tapping mode to recognize the surface or the shape of the sample, that is, AFM with the ferromagnetic probe. After lifting the probe to a certain height which can be selected as desired upon tuning, the second scan along the known trajectory above the same area uses the non-contact mode, and the magnetic gradient of the sample is detected by measuring the deflection of the cantilever equipped with the ferromagnetic probe in the static mode of the MFM operation (Fig. 1.3). During the second scan, the van der Waals force between the probe and the sample almost disappears and the probe mainly responds to magnetic forces. The lateral resolution of the MFM image largely depends on the probe-sample distance and the probe geometry. Close proximity of the probe to the sample surface and sharpening of the probe apex will bring about an improved resolution. It is generally said that the limitation of the lateral resolution is almost identical to the probe-sample distance when a commercial probe is used.
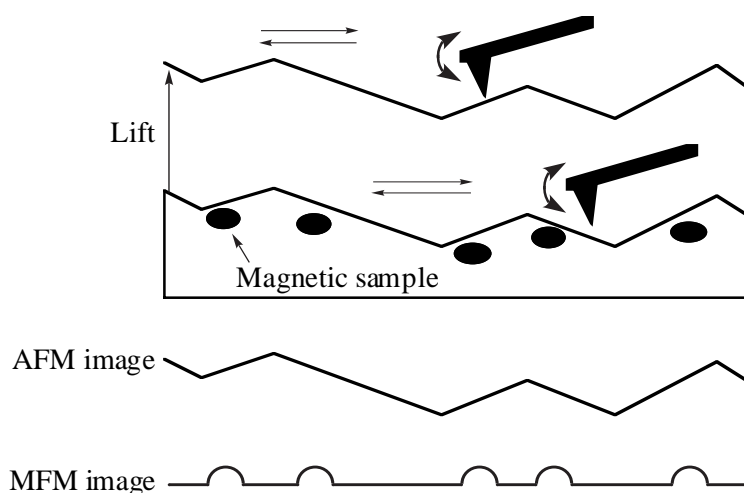

Fig. 1.3. Schematics of magnetic force microscopy operation.

Actual MFM contrasts are recorded as amplitude, phase, or frequency shifts of the cantilever oscillation when a Nanoscope IIIa with a MultiMode AFM/MFM microscope (Digital Instruments, Inc.) is used.   For amplitude detection, the drive frequency of the cantilever is set slightly higher or lower than its resonance frequency and variations in the oscillation amplitude are tracked while raster-scanning across the sample surface. If an attractive force between the probe and the sample is detected, the resonance curve of the cantilever shifts toward a lower frequency.   Consequently, the amplitude at the fixed drive frequency lower than the resonance frequency increases, but it oppositely decreases at the higher drive frequency (Fig. 1.4).   Since topographic information never provides inversion of the image, this method can be useful in verifying that the obtained MFM image is surely derived from the magnetic information.   Phase detection, which measures the phase lag of the cantilever oscillation relative to the piezo drive, provides images with a better signal-to-noise ratio and less contamination of topographic data compared to amplitude detection.   Frequency modulation detection, which directly tracks frequency variations by keeping the cantilever's phase lag at 90 degrees, also has features of an improved signal-to-noise ratio and independence of the cantilever's quality factor.   These are generally superior methods to amplitude detection for more extensive and quantitative MFM images.

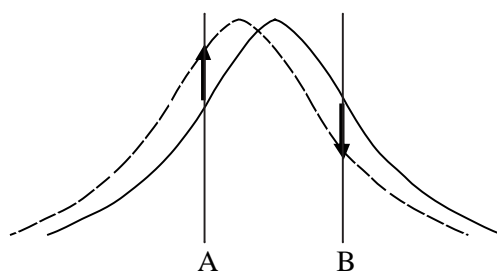
Fig. 1.4.   Shift of resonance curve in amplitude detection.   The initial curve (solid line) is shifted to lower frequency (dotted line) by the attraction between probe and sample.   If the drive frequency is set at point A, which is lower than the resonance frequency, an amplitude shift is positive.   On the contrary, if drive frequency is set at point B, the amplitude shift is negative.

MFM can provide detailed information on a magnetic structure with a nanometer size, unlike other magnetic measurements such as SQUID and ESR that evaluate the magnetic property of a sample as a bulk.   Accordingly, magnetically responsible nanoparticles or nanodots are very suitable for its motif.   In actual measurements, an MFM probe coated with a ferromagnetic alloy is used after being magnetized in the direction perpendicular to the sample surface.   It should be noted here that the MFM image must be interpreted carefully if the nano-sized sample has a weak magnetic moment relative to the ferromagnetic probe.   The magnetic field from the MFM probe might perturb or reverse the sample magnetization upon measurement.   In such a case, the application of an external magnetic field should be a good approach.   Since a strong external magnetic field brings about a motion or pinning of domain walls, it is often used for investigating the dynamics of a magnetic sample.[69-72]   On the other hand, the homogeneous magnetic field applied perpendicular to the sample surface is not detected as an MFM response to some extent.   Therefore, if the external magnetic field will induce the sufficient sample magnetization not to be altered by the ferromagnetic probe, a reliable magnetic image will be attained.   Another approach to gain the proper interpretation of the MFM image is to exchange the probe for a different one with a smaller (or much larger) magnetic moment than that of the sample.[73]   One can obtain more information on the magnetic origin from changes of the magnetic contrast. These methods enable the easy detection of a very weak magnetic moment, which will lead to the widespread applications of MFM in the future technology.

References

1. S. Sun, C. B. Murray, D. Weller, L. Folks, and A. Moser, *Science*, **287**, 1989 (2000).

2. O. Pietzsch, A. Kubetzka, M. Bode, and R. Wiesendanger, *Science*, **292**, 2053 (2001).

3. L. Krusin-Elbaum, T. Shibauchi, B. Argyle, L. Gignac, and D. Weller, *Nature*, **410**, 444 (2001).

4. P. Gambardella, A. Dallmeyer, K. Maiti, M. C. Malagoli, W. Eberhardt, K. Kern, and C. Carbone, *Nature*, **416**, 301 (2002).

5. P. M. Lahti, "Magnetic Properties of Organic Materials," Marcel Dekker, New York, 1999.

6. K. Itoh and M. Kinoshita, "Molecular Magnetism-New Magnetic Materials," Kodansha and Gordon and Breach Science Publishers, Tokyo and Amsterdam, 2000.

7. M. R. Freeman and B. C. Choi, *Science*, **294**, 1484 (2001).

8. D. Braun, in N. M. Bikales (ed.), "Encyclopedia of polymer science and technology, 15," Interscience, New York, 1971, p. 429, and references therein.

9. Y. Kurusu, H. Yoshida, and M. Okawara, *Tetrahedron Lett.*, **37**, 3595 (1967).

10. T. Kurosaki, O. Takahashi, and M. Okawara, *J. Polym. Sci., Polym. Chem. Ed.*, **12**, 1407 (1974).

11. T. Miyazawa, T. Endo, and M. Okawara, , *J. Polym. Sci., Polym. Chem. Ed.*, **23**, 1527 (1985).

12. Y. Miura, M. Kinoshita, and M. Imoto, *Makromol. Chem.*, **146**, 69 (1971).

13. Y. Miura, M. Kinoshita, and M. Imoto, *Makromol. Chem.*, **157**, 51 (1972).

14. F. E. Karrer, *Makromol. Chem.*, **181**, 595 (1980).

15. M. Kamachi, H. Enomoto, M. Shibasaka, W. Mori, and M. Kishita, *Polym. J.*, **18**, 439 (1986).

16. R. B. Upasani, L. Y. Chiang, and D. P. Goshorn, *Mater. Res. Soc. Symp. Proc.*, **173**, 77 (1990).

17. T. Kurosaki, K. Y. Lee, and M. Okawara, *J. Polym. Sci., Polym. Chem. Ed.*, **10**, 3295 (1972).

18. K. Nakahara, S. Iwasa, M. Satoh, Y. Morioka, J. Iriyama, M. Suguro, and E. Hasegawa, *Chem. Phys. Lett.*, **359**, 351 (2002).

19. O. H. Griffith, J. F. W. Keana, S. Rottschaefer, and T. A. Warlick, *J. Am. Chem. Soc.*, **89**, 5072 (1967).

20. M. Kamachi, M. Tamaki, Y. Morishima, S. Nozakura, W. Mori, and M. Kishita, *Polym. J.*, **14**, 363 (1982).

21. F. MacCorquodale, J. A. Crayston, J. C. Walton, and D. J. Worsfold, *Tetrahedron Lett.*, **31**, 771 (1990).

22. J. Allgaier and H. Finkelmann, *Makromol. Chem., Rapid Commun.*, **14**, 267 (1993).

23. P. Ferruti, D. Gill, M. P. Klein, H. H. Wang, G. Entine, and M. Calvin, *J. Am. Chem. Soc.*, **92**, 3704 (1970).

24. T. Osa, U. Akiba, I. Segawa, and J. M. Bobbit, *Chem. Lett.*, **1988**, 1423.

25. U. V. Korshak, T. V. Madvedeva, A. A. Ovchinnikov, and V. N. Spector, *Nature*, **326**, 370 (1987).

26. W. T. Borden and E. R. Davidson, *J. Am. Chem. Soc.*, **99**, 4587 (1977).

27. H. Iwamura, *Adv. Phys. Org. Chem.*, **26**, 179 (1990).

28. H. Iwamura and N. Koga, *Acc. Chem. Res.*, **26**, 346 (1993).

29. A. Rajca, *Chem. Rev.*, **94**, 871 (1994).

30. J. S. Miller and A. J. Epstein, *Angew. Chem. Int. Ed. Engl.*, **33**, 385 (1994).

31. J. A. Crayston, J. N. Devine, and J. C. Walton, *Tetrahedron*, **56**, 7829 (2000).

32. A. Rajca and S. Utamapanya, *J. Am. Chem. Soc.*, **115**, 10688 (1993).

33. A. Rajca, S. Rajca, and S. R. Desai, *J. Am. Chem. Soc.*, **117**, 806 (1995).

34. A. Rajca, K. Lu, and S. Rajca, *J. Am. Chem. Soc.*, **119**, 10335 (1997).

35. S. Rajca and A. Rajca, *J. Solid State Chem.*, **159**, 460 (2001).

36. A. Rajca, S. Rajca, and J. Wongsriratanakul, *J. Am. Chem. Soc.*, **121**, 6308 (1999).

37. A. Rajca, J. Wongsriratanakul, and S. Rajca, *Science*, **294**, 1503 (2001).

38. H. Nishide, *Adv. Mater.*, **7**, 937 (1995).

39. M. Miyasaka, T. Yamazaki, E, Tsuchida, and H. Nishide, *Macromolecules*, **33**, 8211 (2000).

40. Y.-J. Pu, M. Soma, J. Kido, and H. Nishide, *J. Polym. Sci. Part A: Polym. Chem.*, **38**, 4119 (2000).

41. H. Nishide, T. Kaneko, T. Nii, K. Katoh, E. Tsuchida, and K. Yamaguchi, *J. Am. Chem. Soc.*, **117**, 548 (1995).

42. H. Nishide, T. Kaneko, T. Nii, K. Katoh, E. Tsuchida, and P. M. Lahti, *J. Am. Chem. Soc.*, **118**, 9695 (1996).

43. T. Kaneko, S. Toriu, Y. Kuzumaki, H. Nishide, and E. Tsuchida, *Chem. Lett.*, **1994**, 2135.

44. H. Nishide, T. Kaneko, S. Toriu, Y. Kuzumaki, and E. Tsuchida, *Bull. Chem. Soc. Jpn.*, **69**, 499 (1996).

45. H. Nishide, M. Miyasaka, and E. Tsuchida, *Angew. Chem. Int. Ed. Engl.*, **37**, 2400 (1998).

46. H. Nishide, M. Miyasaka, and E. Tsuchida, *J. Org. Chem.*, **63**, 7399 (1998).

47. H. Nishide, T. Ozawa, M. Miyasaka, and E. Tsuchida, *J. Am. Chem. Soc.*, **123**, 5942 (2001).

48. K. K. Anderson and D. A. Dougherty, *Adv. Mater.*, **10**, 688 (1998).

49. F. E. Goodson and J. F. Hartwig, *Macromolecules*, **31**, 1700 (1998).

50. J. Louie and J. F. Hartwig, *Macromolecules*, **31**, 6737 (1998).

51. F. E. Goodson, S. I. Hauck, and J. F. Hartwig, *J. Am. Chem. Soc.*, **121**, 7527 (1999).

52. R. J. Bushby, D. R. McGill, K. M. Ng, and N. Taylor, *J. Mater. Chem.*, **7**, 2343 (1997).

53. R. J. Bushby and D. Gooding, *J. Chem. Soc., Perkin Trans. 2*, **1998**, 1069.

54. R. J. Bushby, D. Gooding, and M. E. Vale, *Phil. Trans. R. Soc. Lond. A,* **357**, 2939 (1999).

55. T. D. Selby and S. C. Blackstock, *J. Am. Chem. Soc.*, **120**, 12155 (1998).

56. K. R. Stickley, T. D. Selby, and S. C. Blackstock, *J. Org. Chem.*, **62**, 448 (1997).

57. M. M. Wienk and R. A. J. Janssen, *J. Am. Chem. Soc.*, **119**, 4492 (1997).

58. K. Babcock, M. Dugas, S. Manalis, and V. Elings, *Mater. Res. Soc. Symp. Proc.*, **355**, 311 (1995).

59. L. A. Bottomley, *Anal. Chem.*, **70**, 425R (1998).

60. S. Porthun, L. Abelmann, and C. Lodder, *J. Magn. Magn. Mater.*, **182**, 238 (1998).

61. L. Folks and R. C. Woodward, *J. Magn. Magn. Mater.*, **190**, 28 (1998).

62. U. Hartmann, *Ann. Rev. Mater. Sci.*, **29**. 53 (1999).

63. R. Proksch, *Curr. Opin. Solid State Mater. Sci.*, **4**, 231 (1999).

64. I. V. Yaminsky and A. M. Tishin, *Russ. Chem. Rev.*, **68**, 165 (1999).

65. H. J. Hug, B. Stiefel, P. J. A. van Schendel, A. Moser, R. Hofer, S. Martin, H.-J. Güntherodt, S. Porthun, L. Abelmann, J. C. Lodder, G. Bochi, and R. C. O'Handley, *J. Appl. Phys.*, **83**, 5609 (1998).

66. Y. Liu and P. Grütter, *J. Appl. Phys.*, **83**, 7333 (1998).

67. R. Proksch, K. Babcock, and J. Cleveland, *Appl. Phys. Lett.*, **74**, 419 (1999).

68. V. Elings, J. Gurley, *US Patent 5 308 974*, Digital Instruments, Santa Barbara, CA, May 3, 1994.

69. R. Proksch, E. Runge, P. K. Hansma, S. Foss, and B. Walsh, *J. Appl. Phys.*, **78**, 3303 (1995).

70. J. Shi, S. Gider, K. Babcock, and D. D. Awschalom, *Science*, **271**, 937 (1996).

71. K. L. Babcock, L. Folks, R. Street, R. C. Woodward, and D. L. Bradbury, *J. Appl. Phys.*, **81**, 4438 (1997).

72. R. D. Gomez, T. V. Luu, A. O. Pak, I. D. Mayergoyz, K. J. Kirk, and J. N. Chapman, *J. Appl. Phys.*, **85**, 4598 (1999).

73. L. Folks, R. Street, R. C. Woodward, and K. Babcock, *J. Magn. Magn. Mater.*, **159**, 109 (1996).

Chapter 2

Preparation of Nanometer-Sized Polyradical Particles and their Single Molecular-Based Magnetic Images

2.1 Introduction

In recent years, magnetic dots consisting of metals or metal oxides of 10–100 nanometer (nm) sizes have been significantly investigated because of their potential use as future high-density magnetic recording media.[1-3]   However, there has been no report, to our knowledge, on a magnetically responsible "dot" composed of purely-organic derived materials.   Among the nm-sized materials, organic macromolecules that possess a single molecular-based size in the nanometer range have received considerable attention, because they are prepared by conventional macromolecular chemistry and their molecular structure is designable.[4]   In particular, the preparation of organic macromolecular particles with a size from 10 nm to μm has been established and their applications have been widely investigated.[5]   The emulsion and dispersion polymerizations are useful for preparing macromolecular particles in that size range.

One of the ways to make non-diamagnetic and paramagnetic organic macromolecules is the accumulation of stable open shell molecules by preparing the macromolecule bearing stable radicals pendantly or integrating them into the main chain.[6,7]   They are often called polyradicals and have been studied as a redox resin and an antioxidant.   Nevertheless, no attempt has been made using a nm-sized polyradical particle composed of persistent organic radical species up to now (the π-conjugated but non-Kekulé-type and high-spin polyradicals with a nm-size has already been reported, but they were not persistent under air at room temperature[8]).   We selected, in this chapter, the 2,2,6,6-tetramethylpiperidine-1-oxyl (TEMPO) radical as a persistent radical, and describe the preparation of nm-sized and single molecular-based particles bearing TEMPO radicals and the detection of a very weak magnetic signal of the polyradical particles by magnetic force microscopy (MFM) as a dot image.

2.2   Experimental section

2.2.1 Materials

Polystyrene-*block*-polybutadiene was purchased from Aldrich and was purified by repeated reprecipitation from chloroform into methanol (30 wt% polystyrene content, $M_n = 1.7 \times 10^5$).   Methacrylic acid and methyl methacrylate were purified by distillation

under reduced pressure before use.   The potassium persulfate was recrystallized from water.   The solvents for the anionic dispersion polymerization were carefully distilled under nitrogen.   The solvents and triethylamine were purified in the usual manner. The other reagents were used as received.

2.2.2 Preparations

An emulsifier-free emulsion polymerization was carried out in a 300 ml round-bottom flask equipped with a reflex condenser, a nitrogen inlet, and an extendable bladed agitator.   The ratio of monomers to water was held constant at 6/94 (g/g).   The monomer feed composition, methyl methacrylate / methacrylic acid / methylenebisacrylamide, was changed from 94/1/5 to 65/30/5 mol%.   The weighed monomers and water, e.g., 4.0 g of methyl methacrylate, 1.55 g of methacrylic acid, and 0.45 g of methylenebisacrylamide in 89 ml of water, were put into the flask and nitrogen was bubbled into the solution for 30 min at 80ºC with stirring at 300 rpm.   An aqueous solution of 0.022 g potassium persulfate (5 ml) was added to initiate the polymerization. The polymerization was continued for 4 h at 80ºC and then allowed to cool to room temperature.   The produced macromolecular particles were purified with water by three centrifugation separations at 12000 rpm for 20 min, and dried in vacuo at 100ºC for 24 h.   A 0.1 g sample of the particles was then dispersed into 10 ml of thionyl chloride and heated to 70ºC for 24 h.   After thoroughly removing the thionyl chloride, 0.1 g of 4-amino-2,2,6,6-tetramethylpiperidine-1-oxyl and 3 g of triethylamine in 5 ml of dichloromethane were added and stirred at room temperature for 24 h.   The polyradical particle was isolated by repeated decantation, washing with dichloromethane, and drying in vacuo.

The anionic dispersion polymerization of 4-methacryloyloxy-2,2,6,6-tetramethylpiperidine-1-oxyl (MOTMP) was carried out in a Schlenk tube under an argon atmosphere.   A typical procedure is as follows.   In the tube were directly placed 5 ml of anhydrous hexane from the distillation apparatus, 0.2 g of MOTMP, and 0.02 g of polystyrene-*block*-polybutadiene, and the mixture was stirred until dissolved.   A 0.2 ml hexane solution of *sec*-butyllithium (1.0 M) was added dropwise with a dried syringe at room temperature.   After stirring for 30 min, the reaction was terminated with methanol.

Linear polyradicals, poly(4-methacryloylamino- and 4-methacryloyloxy-2,2,6,6-

tetramethylpiperidine-1-oxyl), were prepared according to the literature.[9,10] The former was obtained by the chemical oxidation of the precursor macromolecule with hydrogen peroxide in the presence of ethylenediaminetetraacetic acid and sodium tungstate (0.22 spin unit^{-1}; 0.91 mmol g^{-1}, $[\eta] = 1.7$ in acetone at 20°C). The latter was obtained by the anionic polymerization of MOTMP with *sec*-butyllithium in THF at room temperature (0.81 spin unit^{-1}; 3.3 mmol g^{-1}, $M_n = 2.3 \times 10^4$).

The polystyrene-*block*-poly(methyl methacrylate) was prepared by the living radical polymerization of methyl methacrylate using the chlorine atom end-capped polystyrene and CuCl and 2,2'-bipyridine as an initiator at 130°C (25 wt% polystyrene content, $M_n = 9.6 \times 10^4$). [11]

2.2.3 Measurements

Atomic force microscopy (AFM) and MFM measurements were performed using a Nanoscope IIIa multimode AFM/MFM microscope (Digital Instruments, Inc.). A drop of dilute dichloromethane solution or dispersion of the polyradical was transferred onto a highly oriented pyrolytic graphite, and the solvent was carefully blotted off by air-drying. Tapping mode AFM using a Si probe (type TESP) was applied to estimation of the horizontal distance of particles. The size and the shape of probe are known to affect AFM images,[12] therefore, the same probe was used for all measurements. The MFM images were presented by an amplitude or phase shift acquired with the Lift Mode technique. The scan lift height was controlled by the scanning parameters, assuming that the sensitivity of the cantilever was 0.03 V nm^{-1}. A commercially available MFM probe (type MESP) coated with a ferromagnetic CoCr alloy possessing a magnetic moment of 1×10^{-13} emu was used, which was magnetized in the direction perpendicular to the sample surface.

The light scattering measurement was performed with a Coulter N4SD sub-micron particle analyzer. The scanning electron microscope used was a S2500CX (Hitachi) for observing the polyradical particle. The molecular weight of the macromolecules was estimated by GPC (polystyrene gel column, eluent THF, polystyrene calibration).

2.3 Preparation of nitroxide-particle through emulsifier-free emulsion polymerization

It is well known that nm- or sub-μm-sized and monodispersed macromolecular particles are obtained by a dispersion and emulsion polymerization. However, the obtained particles are covered with a stabilizer and an emulsifier that often results in a low yield in the following chemical modification of the particles. We used, in this study, an emulsifier-free emulsion terpolymerization of methacrylic acid, methyl methacrylate, and methylenebisacrylamide to obtain the particles. The feed composition of the methacrylic acid (1–30 %), methyl methacrylate as an oil-phase formation agent (94–65 %), and methylenebisacrylamide as a bifunctional crosslinker (5 %) through the emulsifier-free emulsion polymerization was first examined to obtain the poly(methacrylic acid) particle with a desirable size and applicable to the following reactions to introduce the TEMPO moiety. The more methacrylic acid was subjected to the polymerization, the more carboxyl groups were introduced into the particle, and a stable dispersion was maintained up to 30 % of the methacrylic acid content. Next the carboxyl function of the particle was treated with an excess amount of thionyl chloride to yield the acid chloride, followed by 4-amino-2,2,6,6-tetramethylpiperidine-1-oxyl in dichloromethane solution in the presence of triethylamine. The introduction of TEMPO groups into the particle and its amount were confirmed by elemental analysis. The determined TEMPO amount was ca. 1.4 times larger than that from SQUID measurements shown below (e.g., 1.5 mmol g^{-1} from elemental analysis corresponded to 1.1 mmol g^{-1} from magnetic measurement).

Light scattering measurement on the particle dispersion in dichloromethane indicated, for example, an average diameter of 400 nm and a narrow distribution (±60 nm) for the TEMPO sample derived from the particle prepared by the polymerization of
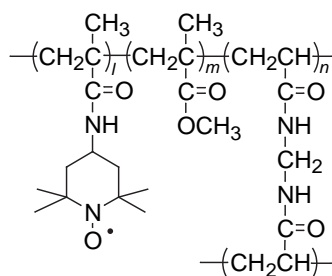
methacrylic acid (20 %), methyl methacrylate (75 %), and methylenebisacrylamide (5%).   A dilute dichloromethane dispersion of the particle was transferred to a highly oriented pyrolytic graphite surface, and was subjected to AFM.   An approximate 280 nm diameter was estimated for the polyradical particle.   AFM gave a slightly smaller diameter than that by the light scattering, probably because of the lack of swelling or a solvent-free sample state for the AFM measurement.

The spin concentration and persistency of the polyradical particle were estimated by SQUID measurements.   The magnetic susceptibility data for all samples obeyed the Curie-Weiss law with a small Weiss constant of less than -1 K.   For four kinds of polyradical particles with almost the same diameter of ca. 300 nm, the spin concentrations (mmol g^{-1}) of 1.1, 0.85, 0.60, and 0.17 were estimated from the slope of the plots in each case.   These values correspond to the maximum yield of ca. 50 % for the methacrylic acid residues in the particle.   All polyradical particles prepared were fully stable at room temperature under atmospheric conditions for at least 6 months.

2.4   Anionic dispersion polymerization of nitroxide monomer

A direct one-step preparation of the desired polyradical particle was tried by the anionic dispersion polymerization of the nitroxide monomer, 4-methacryloyloxy-2,2,6,6-tetramethylpiperidine-1-oxyl (MOTMP).   It has been reported that both the radical and cationic polymerizations of a nitroxide-bearing vinyl monomer did not proceed but the anionic polymerization of the nitroxide monomer, e.g., MOTMP, directly gave a nitroxide polyradical.[10,13,14]   MOTMP was anionically polymerized in hexane with *sec*-butyllithium as an initiator in the presence of polystyrene-*block*-polybutadiene as the stabilizer.   Immediately after the addition of the initiator, there appeared a light orange turbidity, which indicated the progress of the polymerization and the particle formation.   GPC measurement of the resulting macromolecule dissolved in THF indicated the polyradical formation with a molecular weight of $M_n = 3.2 \times 10^3$.   Its spin concentration estimated from the SQUID measurement was 2.0 mmol g^{-1}.   This spin concentration was twice that of the highest one for the polyradical particle prepared by the polymer reaction.   A scanning electron micrograph of the product revealed the formation of a relatively monodispersed particle with ca. 100 nm

diameter and their aggregation. Thus it was concluded that the anionic dispersion polymerization of MOTMP was useful for preparing the corresponding polyradical particle with a high spin concentration in one step. However, the AFM images gave only the aggregate of particles and it was difficult to obtain an image of the dispersed single particle even by replacing the solvent species of the particle suspension and a stabilizer (e.g., polystyrene-*block*-poly(methyl methacrylate)) in the anionic dispersion polymerization. Therefore, this polyradical particle could not be subjected to the subsequent MFM measurement.

CH$_3$
$-$(CH$_2$C$\overset{}{)}_n$$-$
C=O
O
N
O$^\bullet$

MOTMP
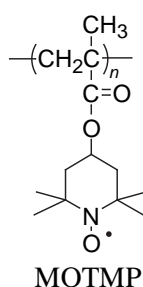
2.5 Magnetic response of polyradical particles

Magnetic force microscopy (MFM) is a scanning probe technique and a powerful tool for sub-μm magnetic imaging.[15,16] The microscope's cantilever equipped with the ferromagnetic probe achieves a local magnetostatic interaction between the probe and a magnetic sample on the substrate or the sample surface. In this study, our sample is paramagnetic and has a weak magnetic moment relative to ferromagnetic materials at which the MFM has generally aimed and been utilized, therefore, we set the sample holder on a powerful magnet to induce the magnetic vector of the sample. The magnet consists of a NdFeB alloy, with which a multimode SPM scanner AS-130 (J) for the Nanoscope IIIa is equipped. The effective external magnetic field at the sample position through a stainless holder was estimated to be ca. 80 G using a Gaussmeter, which seemed to be sufficient to affect the paramagnetic sample in this study. The polyradical sample would sense an adequate external magnetic field, and the ferromagnetic MFM probe would respond to a change in the magnetic permeability at the position of the paramagnetic polyradical sample.

Dilute dichloromethane solution of the linear polyradical, poly(4-methacryloylamino- or 4-methacryloyloxy-2,2,6,6-tetramethylpiperidine-1-oxyl) as a control, was transferred to a graphite surface and subjected to AFM followed by MFM. Both images were obtained at ambient conditions or under air at room temperature. The MFM image appeared exactly on the molecular positions detected by the AFM image. However, the disadvantage of the linear polyradical was unsettled images, which strongly depended on the surface deposition process or evaporation process of the solvent, solvent species, and so on. These often include ellipse images with a broad distribution of diameter consisting of the aggregation of many molecules, taking into account the molecular weight of the macromolecule.

This result was in contrast to the polyradical particle with a controlled and monodispersed diameter. A clear particle or dot shape is observed for the polyradical particle, which was not affected by the deposition process on the graphite substrate. The AFM gave 10^2 nm-sized dot images of the single polyradical particle (Fig. 2.1). The following MFM clearly indicated magnetic gradient responses exactly on the same single polyradical particle positions. The three-dimensional representation of the MFM topography demonstrates "holes" ascribed to the polyradical particle. By switching the drive frequency of the cantilever from higher to lower against the resonance frequency, the MFM image was inverted, which supported the magnetic response of the observed images and denied a noise image caused by surface information in the AFM.

Figure 2.1 shows the effect of the radical or spin concentration of the particle on the MFM image. For all measurements, the same apparatus and the same cantilever were used, and the scan lift height or the distance between the probe and the sample surface was maintained at 30 nm. The intensity of the MFM image, that is, the magnitude of magnetic gradient decreased with a decrease in spin concentration of the polyradical particle. The magnetic gradient response was not observed for the particles without radical, which indicated that the contribution of diamagnetism to the probe at a certain height was almost the same in this series of study. The MFM vertical scale could be, in principle, represented by a force which is related to the detailed magnetic properties of the probe such as the absolute value of the effective magnetic moment and its hysteresis loop, the spring constant of the cantilever upon measurement, and the scan lift height, but it was given as an arbitrary unit here.

AFM image   MFM image   3D-MFM topography

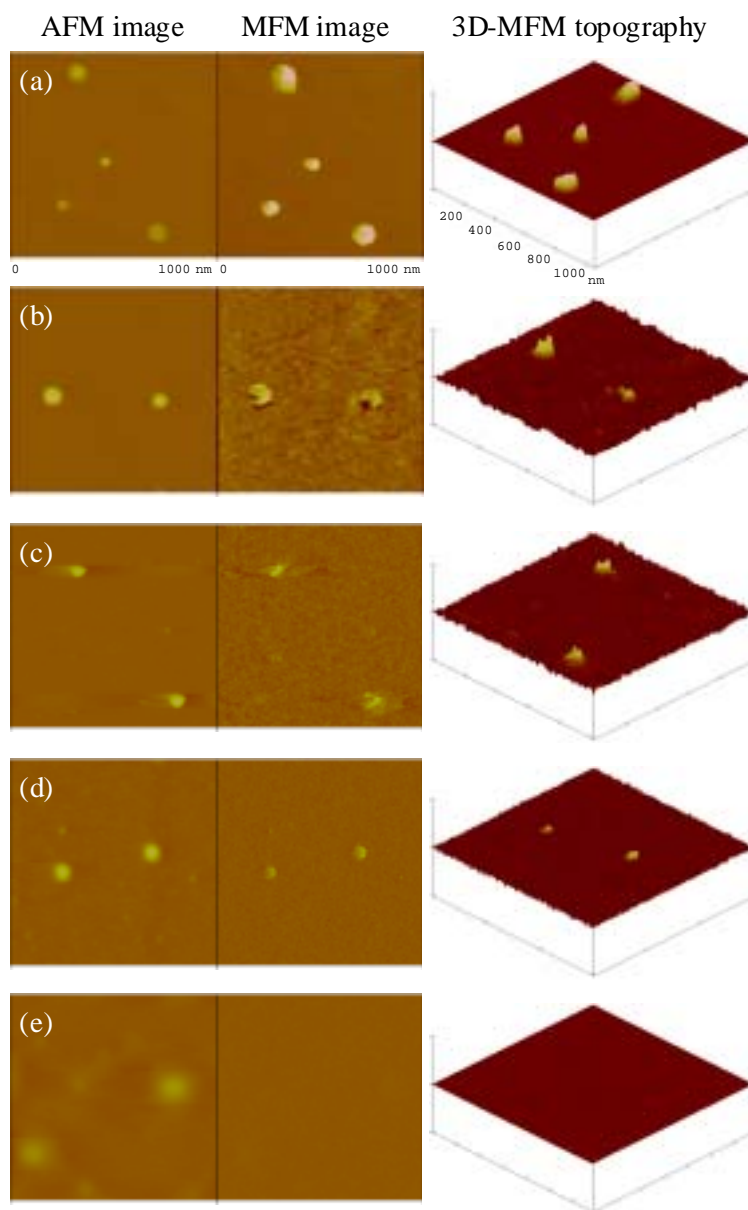**Fig. 2.1.** Effect of the spin concentration of the polyradical particles. (left) AFM, (middle) MFM images obtained by detecting phase shifts in the cantilever oscillation caused by attractive forces acting on the ferromagnetic probe, and (right) three-dimensional representations of the MFM images of the polyradical particles with different spin concentrations (mmol g^{-1}) (a) 1.1, (b) 0.85, (c) 0.60, (d) 0.17, and (e) 0.

The MFM of the particle with a low spin concentration of 0.17 mmol g^{-1} gave an interesting hollow dot image when the scan lift height was adjusted to 35 nm (Fig. 2.2). On this particle sample, the radical group was introduced by the polymer reaction and the radicals are homogeneously distributed only over the particle surface where the reaction initially occurred but not inside.   The magnetic response as the deflection of the cantilever is based on the second differential of the magnetic field in the vertical direction.   A strong magnetic gradient is detected on the perimeter of the particle but is very weak in the interior.   This consideration could explain such a hollow dot image.
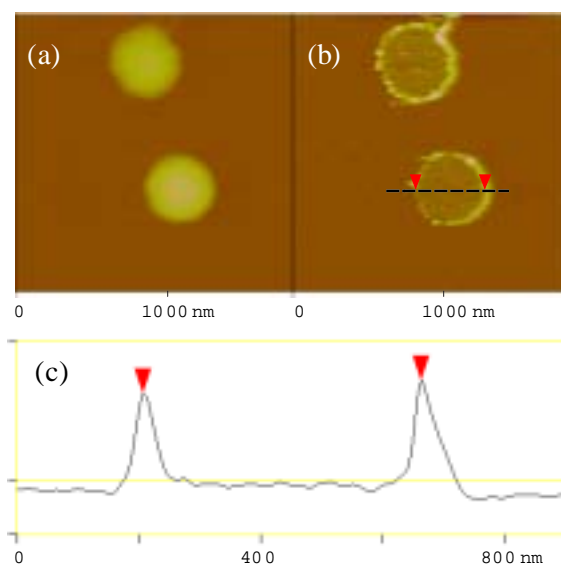
Fig. 2.2.   MFM hollow dot image of the polyradical particle with low spin concentration. (a) AFM, (b) MFM, and (c) cross sectional view of the MFM image.

References

1. F. J. Himpsel, J. E. Ortega, G. J. Mankey, and R. F. Willis, *Adv. Phys.*, **47**, 511 (1998).

2. J.-Q. Wang, L. M. Malkinski, Y. Hao, C. A. Ross, J. A. Wiemann, and J. O'Connor, *Mater. Sci. Eng.*, *B*, **76**, 1 (2000).

3. J. Lohau, S. Kirsch, A. Carl, and E. F. Wassermann, *Appl. Phys. Lett.*, **76**, 3094

(2000).

4. D. A. Tomalia, H. Baker, J. Dewald, M. Hall, G. Kallos, S. Martin, J. Roeck, and P. Smith, *Polym. J.*, **17**, 117 (1985).

5. H. Kawaguchi, *Prog. Polym. Sci.*, **25**, 1171 (2000).

6. P. M. Lahti, "Magnetic Properties of Organic Materials," Marcel Dekker, New York, 1999.

7. K. Ito and M. Kinoshita, "Molecular Magnetism – New Magnetic Materials," Kodansha and Gordon and Breach Science Publishers, Tokyo and Amsterdam, 2000.

8. H. Nishide, T. Ozawa, M. Miyasaka, and E. Tsuchida, *J. Am. Chem. Soc.*, **123**, 5942 (2001).

9. T. Kurosaki, K. W. Lee, and M. Okawara, *J. Polym. Sci., Polym. Chem. Ed.*, **10**, 3295 (1972).

10. M. Kamachi, M. Tamaki, Y. Morishima, S. Nozakura, W. Mori, and M. Kishita, *Polym. J.*, **14**, 363 (1982).

11. J.-S. Wang and K. Matyjaszewski, *J. Am. Chem. Soc.*, **117**, 5614 (1995).

12. S. J. Eppell, F. R. Zypman, and R. E. Marchant, *Langmuir*, **9**, 2281 (1993).

13. O. H. Griffith, J. F. Keana, S. Rottschaefer, and T. A. Warlick, *J. Am. Chem. Soc.*, **89**, 5072 (1967).

14. J. Allgaier and H. Finkelmann, *Makromol. Chem., Rapid Commun.*, **14**, 267 (1993).

15. L. A. Bottomley, *Anal. Chem.*, **70**, 425R (1998).

16. U. Hartmann, *Annu. Rev. Mater. Sci.*, **29**, 53 (1999).

Chapter 3

Synthesis of Stable Poly(acyl nitroxide)

3.1 Introduction

A variety of macromolecules containing stable nitroxide radicals have been investigated as new magnetic materials.[1-7]   In particular, attempts aimed at a ferromagnetic macromolecule require a high spin concentration (the number of unpaired electrons in unit weight) in the macromolecule, because ferromagnetism arises from the cooperative interaction of a large number of unpaired electrons.   Thus far, an increase of the yield in radical generation and radical attachment reactions with a precursor macromolecule and polymerization of a radical monomer without a side reaction have been mainly considered.   From an intrinsic viewpoint, a new approach to minimize the molecular weight per radical unit should be proposed in order to increase the spin concentration of polynitroxide.

The nitroxide radical is well known as one of the most stable radicals.[8-10] Although its reactivity generally increases by substituting the nitrogen atom with electron-withdrawing groups, many types of such stable nitroxides have been reported. For example, Fremy's radical could become commercially available irrespective of the substitution of two sulfonate groups.   Acyl nitroxides, both sides of which are effectively protected with *tert*-carbon atoms, also show enough chemical stability to be handled at room temperature.[11,12]   These examples indicate that a stable polynitroxide with a potentially high spin concentration is possible by replacing a bulky structure such as conventional piperidine ring in 2,2,6,6-tetramethylpiperidine-1-oxyl (TEMPO) with a compact carbonyl or *tert*-butyl group.   If useless atoms without a direct contribution to the radical stability are removed, the ideal low molecular structure having an unpaired electron would be formed.

Nitroxide polyradicals, e.g., TEMPO macromolecules, have also been investigated as an *N*-oxy-mediated oxidizing agent of alcohols and amines.[13,14]   The redox between the nitroxide and oxoammonium salt, that is, the p-type redox reaction of a nitroxide is fully reversible through the catalytic cycle.   On the other hand, there has been no report, to our knowledge, on the stable n-type redox system of a nitroxide. The nitroxide with an electron-withdrawing substituent is expected to have a high electron affinity as compared with TEMPO, which will result in an easy reduction or anodically shift of the overall redox potential.   A search for the electronic structure of such a novel molecule is a very intriguing subject.

In this chapter, the *N*-acyl-*N*-*tert*-butylnitroxide was selected as the radical group with a high spin concentration.   The synthetic process of the macromolecule pendantly bearing the acyl nitroxides, poly(*N*-*tert*-butyl-*N*-methacryloylnitroxide) **1**, and the redox bahavior of the corresponding monoradical, *N*-*tert*-butyl-*N*-pivaloylnitroxide, are described.

3.2 Experimental section

3.2.1 Materials

N-*tert*-Butylmethacrylamide was prepared by the reaction of *tert*-butylamine and methacryloyl chloride.   Yield 60 %. *N*-*tert*-Butylhydroxylamine hydrochloride was treated with aqueous potassium hydroxide solution to yield the desalted compound. Solvents, pyridine, and triethylamine were purified in the usual manners.   The other reagents were used as received.

3.2.2 Synthetic procedure

Poly(*N*-*tert*-butylmethacrylamide) 2.   A benzene solution (3 ml) of *N*-*tert*-butylmethacrylamide (0.50 g, 3.5 mmol) was stirred at 60ºC for 24 h using AIBN (5.8 mg, 3.5×10^{-5} mol) as an initiator.   After cooling to room temperature, the solution was poured into 400 ml of hexane to give a white powder.   Yield 29 %; IR (KBr pellet) 3463 (ν_{N-H}), 1663 ($\nu_{C=O}$), 1511 cm^{-1} (δ_{N-H}); ^{1}H NMR (CDCl$_3$, 500 MHz) δ = 1.05-1.25 (m, -CH$_3$), 1.28, 1.32 (s, *t*-butyl), 1.52-2.17 (m, -CH$_2$-), 5.44, 5.51 (br s, NH).

O-Benzoyl-*N*-*tert*-butylhydroxylamine 3.   Benzoyl chloride (3.9 g, 28 mmol) was added to 30 ml of benzene solution of *N*-*tert*-butylhydroxylamine (2.5 g, 28 mmol) in the presence of pyridine (2.4 g, 30 mmol), and the mixture was stirred under nitrogen at room temperature for 12 h.   After filtration of the deposited salt, the filtrate was concentrated and purified by flash column chromatography (dichlromethane) to give **3** as a pale yellow liquid.   Yield 70 %; IR (liquid membrane) 3224 (ν_{N-H}), 1719 ($\nu_{C=O}$), 1272 cm^{-1} (ν_{C-O-C}); ^{1}H NMR (CDCl$_3$, 500 MHz) δ = 1.12 (s, 9H, *t*-butyl), 5.15 (br s, 1H, NH), 7.31-7.93 (m, 5H, Ar); ^{13}C NMR (CDCl$_3$, 125 MHz) δ = 26.21, 55.69, 128.18, 128.21, 128.88, 132.85, 166.30.

O-Benzoyl-*N*-*tert*-butyl-*N*-methacryloylhydroxylamine   4.   Methacryloyl

chloride (0.66 g, 6.3 mmol) was added to 12 ml of benzene solution of **3** (1.2 g, 6.3 mmol) in the presence of pyridine (0.55 g, 6.9 mmol), and the mixture was stirred under nitrogen at 90°C for 12 h.   After cooling to room temperature, the crude product was filtered off to remove the deposited salt, and the filtrate was purified by flash column chromatography (dichloromethane) to give **4** as a brown liquid.   Yield 62 %; IR (liquid membrane) 1764 ($\nu_{O\text{-acyl C=O}}$), 1666 ($\nu_{\text{amide C=O}}$), 1364 cm^{-1} ($\nu_{\text{N-O}}$); ^{1}H NMR (CDCl$_3$, 500 MHz) δ = 1.46 (s, 9H, *t*-butyl), 1.83 (s, 3H, methyl), 4.93 (s, 1H, vinyl), 5.11 (s, 1H, vinyl), 7.41 (t, 2H, *J* = 8 Hz, Ph), 7.57 (t, 1H, *J* = 8 Hz, Ph), 7.95 (d, 2H, *J* = 8 Hz, Ph); ^{13}C NMR (CDCl$_3$, 125 MHz) δ = 19.33, 27.46, 62.56, 115.91, 127.17, 128.81, 129.94, 134.09, 140.60, 165.62, 172.55.

N-*tert*-Butyl-N-methacryloylhydroxylamine 5.   Hydrazine monohydrate (0.76 g, 15 mmol) was added to the ethanol solution (6 ml) of **4** (0.51 g, 2.0 mmol) and stirred at 40°C for 40 min.   The solution was evaporated and the crude product was purified by column chromatography on silica gel (dichlromethane) to give the deprotection compound **5** as a pale yellow powder.   Yield 36 %; IR (KBr pellet) 3373 ($\nu_{O\text{-H}}$), 1645 ($\nu_{C=O}$), 1576 ($\nu_{C=C}$), 1363 cm^{-1} ($\nu_{\text{N-O}}$); ^{1}H NMR (CDCl$_3$, 500 MHz) δ = 1.45 (s, 9H, *t*-butyl), 1.98 (s, 3H, methyl), 5.14 (s, 2H, vinyl), 8.29 (s, 1H, -OH); ^{13}C NMR (CDCl$_3$, 125 MHz) δ = 20.17, 28.28, 61.23, 116.99, 141.35, 170.73.

Polymerization of 4 and 5.   In a 5 ml ampule tube, the vinyl monomer **4** or **5** and the initiator were placed, and 0.56 ml of the solvent was then added to it.   The tube was attached to a vacuum line, sealed off, and then heated in an oil bath.   After cooling to room temperature, the resulting crude product was poured into methanol or hexane.

O-Benzoyl-N-*tert*-butyl-N-pivaloylhydroxylamine.   In a similar manner to the preparation of **4**, pivaloyl chloride (0.65 g, 5.4 mmol) and **3** (1.0 g, 5.4 mmol) were reacted to yield a pale-yellow powder.   Yield 36 %; IR (KBr pellet) 1766 ($\nu_{O\text{-acyl C=O}}$), 1640 ($\nu_{\text{amide C=O}}$), 1363 cm^{-1} ($\nu_{\text{N-O}}$); ^{1}H NMR (CDCl$_3$, 500 MHz) δ = 1.17 (s, 9H, *t*-butyl), 1.48 (s, 9H, *t*-butyl), 7.53 (t, 2H, *J* = 8 Hz, Ph), 7.67 (t, *J* = 8 Hz, 1H, Ph), 8.10 (t, 2H, *J* = 8 Hz, Ph); ^{13}C NMR (CDCl$_3$, 125 MHz) δ = 26.50, 27.40, 40.68, 64.12, 127.42, 128.99, 129.97, 134.18, 166.14, 179.24.

N-*tert*-Butyl-N-pivaloylhydroxylamine 7.[15]   A 0.2 M methanol solution of sodium hydroxide (30 ml) was added to *O*-benzoyl-*N*-*tert*-butyl-*N*-pivaloylhydroxylamine (0.19 g, 0.67 mmol) and stirred at room temperature for 72 h. The solution was evaporated and the crude product was purified by a recycling

preparative HPLC LC-918R/U (Japan Analytical Industry Co.) to give the deprotection compound as a white powder.   IR (KBr pellet) 3169 (ν_{O-H}), 1590 ($\nu_{C=O}$), 1360 cm^{-1} (ν_{N-O}); ^{1}H NMR (CDCl$_3$, 500 MHz) $\delta = 1.25$ (s, 9H, *t*-butyl), 1.41 (s, 9H, *t*-butyl), 4.98 (s, 1H, -OH); ^{13}C NMR (CDCl$_3$, 125 MHz) $\delta = 27.24, 29.71, 40.62, 61.74, 180.85$.

Oxidation.   Oxidation of poly(*N-tert*-butylmethacrylamide) **2** with *m*-chloroperoxybenzoic acid or hydrogen peroxide was carried out according to the literature.[16]   ESR spectrum of the macromolecule at $g = 2$ was very weak and the spin concentration estimated by careful integration of its signal standardized with that of a TEMPO solution was $<10^{-3}$ %.

3.2.3 Measurements

Cyclic voltammetry was carried out in dichloromethane in the presence of 0.1 M tetrabutylammonium tetrafluoroborate as a supporting electrolyte with a platinum working electrode using a function generator (Nikko Keisoku NPG-3) and potentiogalvanostat (NPGS-301) at room temperature, at the scan rate of 100 mV s^{-1}.

ESR spectrum was taken using a JEOL JES-2XG ESR spectrometer with 100 kHz field modurlation.   The IR, NMR, and mass spectra were measured with JASCO FT/IR-410, JEOL NMR 500Λ, and Shimadzu GC-MS 17A, respectively.   Molecular weight of the macromolecules was estimated by GPC (polystyrene gel column, eluent THF, polystyrene calibration).
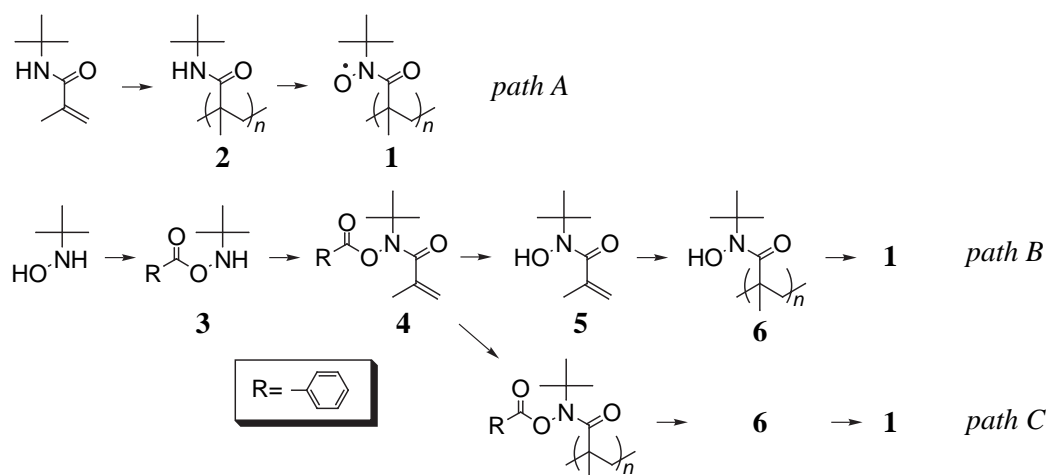
3.3 Synthesis of poly(acyl nitroxide)

The simple route (path A) to poly(*N-tert*-butyl-*N*-methacryloylnitroxide) **1** was at first examined, because the oxidation of the amine to a nitroxide radical is well reported.[16]   *N-tert*-Butylmethacrylamide was polymerized in benzene using AIBN as an initiator to yield poly(*N-tert*-butylmethacrylamide) **2** with the molecular weight of $M_n = 4.9 \times 10^3$.   The oxidation of **2** with conventional oxidants such as *m*-chloroperoxybenzoic acid and hydrogen peroxide hardly proceeded, probably due to the high potential caused by the carbonyl group attached to the nitrogen atom.

Another route via the *N-tert*-butyl-*N*-methacryloylhydroxylamine derivative was newly considered.   The protective group of the hydroxyl moiety is important for the

following reactions.   Among the many candidates, a benzoyl group was selected, which has been reported to give a stable intermediate unlike the acetyl analogue in this case.[17]   *N-tert*-butylhydroxylamine was reacted with benzoyl chloride in benzene in the presence of a small excess of base.   The use of pyridine and triethylamine as a base gave *O*-benzoyl-*N-tert*-butylhydroxylamine **3** in 70 % and 18 % yields, respectively. This yield difference seemed to be related to the basicity of the bases used: The pK_b of pyridine is 8.8, while that of triethylamine is 3.2, which is strong enough to cleave the ester bond in the product **3**.   Although **3** was hardly reacted with methacryloyl chloride at 5°C, the same reaction at 90°C smoothly proceeded to give *O*-benzoyl-*N-tert*-butyl-*N*-methacryloylhydroxylamine **4** in 62 %.   It should be noted here that **4** is a key compound in the synthetic process of the polyradical **1**.   The order of the deprotection reaction and polymerizaton and the polymerization procedure, e.g., radical or anionic polymerization, should be carefully selected.

As the leading route (path B), **4** was converted to **5** in 36 % yield by treatment with hydrazine monohydrate.   However, the polymerization of **5** at 60°C in benzene using AIBN (0.01 equiv. to **5**) as the initiator did not proceed even after 24 h (Table 3.1, Run 1).   Judging from the GPC result that the resulting crude product contains a certain oligomer fraction (27%) other than the unreacted monomer, this is probably due to the hydrogen transfer effect of the hydroxyl group in **5**.

Scheme 3.1.   Synthesis of poly(*N-tert*-butyl-*N*-methacryloylnitroxide) **1**.

We then went back to the hydroxyl-protected monomer **4** and tried the radical polymerization (path C).   The polymerization of **4** under the same conditions as **5** did not afford the macromolecule and also any oligomers (Run 2).   Other polymerization attempts using large amounts of the initiator (0.1 equiv. to **4**), with benzoyl peroxide (BPO) as a different initiator, in other solvents such as THF and toluene, and at higher temperature (100°C) did not succeed.   As one of the reasons for no polymerization, it is considered that the radical chain end and the intramolecular aminooxy (N-O) moiety form an inactive chain end during the reaction under the similar concept of living radical polymerization[18,19].   Therefore, the conventional procedure of the living radical polymerization of styrene using the TEMPO radical was applied to this system, that is, **4** was reacted in *p*-xylene at 130°C (Run 3).   After 24 h a small amount of oligomer was obtained, consistent with the amount of the initiator added, but most of **4** remained unreacted.   The polymerization was also carried out in acidic or basic solvent with a view to change the electronic state of the aminooxy moiety in **4**.   No progress has been made in acetic acid (Run 4), while a component with the higher molecular weight of M_n = 2.0×10^3 was produced in pyridine (Run 5).   Since the use of triethylamine in place of pyridine under the same conditions brought about a decrease in the molecular weight, M_n = 0.8×10^3 (Run 6), the pH is apparently an important factor to accomplish the radical polymerization of **4**.   Further work on the deprotection and oxidation of the resulting macromolecule is in progress.

Table 3.1. Radical polymerization^a of **4** and **5**.

Run	monomer (molecular weight)	initiator	[monomer] /[initiator]	solvent	temperature (^{o}C)	$M_n{}^b$
1	**5** (157)	AIBN	100	benzene	60	389 (27)^c, 210 (73)^c
2		AIBN	100	benzene	60	297
3		BPO	57	*p*-xylene	130	957 (4)^c, 300 (96)^c
4	**4** (261)	AIBN	10	acetic acid	60	327
5		AIBN	10	pyridine	60	2027 (5)^c, 984 (1)^c, 327 (94)^c
6		AIBN	10	triethylamine	60	806 (1)^c, 310 (99)^c

^{a} [monomer] = 1.15 M; Reaction time = 24 h. ^{b} The number-average molecular weight measured by GPC.
^{c} Relative ratio of the peak area (%).

3.4   Redox behavior of acyl nitroxide

In order to gain information on the electronic structure of the acyl nitroxide, *N-tert*-butyl-*N*-pivaloylhydroxylamine **7** was prepared as a control sample of the precursor macromolecule **6**, by referring to the preparation of **5**.   Figure 3.1 illustrates a cyclic voltammogram of **7** in dichloromethane at room temperature.   The anodic sweep from 0 V (vs. Ag/AgCl) provided two obscure oxidation peaks at 1.22 and 1.48 V.   The potential Ia at 1.22 V corresponds to the oxidation of hydroxylamine to the nitroxide radical through the one-electron removal and the following rapid deprotonation.   The subsequent one IIa at 1.48 V is ascribed to the oxidation process from the nitroxide radical to the oxoammonium salt.   However, there is no accompanying cathodic peak, which suggests that the electrochemical process is followed by a chemical reaction or a disproportionation reaction.   A further cathodic sweep showed a peak Ic at 0.27 V due
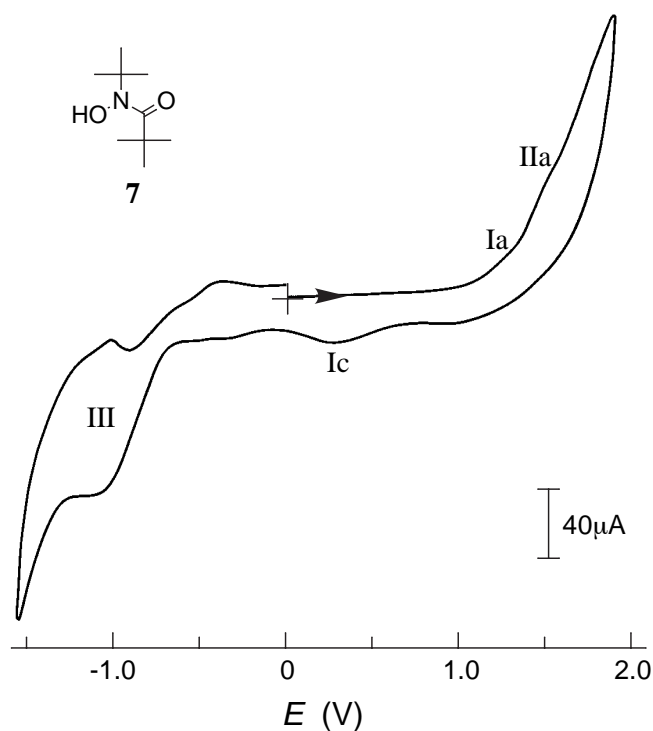

Fig. 3.1.   Cyclic voltammogram of **7** (1 mM) in CH_2Cl_2 with 0.1 M $(C_4H_9)_4NBF_4$ at room temprerature, at 100 mV s^{-1} scan rate.   Potential vs. Ag/AgCl.

to the rapid protonation of trace amounts of the nitroxide and the following one-electron reduction to yield the hydroxylamine.   The electric currents observed for these redox processes were very weak, indicating difficulty in the oxidation or p-type redox reaction of this compound.   On the other hand, a well-defined reversible redox wave III emerged at –1.05 V with the peak-to-peak separation of ca. 60 mV, which has never been seen in other nitroxide radicals like TEMPO.[20]   This wave was reversibly recorded in the repeated sweeps at room temperature.   The stable n-type redox reaction of **7** is probably caused by the substitution of the electron-withdrawing carbonyl group. More extensive information on the redox products of acyl nitroxide will be obtained by changing the electrolyte, solvent, and pH in the electrochemical studies.

References

1. M. Kamachi, in K. Takemoto, R. M. Ottenbritte, M. Kamachi (eds.), "Functional Monomers and Polymers," Marcel Dekker, New York, 1997, p. 149.

2. U. V. Korshak, T. V. Madvedeva, A. A. Ovchinnikov, and V. N. Spector, *Nature*, **326**, 370 (1987).

3. E. J. Vlietstra, R. J. M. Nolte, J. W. Zwikker, W. Drenth, and E. W. Meijer, *Macromolecules*, **23**, 946 (1990).

4. L. Dulog and S. Luts, *Macromol. Chem., Rapid Commun.*, **14**, 147 (1993).

5. P. Swobada, R. Saf, K. Hummel, F. Hofer, and R. Czaputa, *Macromolecules*, **28**, 4255 (1995).

6. H. Nishide, T. Kaneko, S. Toriu, Y. Kuzumaki, and E. Tsuchida, *Bull. Chem. Soc. Jpn.*, **69**, 499 (1996).

7. H. Oka, T. Tamura, Y. Miura, and Y. Teki, *J. Mater. Chem.*, **11**, 1364 (2001).

8. H. G. Aurich, in S. Patai, Z. Rappoport (eds.), "Nitrones, nitronates and nitroxides," Wiley, Chichester, 1989, p. 313.

9. J. F. W. Keana, *Chem. Rev.*, **78**, 37 (1978).

10. M.-E. Brik, *Heterocycles*, **41**, 2827 (1995).

11. J. Perkins and P. Ward, *J. Chem. Soc., Chem. Commun.*, **1973**, 883.

12. P. F. Alewood, S. A. Hussain, T. C. Jenkins, M. J. Perkins, A. H. Sharma, N. P. Y. Siew, and P. Ward, *J. Chem. Soc., Perkin Trans. 1*, **1978**, 1066.

13. T. Miyazawa and T. Endo, *J. Polym. Sci., Polym. Chem. Ed.*, **23**, 2487 (1985).

14. F. MacCorquodale, J. A. Crayston, J. C. Walton, and D. J. Worsfold, *Tetrahedron Lett.*, **31**, 771 (1990).

15. This compound has already been reported, but the yield was trace; H. G. Aurich and J. Trösken, *Chem. Ber.*, **106**, 3483 (1973).

16. E. Rozantzev, "Free Nitroxyl Radicals," Plenum, London, 1970.

17. P. F. Alewood, I. C. Calder, and R. L. Richardson, *Synthesis*, **1981**, 121.

18. M. K. Georges, R. P. N. Veregin, P. M. Kazmaier, and G. K. Hamer, *Trends Polym. Sci.*, **2**, 66 (1994).

19. C. J. Hawker, *Acc. Chem. Res.*, **30**, 373 (1997).

20. J. R. Fish, S. G. Swarts, M. D. Sevilla, and T. Malinski, *J. Phys. Chem.*, **92**, 3745 (1988).

Chapter 4

Complexation of Gadolinium Ion with a Poly(methacrylic acid) Nanoparticle and its Magnetic Image

4.1 Introduction

In previous chapters, it was shown that a nitroxide radical macromolecule with a nm-size is a promising material for nm-sized MFM imaging, in which a spin concentration of the macromolecule can express the image in different ways, and that the spin concentration of the macromolecule can be enhanced by molecular design. However, the nitroxide radicals mentioned there were completely paramagnetic with a very weak intermolecular antiferromagnetic interaction between radicals, that is, the spin quantum number (S) of the polynitroxides was 1/2.   Here one doubts what type of MFM image will be obtained for a magnetic sample with a higher S value.

Among atoms, gadolinium(III) (Gd^{3+}) ion has the largest S value of 7/2 based upon 7 unpaired 4f electrons.   Macromolecular-complexes with Gd^{3+} ions have mainly been investigated in view of possibly using them as a contrast agent for magnetic resonance imaging in medical uses,[1,2] but there has been few reports on their magnetism. If a nm-sized macromolecular particle containing effective functional groups for the complexation with Gd^{3+} ions can be prepared, it will be a control sample for the comparison with the MFM image of the polynitroxide particles.   As a good illustration for this purpose, the complexation of lanthanide ions with macromolecules bearing effective functional groups has been well studied to provide an organic macromolecule with the physicochemical properties of lanthanide.[3]   As for the Gd^{3+} ion, for example, it has been reported that poly(methacrylic acid) formed a bis-carboxylate coordinate complex, while its copolymer produced a tris-coordinate one with a large overall complexation constant.[4,5]

A nm-sized macromolecular particle can be prepared by using emulsion, emulsifier-free emulsion, and dispersion polymerizations.[6,7]   Since emulsifiers were not expected to interfere with the complexation unlike the polymer reaction in the synthesis of polynitroxide particles, we selected the emulsion polymerizaion to obtain a smaller particle.   In addition, a hydrophilic monomer such as methacrylic acid needs a comonomer as an oil-phase formation agent in the emulsion polymerization, which well meets the present objective of the tris-coordinate complexation of Gd^{3+} ion with the macromolecular (poly(methacrylic acid) in this case) particle.

In this chapter, the preparation of a 100 nm-sized poly(methacrylic acid) particle by emulsion polymerization, the complexation of the Gd^{3+} ion with the particle, and

detection of their magnetic signal by MFM as a dot image are described.

4.2 Experimental section

4.2.1 Materials

Methacrylic acid, ethyl acrylate, and allyl methacrylate were purified by distillation under reduced pressure before use.   Potassium persulfate was recrystallized from water.   Dichloromethane was purified in the usual manner.   Gadolinium(III) nitrate hexahydrate, sodium dodecyl sulfate, and the other reagents were used as received.

4.2.2 Preparations

Emulsion polymerization of methacrylic acid, ethyl acrylate, and allyl methacrylate was carried out in a 300 ml round-bottom flask equipped with a reflex condenser, a nitrogen inlet, and an extendable bladed agitator.   The monomers and sodium dodecyl sulfate with various feed ratios and 50 ml of aqueous solution were put into the flask and nitrogen was bubbled into the solution for 30 min at 80°C with stirring at 200 rpm.   An aqueous solution (5 ml) of 0.0123 g potassium persulfate (KPS) was added to initiate the polymerization.   After 15 min the solution was cooled and the produced macromolecular particles were purified with water by three ultracentrifugation separations at 19000 rpm for 2 h, and freeze-dried.

A 0.5 g sample of the particles was immersed in 20 ml of CO_2-free water.   After reaching equilibrium swelling, a dilute aqueous solution of sodium hydroxide was added to keep pH 5.   To this dispersion was added dropwise an aqueous solution of 0.0123–0.462 g gadolinium(III) nitrate hexahydrate (3 ml).   The pH of the system was adjusted to 5 with the sodium hydroxide solution during the experiments.   Stirring was then continued for 1 h and the resulting particles were centrifuged at 12000 rpm for 10 min to remove soluble and uncomplexed Gd^{3+} ions, and freeze-dried.


4.2.3 Measurements

For the magnetic susceptibility using a SQUID magnetometer and AFM, MFM, and SEM images, the details have been described in Chapter 2.   In AFM and MFM

measurements, a drop of dilute dichloromethane dispersion of the particle with Gd^{3+} ions (0.01g l^{-1}) was transferred onto mica surface, and the solvent was evaporated in vacuo.   The IR spectra were measured as a KBr pellet using a JASCO FT/IR-410 and the ESR spectra were taken as a neat sample on a JEOL JES-2XG ESR spectrometer with 100-kHz field modulation.

Potentiometric titrations were carried out under nitrogen at 30°C using CO_2-free water.   Hydrogen ion activities were determined with a HORIBA F-12 type pH meter. Sodium nitrate (0.1 M) was added as the supporting electrolyte.   The methacrylic acid content in the particle was estimated by back-titration using a standard 0.01 M hydrogen chloride solution as a titrant and bromothymol blue as an indicator, and the acid dissociation constant α was determined by titration with a standard 0.1 M sodium hydroxide solution.   Titration for estimation of the formation constants was carried out at the ratio of $[Gd^{3+}]/[COOH] = 0.07$ with an initial Gd^{3+} concentration of 0.3 mM.

4.3 Preparation of poly(methacrylic acid) nanoparticle

Poly(methacrylic acid) particles were prepared by emulsion polymerization.   In order to approach the ideal emulsion polymerization of a hydrophobic monomer, which was quantitatively analyzed by Smith and Ewart,[8] a large distribution ratio of methacrylic acid (MAA) into a comonomer as an oil-phase formation agent is required. In theory, the distribution ratio of MAA increases with a decrease in the pH to reach the maximum value at pH 4.6 or the pK_a of MAA, and it remains constant below pH 4.6 if the dimerization of MAA is not assumed to occur in an oil-phase.   An increase in a total amount of monomers results in an increase of the distribution ratio, but there is also a substantial requisite to depress the aggregation of the produced particles.   Taking into account these factors, we selected ethyl acrylate (EA) as a comonomer for MAA
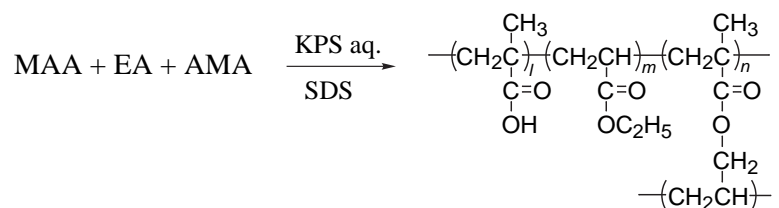
Scheme 4.1.   Preparation of poly(methacrylic acid) nanoparticle.

because of its larger distribution coefficient of 9.0 than those of other typical hydrophobic monomers, e.g., 6.5 for methyl methacrylate and 1.9 for styrene, and examined the monomer feed composition in the polymerization. A small amount of allyl methacrylate (AMA) was used as a bifunctional crosslinker for a single macromolecular-based particle in the emulsion polymerization.

Table 4.1 summarizes the polymerization results. The polymerization at the feed ratio of [MAA]/[EA] = 3/7 in a 0.01 M HCl aqueous solution gave macromolecular particles with an average diameter of 710 nm, which was larger than that obtained in water (Runs 1 and 2). The decrease in the [MAA]/[EA] ratio below pH 4.6 in principle should bring about the largest distribution ratio of MAA. However, this result suggests that the effect of the electrostatic repulsion of MAA and the anionic emulsifier or sodium dodecyl sulfate (SDS) in the particle surface, which contributes to a smaller size of the produced particles and their stable dispersion, also decreased under the acidic condition. Although an increase in the emulsifier amount relative to the monomers is also known to lead to a smaller particle size, the ineffectiveness of the emulsifier under acidic conditions was pointed out by gelation when doubling the SDS amount (Runs 3 and 4). The polymerization using the original SDS amount at the limiting feed ratio of [MAA]/[EA] = 1/1, which mostly ruled out the occurrence of the solution polymerization of MAA, yielded the smaller particles with an average diameter of 190 nm and their stable dispersion even in a 0.01 M HCl aqueous solution (Run 5). The polymerization in water under the same condition made the generated particles nanometer-sized (100 nm) and monodispersed (Run 6).

Table 4.1. Effect of monomer and emulsifier compositions on emulsion polymerization[a].

Run	solvent	MAA/EA/AMA (mmol)	SDS (mmol)	diameter[b] (nm)
1	water	30.1/70.0/1.51	5.00	470
2	HCl aq.: 0.01N	30.2/70.0/1.50	5.00	710
3	HCl aq.: 0.01N	26.6/27.6/0.761	1.06	200
4	HCl aq.: 0.01N	26.4/27.0/0.941	2.15	gelation
5	HCl aq.: 0.01N	52.7/53.4/2.01	2.12	190
6	water	52.2/52.1/3.29	2.10	100

[a] [KPS] = 0.91 mM in 50 ml of solvent; Under N_2 at 80°C; Reaction time = 15 min. [b] The average diameter was estimated from the SEM images of the freeze-dried samples.

4.4 Complexation of gadolinium ion

To a suspension of the poly(methacrylic acid) particle with 100 nm diameter was added a Gd^{3+} ion salt aqueous solution to yield three kinds of paramagnetic nanoparticles with different complexed concentrations.   The shape and the average diameter of the nanoparticles and their stable dispersion in water were almost unchanged even after the complexation (Fig. 4.1).   The amount and spin quantum number (S) of the complexed Gd^{3+} ion were estimated by measuring the static magnetic susceptibility and magnetization of the particles using a SQUID magnetometer.   The Gd^{3+} ion concentrations in the particles were estimated to be 0.89, 0.26, and 0.049 mmol g^{-1} from the slope of the Curie-Weiss plots in each case.   The normalized magnetization (M/M_s) plots for all samples were exactly on the Brillouin curve for $S = 7/2$, which indicated that the Gd^{3+} ion definitely complexed with the methacrylic acid residues in the particle.   The stretching vibration of the carboxylate anion emerged at 1540 cm^{-1} for the complexed nanoparticles and the intensity increased with an increase in the amount of the complexed Gd^{3+} ion, while the intensity of the stretching vibration at 1730 cm^{-1} derived from carboxylic acid decreased.
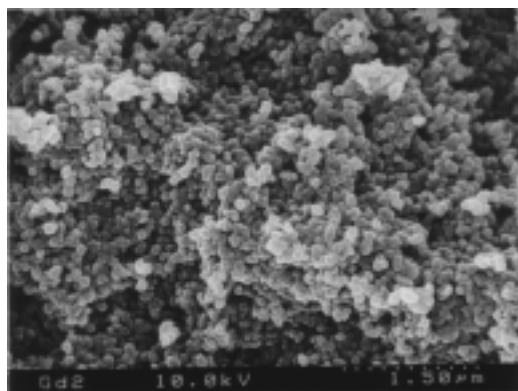

Fig. 4.1.   SEM photograph of poly(metahcrylic acid) nanoparticles complexed with Gd^{3+} ions.

The ESR spectra were also dependent on the Gd^{3+} ion concentration in the particle. Figure 4.2 shows the spectra observed for the particles with different Gd^{3+} ion concentrations at room temperature.   The particle with the high Gd^{3+} ion concentration
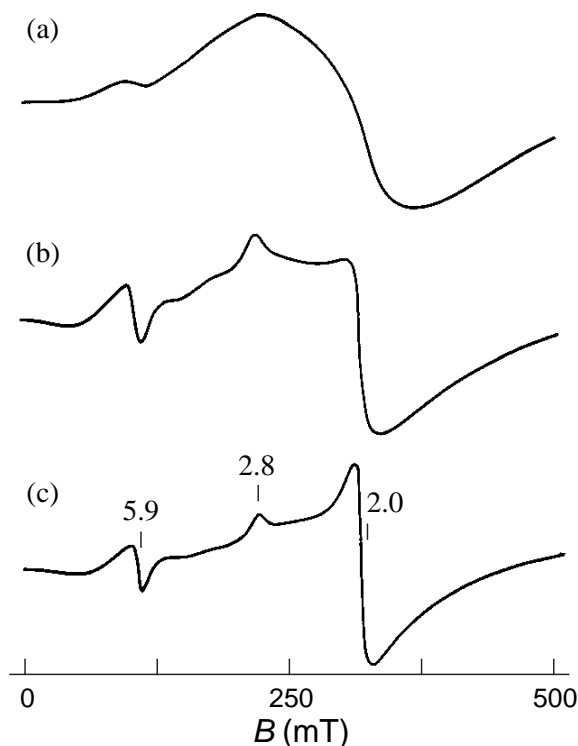
Fig. 4.2. ESR spectra of the poly(methacrylic acid)-Gd^{3+} ion nanoparticles with Gd^{3+} ion concentration of (a) 0.89, (b) 0.26, and (c) 0.049 mmol g^{-1}, at room temperature.

of 0.89 mmol g^{-1} exhibited a signal at $g = 5.9$ and a broad singlet line at $g = 2.8–2.0$, while the particles with the medium and the low Gd^{3+} ion concentrations of 0.26 and 0.049 mmol g^{-1}, respectively, provided the well-defined structures at $g = 5.9$, 2.8, and 2.0. The line at $g = 5.9$ is derived from a distorted tetrahedral environment for the complexed Gd^{3+} ions, which are rigidly bound to the poly(methacrylic acid) particle. On the other hand, the signal at $g = 2.0$ is due to the Gd^{3+} ions in an environment close to octahedral and is sensitive to hydration of the ion.[9] When an insufficient amount of Gd^{3+} ions with respect to the carboxylic acid residues in the particle was subjected to the complexation, many water molecules would remain and be easily accessible to the complexed Gd^{3+} ions in the particle, which provided the strong absorption at $g = 2.0$. On the other hand, when an excess amount of Gd^{3+} ions was subjected to the complexation, a strong dipolar interaction between the Gd^{3+} ions mainly acted to collapse the structure at $g = 2.8–2.0$.

45

The formation constants were determined by potentiometric titration for an aqueous medium of Gd^{3+} ion with the poly(methacrylic acid) nanoparticle at 30°C. The modified Bjerrum method was applied to the poly(methacrylic acid)-Gd^{3+} ion complex as a polyelectrolyte.[10,11]

First, the acid dissociation constant K_a of the poly(methacrylic acid) particle was estimated to be 4.8×10^{-7} M from Henderson-Hasselbach plots (Fig. 4.3(a)). Interestingly there was an inflection point in the plots at a low degree of dissociation similar to linear poly(methacrylic acid)[12,13]. Considering the previous report that this feature is due to a molecular confomational transition of the poly(methacrylic acid), the contracted structure of the macromolecular particle caused by a hydrophobic interaction between the α-methyl groups in the poly(methacrylic acid) moiety seemed to be destroyed by the partial generation of carboxylate anions at the low degree of dissociation, which resulted in a change in the macromolecular structure to a mobile one even in the network form.

Using the constants obtained from the Henderson-Hasselbach plots, the formation curve for the Gd^{3+} ion complex with the poly(methacrylic acid) particle was calculated (Fig. 4.3(b)). Extrapolation of the curve seemed to closely approach a maximum coordination number of 3, which revealed a completion of the complexation at the ratio of Gd(carboxylate)$_3$. According to the previous work, the complexation of a linear
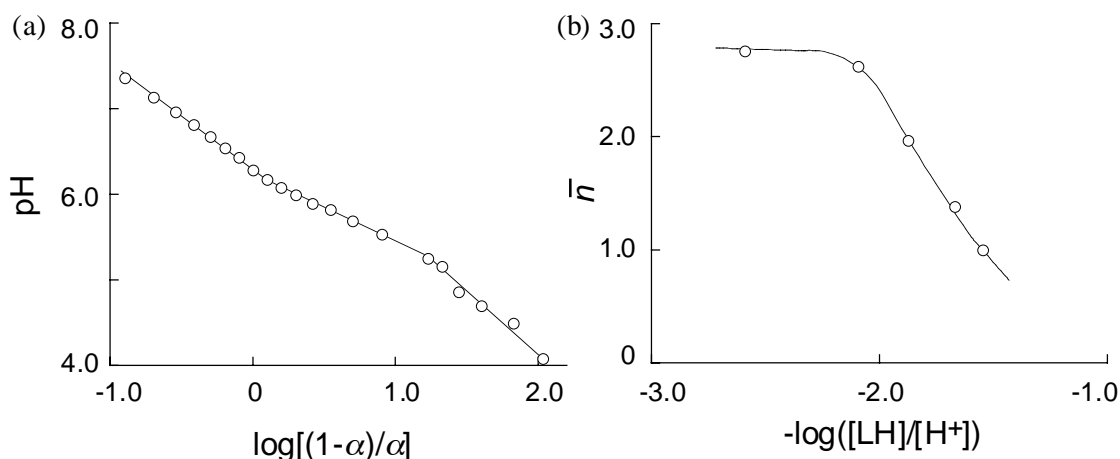

Fig. 4.3. (a) Henderson-Hasselbach plots and (b) Bjerrum's formation curve for the Gd^{3+} ion-complex with the poly(methacrylic acid) nanoparticle. $\bar{n}$ is the average number of the complexed carboxylate groups per Gd^{3+} ion and [LH] denotes the concentration of carboxylic acid.

Table 4.2. Complexation constants of the Gd^{3+} ion complexes.

macromolecule	$\bar{n}$	$\log k_1$	$\log k_2$	$\log k_3$	$\log \beta_n$
poly(methacrylic acid)^a	2.0	4.6	4.3		8.9
poly(methacrylic acid-*co*-acrylamide)^a	3.0	4.3	3.8	3.5	11.6
poly(methacrylic acid) nanoparticle	2.8	4.9	4.6	4.2	13.7

[a] Reference 4

poly(methacrylic acid) with Gd^{3+} ion cannot proceed to the third step due to the steric hindrance of the polymer chain and a large Gd^{3+} ion size, while the copolymer of MAA and acrylamide can form the tris-coordinate complex.[3] Since the poly(methacrylic acid) particle is a network copolymer of MAA, EA, and AMA, it would form the tris-coordinate complex with the Gd^{3+} ion. Successive formation constants k_i and the overall formation constant β_n estimated from the formation curve are summarized in Table 4.2. All successive formation constants for the Gd^{3+} ion complex with the poly(methacrylic acid) particle were larger than those for the linear ones, and its overall formation constant was consequently over 100 times greater at ca. 10^{14} M^{-3}, which suggested a formation of the very stable tris-coordinate complex with the Gd^{3+} ion.

4.5 Magnetic image of nanoparticle containing gadolinium ion

A dilute dichloromethane dispersion of the nanoparticles complexed with Gd^{3+} ions was transferred to a mica surface, and subjected to AFM followed by MFM. AFM gave monodispersed dot images with the horizontal distance of ca. 100 nm, which was consistent with their SEM images. The corresponding magnetic gradient responses on the particle position were observed in the following MFM. For amplitude detection, the MFM image was detected as holes when the drive frequency of the cantilever was set lower than the resonance frequency, while the image was inverted to convex topographies when the drive frequency was set higher. This result ruled out the possibility of contamination of the AFM topography.

The MFM of the particle with the high Gd^{3+} ion concentration of 0.89 mmol g^{-1} provided a half-sphere shape with a strong magnetic response in the vertical direction,

indicating the homogeneous distribution of the Gd^{3+} ions in the particle (Fig. 4.4(a)). The decrease in the Gd^{3+} ion concentration in the particle (0.26 mmol g^{-1}) gave rise to a weaker magnetic response especially in the top of the half-sphere (Fig. 4.4(b)). The change was emphasized for the particle with the low Gd^{3+} ion concentration of 0.049 mmol g^{-1}, whose MFM image consisted of a clear hollow dot structure (Fig. 4.4(c)). On this particle sample, Gd^{3+} ions readily complexed due to the large overall formation constant and their deficiency against methacrylic acid residues in the particle brought about the homogeneous distribution only over the particle surface but not inside. A distribution of Gd^{3+} ions in the vertical direction is supposed to be responsible for the characteristic images in MFM.
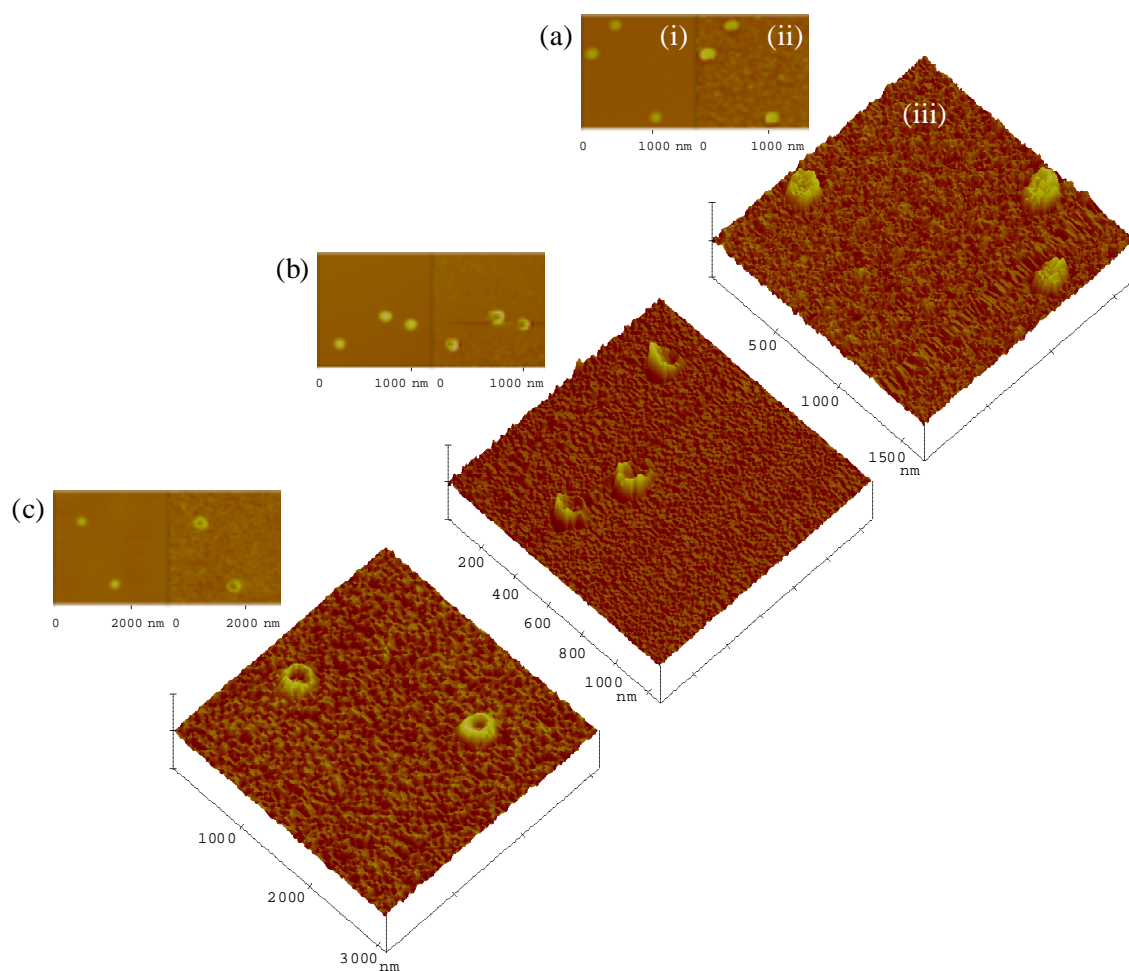

Fig. 4.4. Effect of Gd^{3+} ion concentration in 100 nm-sized nanoparticles. (i) AFM images, (ii) MFM images obtained by phase shift detection at the probe-sample distance of 30 nm, and (iii) three-dimensional representations of MFM images of the nanoparticles with various Gd^{3+} ion concentrations (mmol g^{-1}) (a) 0.89 (b) 0.26 (c) 0.049.

In this manner, the MFM images of the particle complexed with Gd^{3+} ions essentially have the same tendency as the polynitroxide particles described in Chapter 2. However, the images for the sample containing Gd^{3+} ions showed good sensitivity even at the longer probe-sample distance of 40 nm, unlike the polynitroxide particle. This is probably because of high-spin alignment of the 7 unpaired 4f electrons in a Gd^{3+} ion, which produces the square root of three times larger magnetic moment than that of 7 free electrons without any interaction. Thus it has been shown that the nanometer-sized magnetic macromolecules with different spin quantum numbers could also express the MFM images in different ways.

References

1. P. Caravan, J. J. Ellison, T. J. McMurry, and R. B. Lauffer, *Chem. Rev.*, **99**, 2293 (1999).

2. C. H. Reynolds, N. Annan, K. Beshah, J. H. Huber, S. H. Shaber, R. E. Lenkinski, and J. A. Wortman, *J. Am. Chem. Soc.*, **122**, 8940 (2000).

3. Y. Okamoto, S. S. Wang, K. J. Zhu, E. Banks, B. Garetz, and E. K. Murphy, in J. E. Sheats (ed.), "Metal-Containing Polymeric Systems," Plenum, New York, 1985, p. 425.

4. N. Yoshioka, H. Nishide, and E. Tsuchida, *Inorg. Chim. Acta*, **128**, 135 (1987).

5. H. Nishide, T. Izushi, H. Arai, N. Yoshioka, and E. Tsuchida, *J. Macromol. Sci. - Chem.*, **A24**, 343 (1987).

6. R. Arshady, *Colloid Polym. Sci.*, **270**, 717 (1992).

7. D. Kumar and G. B. Butler, *J. Macromol. Sci. -Rev. Macromol. Chem. Phys.*, **C37**, 303 (1997).

8. W. V. Smith and R. W. Ewart, *J. Chem. Phys.*, **16**, 592 (1948).

9. A. V. Kucherov, A. A. Slinkin, and M. Shelef, *Catal. Lett.*, **50**, 1 (1998).

10. H. P. Gregor, L. B. Luttinger, and E. M. Loebl, *J. Phys. Chem.*, **59**, 34 (1955).

11. G. K. Hoeschele, J. B. Andelman, and H. P. Gregor, *J. Phys. Chem.*, **62**, 1239 (1958).

12. J. C. Leyte and M. Mandel, *J. Polym. Sci.*, **A2**, 1879 (1964).

13. M. Nagasawa, T. Murase, and K. Kondo, *J. Phys. Chem.*, **69**, 4005 (1965).

Chapter 5

*Synthesis of Stable Triplet Molecules Composed of Aminium Cationic Radical*

5.1   Introduction

An attempt to realize very high-spin organic molecules using intramolecular through-bond magnetic ordering has become of great interest.   Among them, many π-conjugated, but non-Kekulé type, biradical molecules have been prepared by taking into account their topological symmetry and spin polarization in their alternant conjugations.[1-6]   While some of them succeeded in forming triplet ground-state molecules built in the π-conjugated skeleton, an important aspect of the triplet molecules depended on the spin sources.   For example, the spin density of the triarylmethine radical is delocalized into the π-conjugated skeleton, which enhances the exchange interaction between the two radicals on the biradical molecules.[2,4]   However, this spin density delocalization increases the radical reactivity of the sterically unprotected skeleton, which often leads to chemical destabilization of the molecules. On the other hand, the galvinoxyl radical, whose spin density is localized on the radical moiety, has a substantial chemical stability.[1]   However, the localized spin reduces the exchange interaction on their biradical molecules.   Therefore, a spin source, which is to be introduced into the π-conjugated skeleton, should be carefully selected from the list of radical species in order to satisfy both the sufficient exchange interaction and chemical stability for the multiple radical molecules.

Cationic radicals of tri-*p*-arylamine (aminium cationic radicals) are known as one of chemically persistent radicals which can be isolated under ambient conditions.[7-10]   It is also known that the spin density of the triarylaminium cationic radicals is delocalized into the aryl groups.   The bis- and tris(aminium cationic radical)s of the *m*-bis(diphenylamino)- and 1,3,5-tris(diphenylamino)benzenes have been studied to reveal their ground-state triplet and quartet, respectively.[11,12]   More recent research on the bis- and tris(aminium cationic radical)s using the field-swept 2D electron spin transient nutation method clearly described their triplet and quartet states and ferromagnetic coupling capability of the *m*-phenylene and 1,3,5-benzenetriyl π-conjugations.[13]   These papers indicated that the triarylaminium cationic radicals, which have both the chemical stability and an effective distribution of the spin density, are one of the promising spin sources for synthesizing very high-spin organic molecules.

To our knowledge, all of the triplet and quartet molecules based on the triarylaminium cationic radicals are the bis- and tris(cationic radical)s connected to *m*-

phenylene and the 1,3,5-benzenetriyl groups, that is, no bis(aminium cationic radical) connected with π-conjugated skeletons other than *m*-phenylene has been previously studied.   Therefore new non-Kekulé type biradical molecules derived from triarylamines were desired to evaluate the spin polarization ability of the aminium cationic radical and their chemical stability from a different viewpoint.   In this chapter, 3,4'-disubstituted stilbene was for the first time selected as a ferromagnetic skeleton to connect the aminium cationic radicals (IUPAC recommended name: ammoniumyl radical); The syntheses of 3,4'-bis[bis(*p-t*-butylphenyl)amino]stilbene **1a**, 3,4'-bis[bis(*p*-methoxyphenyl)amino]stilbene   **1b**,   and   5,4'-bis[bis(*p*-methoxyphenyl)amino]-2-methoxystilbene **1c**, the formation of the corresponding bis(aminium cationic radical)s **2**, and their magnetic properties are described.
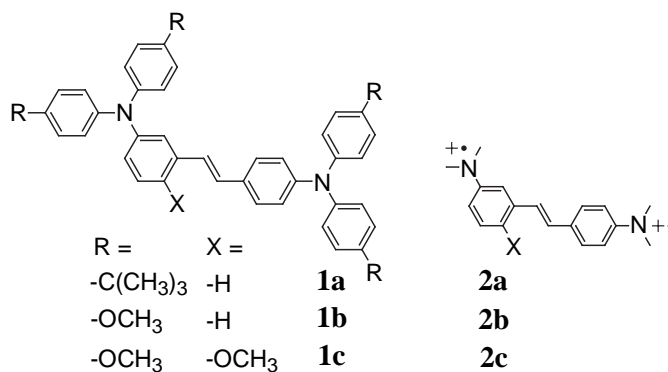
5.2   Experimental section

5.2.1 Materials

Bis(4-*t*-butylphenyl)amine **4a** was prepared by the reaction of 1-bromo-4-*t*-butylbenzene (4.7 g, 22 mmol) and 4-*t*-butylaniline (3.2 g, 21 mmol) in the presence of tris(dibenzylideneacetone)dipalladium (0.51 g, 0.56 mmol), BINAP ((*S*)-(−)-2,2'-bis(diphenylphosphino)-1,1'-binaphthyl) (1.0 g, 1.6 mmol), and sodium *t*-butoxide (6.2 g, 65 mmol) for 18 h at 110ºC.   Yield 82%; mp 111ºC (mp 107-108ºC in the lit[14]). Bis(4-methoxyphenyl)amine   **4b**   was   prepared   from   4-bromoanisole   and   4-methoxyaniline.   Yield 78%; mp 105ºC (mp 103ºC in the lit[15]).

Tris(4-*t*-butylphenyl)amine **3a** was prepared by the reaction of 1-bromo-4-*t*-

butylbenzene (0.53 g, 2.5 mmol) and bis(4-*t*-butylphenyl)amine (0.68 g, 2.4 mmol) in the presence of tris(dibenzylideneacetone)dipalladium (31 mg, 0.0034 mmol), tri-*o*-tolylphosphine (54 mg, 0.18 mmol), and sodium *t*-butoxide (6.2 g, 65 mmol) for 18 h at 100°C. Yield 90%; mp 269°C (mp 265°C in the lit[16]). Tris(4-methoxyphenyl)amine **3b** was prepared from 1-bromo-4-methoxybenzene and bis(4-methoxyphenyl)amine. Yield 70%; mp 93°C (mp 94.5°C in the lit[17]).

      3,4'-Dibromostilbene was prepared from 3-bromostyrene and 1-bromo-4-iodobenzene using palladium(II) acetate and tri-*o*-tolylphosphine as catalysts and triethylamine as a base. Yield 75%; mp 90°C (mp 88°C in the lit[3]). 4-Bromo-2-iodoanisole was prepared from 4-bromoanisole and iodine monochloride. Yield 77%; mp 65°C (mp 64°C in the lit[18]).

      The reagents without any specific notes were used as received. Solvents were purified in the usual manners.

5.2.2 Synthetic procedure

    5,4'-Dibromo-2-methoxystilbene. A volume of palladium(II) acetate (73 mg, 0.32 mmol), tri-*o*-tolylphosphine (0.19 g, 0.61 mmol), and triethylamine (7.8 g, 77 mmol) were added to 16 ml of an acetonitrile solution containing 4-bromostyrene (2.8 g, 15 mmol) and 4-bromo-2-iodoanisole (4.8 g, 15 mmol) under a nitrogen atmosphere. The solution was then stirred at 55°C for 14 h. The solution was evaporated, washed with 10% aqueous hydrogen chloride, and extracted with chloroform. After drying over anhydrous sodium sulfate, the solution was evaporated and the crude product was purified by column chromatography on silica gel (hexane/chloroform = 3/1) to give the stilbene compound as a white needle crystal. Yield 63%; mp 94°C; IR (KBr pellet): 1245, 1032 ($\nu_{\text{C-O-C}}$), 971 cm^{-1} ($\delta_{trans\text{CH=CH}}$); ^{1}H NMR (CDCl$_3$, 500 MHz) $\delta = 3.86$ (s, 3H, -OCH$_3$), 6.75-7.66 (m, 9H, ArH and -CH=CH-); ^{13}C NMR (CDCl$_3$, 125 MHz) $\delta = 55.76$, 112.63, 113.24, 121.47, 122.78, 128.14, 128.16, 128.94, 128.96, 131.23, 131.74, 136.39, 155.94; MS *m/z* 368 (M$^+$).

    3,4'-Bis[bis(*p-t*-butylphenyl)amino]stilbene 1a. 3,4'-Dibromostilbene (0.59 g, 1.7 mmol) and bis(4-*t*-butylphenyl)amine (1.0 g, 3.6 mmol) were dissolved in 13 ml of toluene. Sodium *t*-butoxide (0.54 g, 5.6 mmol), tris(dibenzylideneacetone)dipalladium (46 mg, 0.051 mmol), and tri-*o*-tolylphosphine (77 mg, 0.25 mmol) were added to the solution, and the reaction mixture was stirred at 100°C for 19 h under nitrogen. After

cooling to room temperature, the resulting solution was quenched by adding aqueous ammonia (15 ml) and taken up in chloroform. The crude product was purified by flash chromatography on silica gel (hexane/chloroform = 2/1) to afford 1.1 g of **1a** as a green-yellow solid. Yield 88%; mp 235°C; IR (KBr pellet): 1322 (ν_{C-N}), 959 cm^{-1} ($\delta_{trans CH=CH}$); ^{1}H NMR (CDCl$_3$, 500 MHz) δ = 1.28 (s, 18H, *t*-butyl), 1.30 (s, 18H, *t*-butyl), 6.84-7.30 (m, 26H, ArH and -CH=CH-); ^{13}C NMR (CDCl$_3$, 125 MHz) δ = 31.44, 31.46, 34.26, 34.28, 119.82, 121.70, 122.61, 122.72, 123.70, 124.09, 125.99, 126.03, 126.60, 127.19, 128.36, 129.27, 130.72, 138.75, 144.84, 145.15, 145.41, 145.82, 147.69, 148.47; MS *m/z* 739 (M$^+$). Found: C, 87.6; H, 8.4; N, 4.0%. Calcd for C$_{54}$H$_{62}$N$_2$: C, 87.7; H, 8.5; N, 3.8%.

3,4'-Bis[bis(*p*-methoxyphenyl)amino]stilbene 1b. A toluene solution (13 ml) of 3,4'-dibromostilbene (0.59 g, 1.7 mmol) and bis(*p*-methoxyphenyl)amine (0.83 g, 3.6 mmol) was reacted at 100°C for 19 h in the presence of sodium *t*-butoxide (0.54 g, 5.6 mmol), tris(dibenzylideneacetone)dipalladium (46 mg, 0.051 mmol), and tri-*o*-tolylphosphine (77 mg, 0.025 mmol). Yield 80%; mp 70°C; IR (KBr pellet): 1320 (ν_{C-N}), 1242, 1036 (ν_{C-O-C}), 963 cm^{-1} ($\delta_{trans CH=CH}$); ^{1}H NMR (CDCl$_3$, 600 MHz, ^{1}H-^{1}H COSY cross-peaks in aryl region) δ = 3.79 (s, 6H, -OCH$_3$), 3.80 (s, 6H, -OCH$_3$), 6.78 (dd, 1H, *J* = 4, 8 Hz, 6.81-6.83, 7.13), 6.80 (d, 1H, *J* = 17 Hz, 6.89), 6.81-6.83 (overlapped, 8H, 7.03-7.06), 6.87 (d, 2H, *J* = 8 Hz, 7.25), 6.89 (d, 1H, *J* = 17 Hz, 6.80), 7.02 (d, 1H, *J* = 8 Hz, 7.13), 7.03-7.06 (overlapped, 9H, 6.78, 6.81-6.83), 7.13 (t, 1H, *J* = 8 Hz, 6.78, 7.02), 7.25 (d, 2H, *J* = 8 Hz, 6.87); ^{13}C{^{1}H} DEPT(135°) NMR (CDCl$_3$, 150 MHz): nonquaternary region, expected, 14 resonances; found, 13 resonances δ = 55.48, 114.65, 114.68, 118.46, 119.13, 120.06, 120.46, 126.17, 126.33, 126.57, 127.18, 128.25, 129.14; quaternary region, expected, 8 resonances; found, 8 resonances δ = 129.59 (q), 138.66 (q), 140.76 (q), 141.15 (q), 148.22 (q), 149.06 (q), 155.66 (q), 155.90 (q); MS *m/z* 635 (M$^+$). Found: C, 79.3; H, 6.3; N, 4.6%. Calcd for C$_{42}$H$_{38}$N$_2$O$_4$: C, 79.5; H, 6.0; N, 4.4%.

5,4'-Bis[bis(*p*-methoxyphenyl)amino]-2-methoxystilbene 1c. A toluene solution (8.5 ml) of 5,4'-dibromo-2-methoxystilbene (0.56 g, 1.5 mmol) and bis(*p*-methoxyphenyl)amine (0.70 g, 3.1 mmol) was reacted at 100°C for 20 h in the presence of sodium *t*-butoxide (0.42 g, 4.4 mmol), tris(dibenzylideneacetone)dipalladium (21 mg, 0.023 mmol), and BINAP (42 mg, 0.068 mmol). Yield 30%; mp 87°C; IR (KBr pellet): 1319 (ν_{C-N}), 1239, 1034 (ν_{C-O-C}), 968 cm^{-1} ($\delta_{trans CH=CH}$); ^{1}H NMR (CDCl$_3$, 600

MHz, ^{1}H-^{1}H COSY cross-peaks in aryl region, 243 K) δ = 3.82 (s, 6H, -OCH$_3$), 3.83 (s, 6H, -OCH$_3$), 3.86 (s, 3H, -OCH$_3$), 6.78 (d, 1H, J = 9 Hz, 6.89), 6.82 (d, 4H, J = 9 Hz, 7.03), 6.85 (d, 4H, J = 9 Hz, 7.09), 6.87 (d, 1H, J = 15 Hz, 7.27), 6.89 (dd, 1H, J = 3, 9 Hz, 7.34, 6.78), 6.90 (d, 2H, J = 9 Hz, 7.33), 7.03 (d, 4H, J = 9 Hz, 6.82), 7.09 (d, 4H, J = 9 Hz, 6.85), 7.27 (d, 1H, J = 15 Hz, 6.87), 7.33 (d, 2H, J = 9 Hz, 6.90), 7.34 (d, 1H, J = 3 Hz, 6.89); ^{13}C{^{1}H} DEPT(135°) NMR (CDCl$_3$, 150 MHz, 243 K): nonquaternary region, expected, 14 resonances; found, 13 resonances δ = 55.40, 55.57, 111.11, 113.95, 114.14, 119.27, 119.88, 121.08, 123.72, 124.26, 126.36, 127.05, 128.50; quaternary region, expected, 9 resonances; found, 9 resonances δ = 126.80 (q), 129.26 (q), 140.22 (q), 141.23 (q), 141.49 (q), 147.52 (q), 151.74 (q), 153.98 (q), 155.11 (q); MS *m/z* 665 (M$^+$).

Oxidation. A dichloromethane solution (0.55 ml) of NOBF$_4$ or NOPF$_6$ (8.7 μmol) solubilized with a minimum amount of 18-crown-6 was added to a dichloromethane solution (0.10 ml) of **1** (6.0 unit μmol) under a nitrogen atmosphere in a glove box.   The solution rapidly turned deep blue but was stirred for a few minutes to complete the reaction.   A small amount of trifluoroacetic acid (5 vol%) was added in some cases.

5.2.3 Measurements

Cyclic voltammetry and rotating-disk voltammetry were carried out with a platinum working electrode using a function generator (Nikko Keisoku NPG-3), potentiogalvanostat (NPGS-301), and motor speed controller (SC-5) at the scan rate of 100 and 5 mV s^{-1}, respectively.   The differential pulse voltammetry was carried out using a BAS 100B/W electrochemical analyzer.   The sample solution was under an argon atmosphere during the measurement and the pulse width was 50 mV.   For coulometry, a large carbon felt electrode was used with a digital coulomb meter (Nikko Keisoku DDCM-2).   All of the electrochemical experiments were carried out in dichloromethane in the presence of 0.1 M tetrabutylammonium tetrafluoroborate as the supporting electrolyte.

Magnetization and static magnetic susceptibility were measured with a Quantum Design MPMS-7 SQUID magnetometer.   Powder samples for measurement were prepared as follows.   A dichloromethane solution of the biradical **2** was mixed with a dichloromethane solution of polystyrene ([polystyrene]/[**2**] = 100 w/w).   The solvent

was thoroughly removed in vacuo, and the resulting powder was transferred to a diamagnetic capsule. The magnetization was measured from 0.5 to 7 T at 1.8, 2, 2.25, 2.5, 3, 5, 10, 15, and 20 K. The static magnetic susceptibility was measured from 2 to 200 K in a field of 0.5 T. The quantity of the ferromagnetic impurities and diamagnetic susceptibility of the matrix and the capsule were determined by the Honda-Owen and Curie plots, respectively, and were subtracted from the measured magnetization.

The paramagnetic ^{1}H NMR spectra of the biradicals by the Evans method[19,20] were taken in CDCl$_3$ containing 0.1% TMS and 5% trifluoroacetic acid solution at 302 K on a JEOL NMR 500Λ. The biradical solution was put into a 2 mm diameter capillary tube, which was then placed inside an NMR tube with CDCl$_3$ containing 0.1% TMS and 5% trifluoroacetic acid. The chemical shift difference of the TMS resonance was measured and the mass susceptibility of the paramagnetic molecule was calculated by the conventional method[21,22].

The ESR, IR, NMR, mass, and UV/vis spectra were measured with a JEOL JES-2XG ESR spectrometer, a JASCO FT/IR-410, a JEOL NMR 500Λ or a Bruker NMR AVANCE-600, a Shimadzu GC-MS 17A, and a JASCO V-550 spectrometers, respectively. A 2 mm light-path length cell was used for the UV/vis measurements.

5.3   Synthesis of bis(diphenylamino)stilbenes

The diphenylamines **4** were prepared by a palladium-catalyzed amination[23,24] of the bromobenzene derivatives; BINAP was an effective ligand of palladium for the selective monoarylation to give **4** in high yield. *m-* or *p*-Bromostyrene was coupled with bromoiodobenzene derivatives, which selectively proceeded at the iodo position using a catalyst of palladium(II) acetate and tri-*o*-tolylphosphine to give *m,p'*-dibromostilbenes. The palladium-catalyzed amination of the dibromostilbenes with bis(*p-t*-butyl- or *p*-methoxy-phenyl)amine, **4a** or **4b**, yielded 3,4'-bis[bis(*p-t*-butyl- or *p*-methoxy-phenyl)amino]stilbene, **1a** or **1b**, in a yield of more than 80% and 5,4'-bis[bis(*p*-methoxyphenyl)amino]-2-methoxystilbene **1c** in a moderate yield, which were higher than those from the preparation using Ullmann's copper chemistry.[25,26]

The diaminostilbenes **1** were characterized by NMR spectroscopy. The ^{1}H NMR
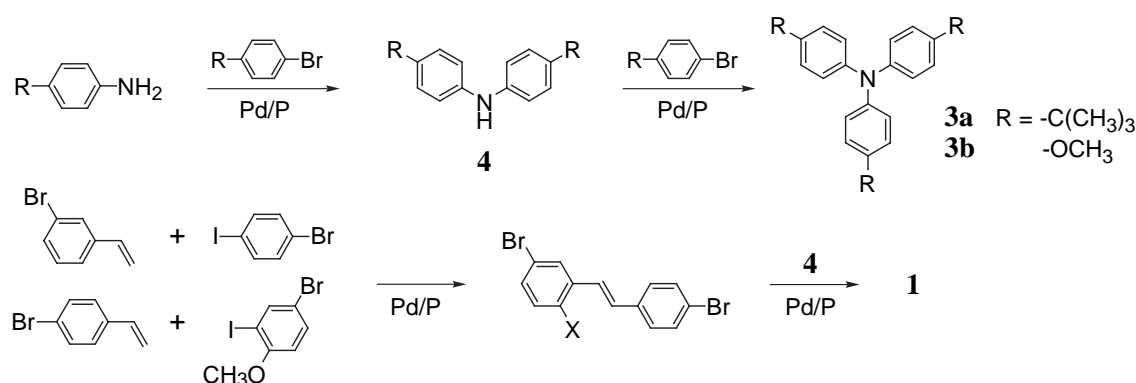
Scheme 5.1.

of **1c** at 243 K clearly characterized its structure though part of the spectrum was broadened at 303 K. On the other hand, the ^{1}H NMR of **1a** and **1b** gave unambiguous spectra even at room temperature. It is considered that the rotation of the tris(*p*-methoxyphenyl)amine moiety on the vinylene bridge of **1c** is suppressed by the introduction of the methoxy group due to its steric interaction with the ethylenic hydrogen. The rotational barrier was estimated to be 64 kJ mol^{-1} from the temperature-variable experiment of the ^{1}H NMR. The aromatic regions were analyzed with the help of ^{1}H-^{1}H COSY, HMQC, and HMBC experiments. For example, the ^{1}H-^{1}H COSY spectrum of **1b** clearly resolved the complex ^{1}H NMR signals in the aromatic region, which showed four sets of phenylene rings and a set of off-diagonal resonances attributed to the vinylene unit (Fig. 5.1). HMQC and HMBC also substantiated the assignment and clarified the correlation of the ^{13}C NMR signals (see Experimental section). The ^{13}C DEPT/NMR spectra were analyzed by comparing the numbers of expected and measured resonances in distinct spectral regions (e.g., aromatics). The diaminostilbenes, **1a**, **1b**, and **1c**, which lacked elements of symmetry in the aromatic regions, contained 24, 21, and 22 nonequivalent carbon atoms, respectively. The exact assignments of the methyl, methine, and the quaternary carbons were accomplished by the combination of an approximation based on the additive law in the HMQC and HMBC spectra. The ^{13}C DEPT experiment of **1b** revealed a total of 21 carbon signals, of which one was attributed to the methyl, twelve to the methine, and eight to the quaternary carbons; these were consistent with the molecular structure. The *trans*-stilbene structure was supported by a strong fluorescence at 490nm (λ_{ex} = 375 nm) and IR absorption at $\delta_{CH=CH}$ = 963 cm^{-1}.
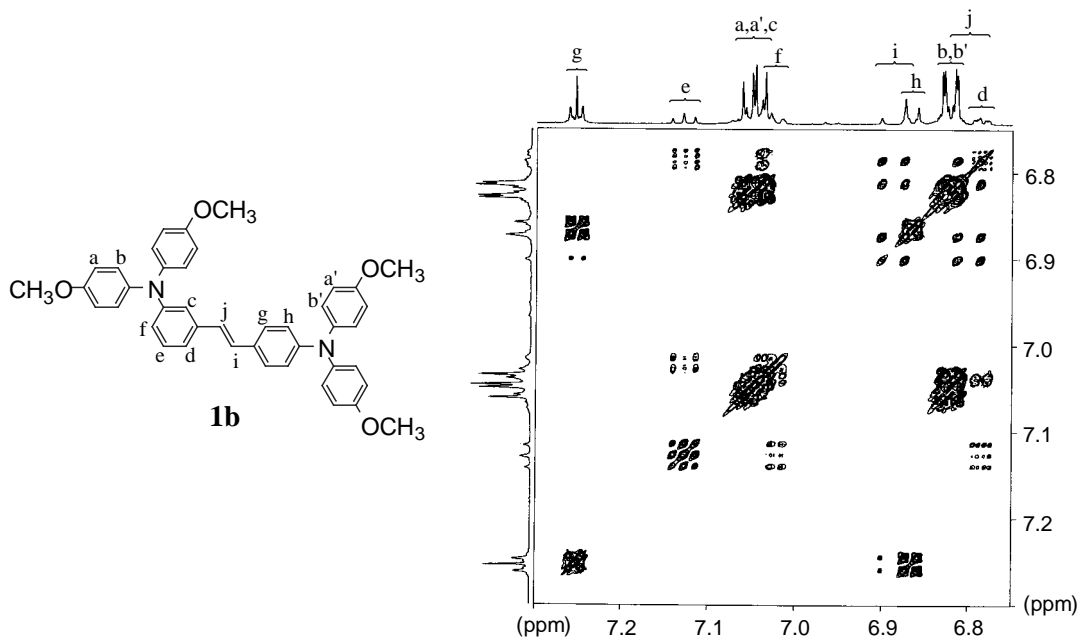
Fig. 5.1. ^{1}H-^{1}H COSY correlation (600 MHz, in CDCl$_3$) in the aromatic region of the diaminostilbene **1b**.

5.4 Electrochemical and spectral analyses in radical generation

The diaminostilbenes **1** displayed complete reversible redox waves during cyclic voltammetry (Fig. 5.2). The biradicals **2** were stable in solution even at room temperature on the time scale of the voltammetry experiment. Compounds **3** also showed reversible redox waves; however, triphenylamine gave only a simple oxidation wave. The chemical stability of **1** in the redox reaction is considered to be realized by the introduction of the *p*-substituents, which prevent dimerization to form benzidine derivatives. The collapsed redox potentials (vs. Ag/AgCl), 0.93 and 0.75 V for **1a** and **1b**, respectively, were anodically shifted relative to those of the corresponding *p*-substituted triphenylamines, 0.89 and 0.65 V for **3a** and **3b**, respectively, while the first potential $E^{\circ\prime}(1)$ of 0.63 V for **1c** was almost the same as that of **3b**. The potentials were also explained by the electron-donating effect of the *t*-butyl and methoxy groups. Differential pulse voltammetry was applied to the oxidation process of the diaminostilbenes **1a** and **1b**. Figure 5.2 displayed two oxidation responses ascribed to
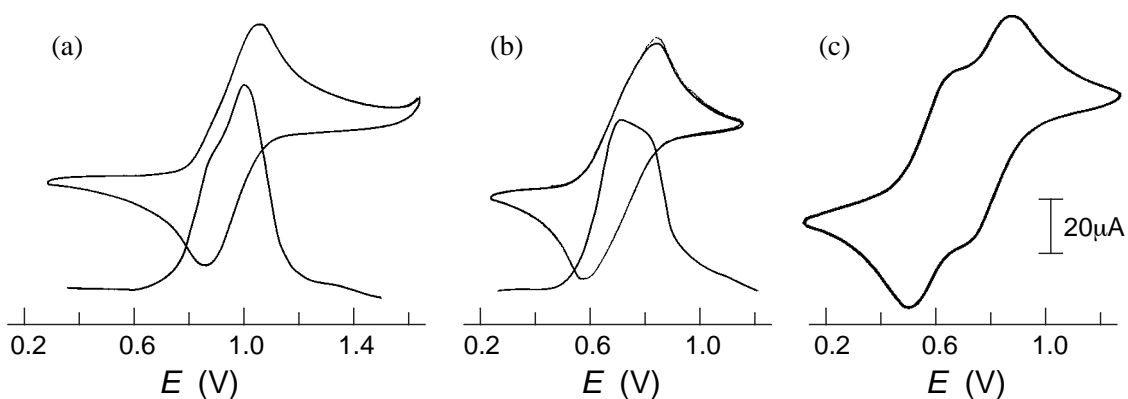
Fig. 5.2. Cyclic voltammograms and differential pulse voltammograms for (a) **1a**, (b) **1b**, and (c) **1c** (1 mM/radical unit) in CH_2Cl_2 with 0.1 M $(C_4H_9)_4NBF_4$ at room temprerature. Potential vs. Ag/AgCl.
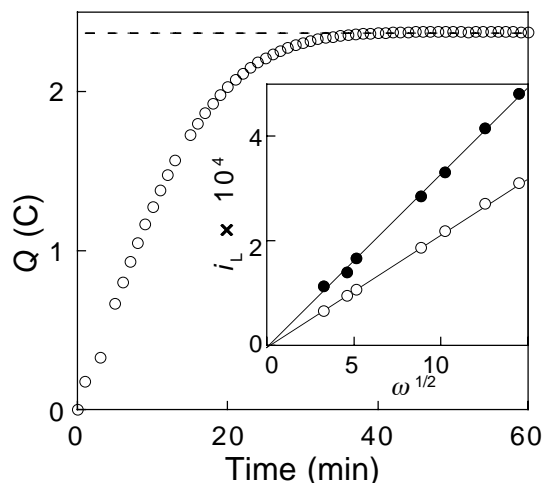

Fig. 5.3. Controlled potential coulometric oxidation of the diaminostilbene **1b** (1.23×10^{-5} mol) in CH_2Cl_2. The dashed line is the theoretical quantity of electricity for stoichiometric oxidation ($Q = 2.37$ C). Inset: Plots of limiting current vs. square root of rate (ω) for **1b** ( ) and **3b** ( ).

the two amine sites (potential difference of ca. 0.1 V). In contrast the second potential $E^{o'}(2)$ of **1c** clearly appeared at 0.77 V without any differential technique. Cation-cation repulsion through the π-conjugation and/or steric closeness in the stilbene linkage of **1** separates the first and second oxidation steps of the amine sites.

The coulometric oxidation of **1b** under the application of 1.2 V with a carbon felt electrode was completed close to the electricity of two-equivalents for the **1b** molecule,

60

and indicated the stoichiometric oxidation of the two amine sites (Fig. 5.3). The rotating-disk voltammetry of **1b** and **3b** was carried out under the same conditions to support the oxidation of **1** via a two-electron transfer reaction. The limiting current for **1b** was ca. 1.5-times larger than the one-electron oxidation current for **3b**. Plots of the limiting current vs. the square root of the rotation rate gave straight lines (Fig. 5.3). The diffusion coefficients of **1b** and **3b** were estimated to be 7.3×10^{-6} and 1.1×10^{-5} cm^2 s^{-1}, respectively, by the Levich equation.[27] The ratio of the diffusion coefficients was approximately consistent with the inverse square-root value of the ratio of the molecular weights of **1b** and **3b**. This result supported the validity of the voltammetry and the two-electron oxidation of **1b** to form the biradical **2b**.

The chemical oxidation of **1** was carried out using NOBF$_4$ or NOPF$_6$ solubilized in dichloromethane with 18-crown-6 at room temperature. The dichloromethane solution of **1** turned deep blue through the oxidation, being accompanied by a new absorption (λ_{max} = 689, 769, and 742 nm for **1a**, **1b**, and **1c**, respectively), which is characteristic of triphenylaminium cationic radicals[28,29] (Fig. 5.4). This spectral change in the UV/vis region had an isosbestic point (at 332, 345, and 346 nm for **1a**, **1b**, and **1c**, respectively), which could negate any side reaction during the oxidation. The radical formation was also supported by the appearance of an ESR signal at g = 2.003. The ESR spectra of the radicals with low spin concentrations gave five-line signals ascribed
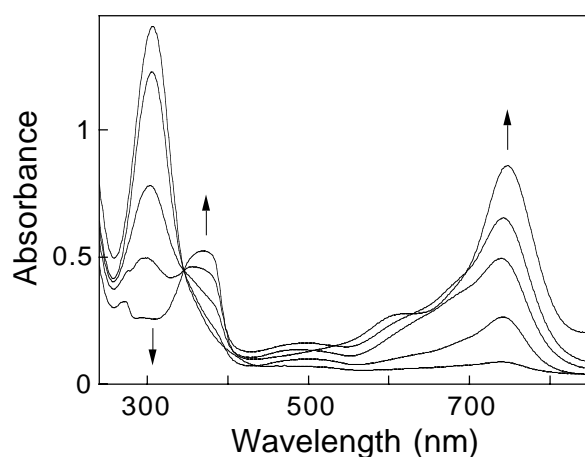

Fig. 5.4. UV/vis spectra of **1b** during the oxidation with NOBF$_4$. [NOBF$_4$]/[**1b**] = 0.35, 0.70, 0.90, 1.05, and 1.40. [**1b**] = 0.2 mM in CH$_2$Cl$_2$.

to the hyperfine coupling with two nitrogen nuclei. These spectra successively changed to three-line and unimodal signals with increasing spin concentration, which was ascribed to an exchange broadening. A small excess of the oxidizing agent (ca. 1.45 equiv. to amine unit) was added for the formation of the biradical **2**, which was judged by the saturations of the visible absorption and ESR signal intensity. Chemical stability of the radicals was enhanced by the process of adding a small amount of trifluoroacetic acid, followed by dilution with polystyrene, and removal of the solvent. The half-life of the biradical **2c** estimated by ESR was approximately 2 months even under ambient conditions. No other aminium cationic biradicals reported up to now have such a substantial chemical stability.

5.5   Magnetic property of bis(aminium cationic radical)s

The ESR of the biradicals **2** gave a fine structure in the $\Delta M_s = \pm 1$ region and a $\Delta M_s = \pm 2$ forbidden transition, which are characteristic of a triplet species. The spectrum of the biradical **2c** at 100 K showed a six-line pattern in the $\Delta M_s = \pm 1$ region (Fig. 5.5). From the peak-to-peak line width of three pairs of absorption, the zero-field splitting parameters, $|D/hc|$ and $|E/hc|$, are estimated to be 0.0028 and 0.0003 cm^{-1}, respectively. The D value, which corresponds to an average distance between the two radical centers of 9.8 Å, is much smaller than that observed for the biradical **2b** (ca.
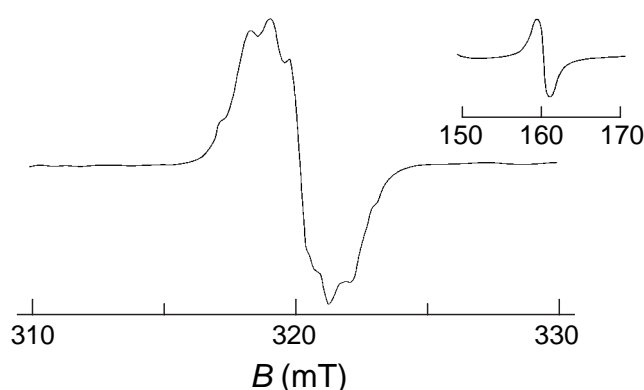

Fig. 5.5.   ESR spectrum of the biradical **2c** (0.025 mM) in CH$_2$Cl$_2$/CF$_3$COOH (95/5 v/v) at 100 K.   Inset: $\Delta M_s = \pm 2$ transition.
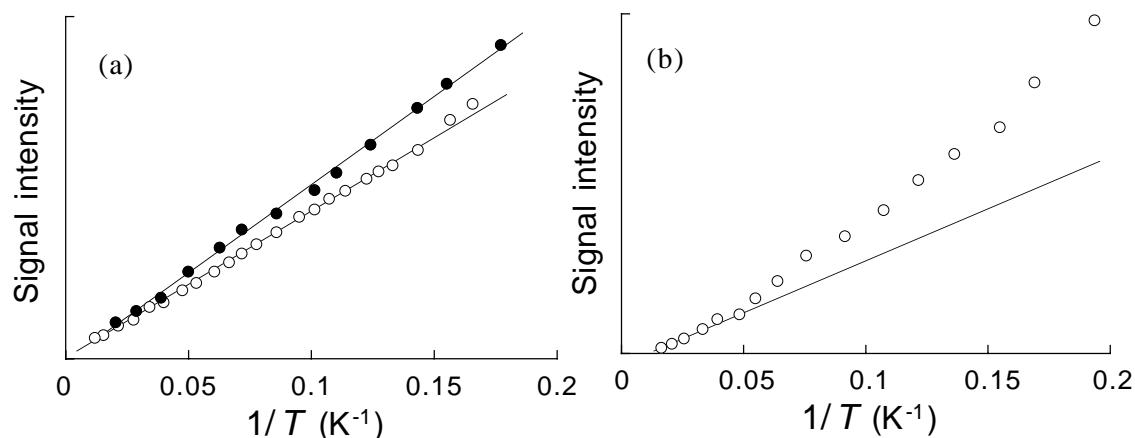
Fig. 5.6. Temperature dependence of the ESR $\Delta M_s = \pm 2$ signal intensity of (a) **2a** (   ) and **2b** (   ) and (b) **2c** (   ).

0.0037 cm^{-1}), presumably because of the restricted π-coplanarity in the stilbenoid framework.   The ESR spectrum of the biradical **2b** recorded under the same conditions only gave a two-line pattern without a well-defined fine structure.   This could be explained by several conformers for the biradical **2b** with slightly different ESR parameters.   On the other hand, the biradical **2c** seems to have a more stable conformation at lower temperature, which leads to the zero-field splitting.

The doubly integrated signal intensities of the $\Delta M_s = \pm 2$ transition for the biradicals **2a** and **2b** were proportional to the reciprocal of the absolute temperature in the temperature range of 5—100 K (Fig. 5.6(a)).   The signal intensity for the biradical **2c** also obeyed Curie's law in the higher temperature region, but the plots deviated upward in the lower temperature region (Fig. 5.6(b)).   These temperature dependences are consistent with **2** being the triplet ground state biradicals.   However, it does not rule out the possibility of a degenerate singlet/triplet state for **2a** and **2b**.

Magnetization and static magnetic susceptibility of the biradicals **2** were measured using a SQUID magnetometer.   Polystyrene was used as a diamagnetic diluent of the biradicals to minimize any intermolecular interactions.   The magnetization (M) normalized by the saturated magnetization (M_s), M/M_s, plots of **2a** were presented between the theoretical Brillouin curves for $S = 1/2$ and $2/2$, and those of **2b** and **2c** were close to the curve for $S = 2/2$, indicating a triplet ground state of the biradicals (Fig. 5.7).
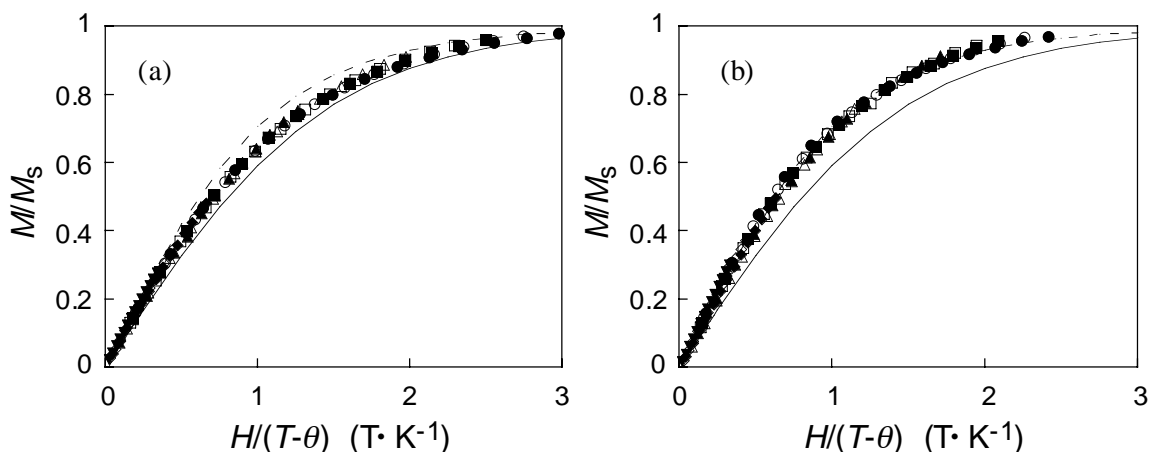
63

Fig. 5.7. Normalized plots of magnetization (M/M_s) vs. the ratio of magnetic field and temperature ($H/(T-\theta)$) for the biradical (a) **2a** and (b) **2b** with the spin concentration of 0.18 and 0.50 spins/radical unit, respectively. Powder samples diluted with polystyrene. $T =$ 1.8 ( ), 2 ( ), 2.25 ( ), 2.5 ( ), 3 ( ), 5 ( ), 10 ( ), 15 ( ), 20 ( ) K and theoretical curves corresponding to the $S = 1/2$ and $2/2$ Brillouin functions.

The temperature dependence of the ratio of the effective magnetic moments (μ_{eff}) and the Bohr magneton (μ_B), μ_{eff}/μ_B, is shown in Figure 5.8. The μ_{eff}/μ_B values of **2a** and **2b** were higher than the theoretical value of 2.45 for $S = 1/2 \times 2$ and almost constant in the range 20—200 K or even at the higher temperature, as compared with those of **2c**. For **2a**, the intermediate value (ca. 2.6) between 2.45 and 2.83 for $S = 1/2 \times 2$ and 1, respectively, could be explained by the still low spin concentration of 0.18 which was determined by the saturated magnetization. The improved spin concentration of 0.50 for **2b** brought about a smaller monoradical fraction, so that the plots were close to 2.83. In contrast, **2c** behaved as two independent free radicals at higher temperature, irrespective of the higher spin concentration of 0.82, and the μ_{eff}/μ_B plots increased with decreasing temperature (<80 K), indicating the ferromagnetic interaction. Curve fitting of the data to the Bleany-Bowers expression[30] gave the triplet-singlet energy gap (2J) of $\gg kT$ for **2a** and **2b** and 71 cm^{-1} for **2c**. The plots obviously decreased below 20 K, probably because of an intermolecular antiferromagneic interaction.
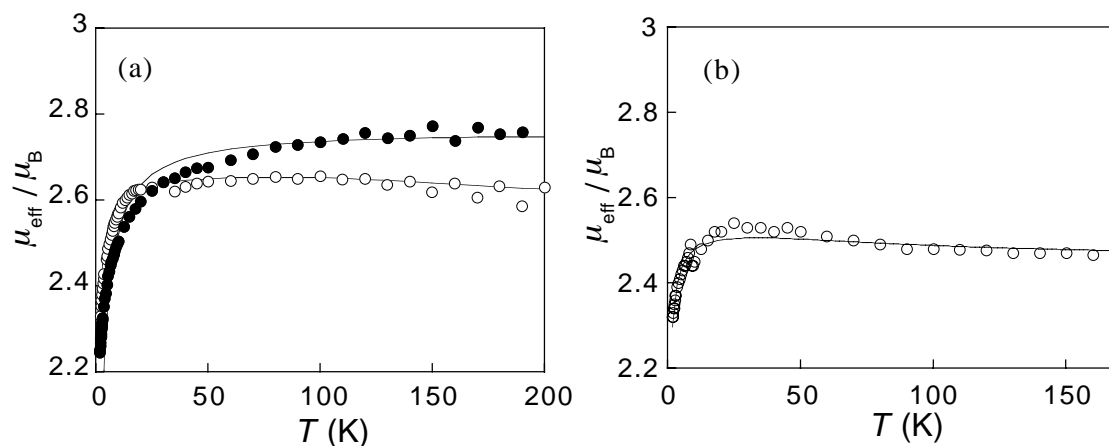
Fig. 5.8. The ratio of the effective magnetic moment and the Bohr magneton ($\mu_{\text{eff}}/\mu_{\text{B}}$) vs. temperature ($T$) plots for the biradical (a) **2a** ( ) and **2b** ( ) and (b) **2c** ( ).   Solid lines are the simulated curves calculated using the Bleany-Bowers expression with the parameters $x_1 = 0.45$, $\theta = -0.55$ K, and $J \gg kT$ for **2a**, $x_1 = 0.30$, $\theta = -1.1$ K, and $J \gg kT$ for **2b**, and $x_1 = 0.81$, $\theta = -0.38$ K, and $J = 71$ cm^{-1} for **2c**.

       The biradicals **2b** and **2c** showed the quite different magnetic behavior, especially at higher temperature.   Susceptibility measurements were carried out at 302 K using the NMR Evans method to clarify this difference.   The $\mu_{\text{eff}}/\mu_{\text{B}}$ values of the biradicals **2b** and **2c** in CDCl$_3$/CF$_3$COOH (95/5 v/v) were 2.7$_9$ and 2.3$_1$, respectively.   The former represents the ferromagnetic spin-alignment in the molecule even at high temperature, while the latter denotes a non-interaction between the two radicals.

       It is concluded that the biradicals **2a** and **2b** had a triplet ground state stabilized from the singlet state with an energy gap greater than kT and that the biradical **2c** has realized a remarkable chemical stability, but the de-conjugative twisting on the 2,5,4'-substituted stilbene framework might concomitantly bring about a decrease in the spin-exchanging ability in **2c**.

References

1. K. Mukai, *Bull. Chem. Soc. Jpn.,* **48**, 2405 (1975).

2. J. Veciana, C. Rovira, M. I. Crespo, O. Armet, V. M. Domingo, and F. Palacio, *J. Am. Chem. Soc*., **113**, 2552 (1991).

3. N. Yoshioka, P. M. Lahti, T. Kaneko, Y. Kuzumaki, E. Tsuchida, and H. Nishide, *J. Org. Chem*., **59**, 4272 (1994).

4. A. Rajca and S. Rajca, *J. Am. Chem. Soc*., **118**, 8121 (1996).

5. R. J. Bushby, D. R. McGill, K. M. Ng, and N. Taylor, *J. Chem. Soc., Perkin Trans. 2,* **1997**, 1405.

6. K. Hamachi, K. Matsuda, T. Itoh, and H. Iwamura, *Bull. Chem. Soc. Jpn*., **71**, 2937 (1998).

7. R. I. Walter, *J. Am. Chem. Soc*., **77**, 5999 (1955).

8. E. T. Seo, R. F. Nelson, J. M. Fitsch, L. S. Marcoux, D. W. Leedy, and R. N. Adams, *J. Am. Chem. Soc*., **88**, 3498 (1966).

9. L. Hagopian, K. Günter, and R. I. Walter, *J. Phys. Chem*., **71**, 2290 (1967).

10. S. Sasaki and M. Iyoda, *Chem. Lett*., **1995**, 1011.

11. K. Yoshizawa, A. Chano, A. Ito, K. Tanaka, T. Yamabe, H. Fujita, J. Yamauchi, and M. Shiro, *J. Am. Chem. Soc.*, **114**, 5994 (1992).

12. K. R. Stickley and S. C. Blackstock, *J. Am. Chem. Soc*., **116**, 11576 (1994).

13. K. Sato, M. Yano, M. Furuichi, D. Shiomi, T. Takui, K. Abe, K. Itoh, A. Higuchi, K. Katsuma, and Y. Shirota, *J. Am. Chem. Soc*., **119**, 6607 (1997).

14. D. Craig, *J. Am. Chem. Soc*., **57**, 195 (1935).

15. H. Wieland, *Ber. Dtsch. Chem. Ges*., **41**, 3493 (1908).

16. R. I. Walter, *U. S. Dept. Com., Office Tech. Serv., PB Rept*., **154**, **498**, 63 (1960); *Chem. Abstr*., **59**, 416d (1963).

17. H. Wieland and E. Wecker, *Ber. Dtsch. Chem. Ges*., **43**, 705 (1910).

18. S. J. Branch and B. Jones, *J. Chem. Soc*., **1957**, 3301.

19. D. F. Evans, *J. Chem. Soc*., **1959**, 2003.

20. D. H. Live and S. I. Chan, *Anal. Chem*., **42**, 791 (1970).

21. S. K. Sur, *J. Magn. Reson*., **82**, 169 (1989).

22. K. R. Stickley, T. D. Selby, and S. C. Blackstock, *J. Org. Chem*., **62**, 448 (1997).

23. J. P. Wolfe, S. Wagaw, J.-F. Marcoux, and S. L. Buchwald, *Acc. Chem. Res*., **31**, 805

(1998).

24. J. F. Hartwig, *Angew. Chem. Int. Ed. Engl.*, **37**, 2046 (1998).

25. F. D. King and D. R. M. Walton, *J. Chem. Soc., Chem. Commun.*, **1974**, 256.

26. P. Strohriegl, G. Jesberger, J. Heinze, and T. Moll, *Makromol. Chem.*, **193**, 909 (1992).

27. A. J. Bard and L. R. Faulker, "Electrochemical Methods," Wiley, New York, 1980.

28. F. A. Neugebauer, S. Bamberger, and W. R. Groh, *Chem. Ber.*, **108**, 2406 (1975).

29. W. Schmidt and E. Steckhan, *Chem. Ber.*, **113**, 577 (1980).

30. $\mu_{\text{eff}}/\mu_{\text{B}} = [6g^2T(1 - x_1)(T - \theta)^{-1}\{3 + \exp(-2J/kT)\}^{-1}+3g^2Tx_1\{2(T - \theta)\}^{-1}]^{1/2}$; B. Bleaney and E. R. Davidson, *J. Am. Chem. Soc.*, **99**, 4587 (1977).

Chapter 6

Synthesis and Magnetic Property of Two-Dimensionally Extended Aromatic Poly(aminium cationic radical)s

6.1   Introduction

In the previous chapter it was demonstrated that the bis(aminium cationic radical)s could realize both the efficient spin-exchange interaction between radicals and the stability of the biradical when they composed of a reasonable stilbene framework. This means that aminium cationic radicals are certainly attractive spin sources to extend them to tractable high-spin polyradicals even at room temperature.   Since Torrance et al. reported the specific preparation of poly(1,3,5-triaminobenzene) and its ferromagnetic behavior up to 400ºC in 1987[1], much effort to synthesize diarylamine and triarylamine macromolecules with a well-defined non-Kekulé and nondisjoint structure has been made.   Tanaka et al. synthesized poly(*m*-aniline) and its derivatives using the copper Ullmann reaction.[2]   However, Ullmann chemistry generally requires drastic conditions such as high temperature and a long reaction time to give the desired product in modest yield.   The recent development of palladium-catalyzed amination chemistry made it possible to synthesize complicated aromatic polyamines under mild conditions in high yield.   Hartwig et al. reported the synthesis of high molecular weight triarylamine macromolecules and dendrimers using a multistep growth strategy and the triplet character of the corresponding polyradicals.[3-5]   Linear and hyperbranched poly(*m*-aniline)s with little structural defects were likewise synthesized via one-pot polycondensations by other groups.[6,7]

p-Phenylenediamine-based cationic radical is also known as one of the aminium cationic radicals, which is more stable than triarylaminium cationic radicals.   A series of oligoradicals and the linear polyradicals linked with an adequate ferromagnetic coupler have been synthesized to evaluate the radicals as a spin source in high-spin molecules.[3,8-15]   However, there has been no report, to our knowledge, on a two-dimensionally extended polyradical composed of these aminium cationic radicals, except for the Bushby's report[16-18].   During the course of polyradical investigations, the two-dimensional extension of π-conjugation in a non-Kekulé and nondisjoint fashion has brought about an increase in the spin quantum number (*S*).   The most successful example is the calix[4]arene-based network polyradical, which showed an exceedingly high *S* value of >5000.[19]   Poly(4-phenoxyl-1,2-phenylenevinylene) was planarily extended and exhibited a relatively high *S* value of 5.[20]   These macromolecules were prepared by the polycondensation of two multi-functionalized monomers, which is

advantageous over the self-condensation of a monomer bearing two kinds of functional groups, because the molecular weight or the degree of polymerization and the terminal structures of the resulting macromolecule can be easily controlled by the feed ratio of the two monomers.   Moreover, arylamine macromolecules extended in two- or three-dimensions can also possess a new redox feature applicable to molecular-based information storage[21-23], and most importantly such macromolecules form the single molecule with a nanometer-sized cylindrical or spherical shape, which will be detected using a conventional scanning probe microscopy.

In   this   chapter,   we   noted   that   the   tris(cationic   radical)s   of   1,3,5-tris(dianisylamino)benzene **1**   and   *N,N',N''*-tris[4-(diphenylamino)phenyl]-*N,N',N''*-triphenyl-1,3,5-benzenetriamine **2** have been investigated in detail to be a quartet ground state molecule[24-28], that is, we selected 1,3,5-tris(anisylamino)benzene or *N,N',N''*-tris[4-(phenylamino)phenyl]-*N,N',N''*-triphenyl-1,3,5-benzenetriamine   as   a quartet radical core and extended it to a series of two-dimensional network macromolecules by the palladium-catalyzed polycondensation with an aryl di- or tri-halide.   The electrochemical and magnetic properties of the corresponding polyradicals and their molecular images are also discussed.

1   **2**
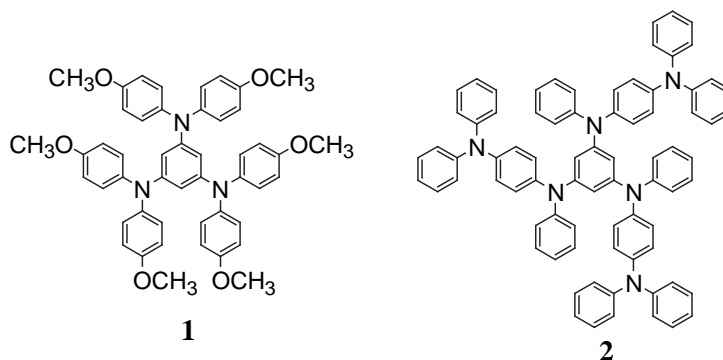
6.2   Experimental section

6.2.1 Materials

1,3,5-Tris(anisylamino)benzene   **4**   and   *N,N'*-bis(4-methoxyphenyl)-1,4-phenylenediamine **6** were prepared according to the literature.[29,15]   The other reagents were used as received.   Solvents were purified in the usual manners.

71

6.2.2 Synthetic procedure

N,N'-Bis(3-bromophenyl)-N,N'-diphenyl-1,4-phenylenediamine 7. N,N'-Diphenyl-1,4-phenylenediamine (1.0 g, 3.8 mmol) and 1,3-dibromobenzene (9.1 g, 38 mmol) were dissolved in 38 ml of toluene. Sodium *t*-butoxide (1.1 g, 12 mmol), palladium(II) acetate (35 mg, 0.16 mmol), and 1,1'-bis(diphenylphosphino)ferrocene (0.17 g, 0.31 mmol) were added to the solution, and the reaction mixture was stirred at 110°C for 24 h under nitrogen. After cooling to room temperature, the resulting solution was treated with a saturated ammonium chloride solution (300 ml) and extracted with dichloromethane. After washing the organic phase with brine, the crude product was purified by flash chromatography on silica gel (hexane/ethylacetate = 20/1) to yield 1.2 g of **7** as a white solid. Yield 53%; ^{1}H NMR (C_6D_6, 500 MHz) δ = 6.66 (t, 2H, *J* = 8 Hz, ArH), 6.80 (s, 4H, *p*-Ph), 6.80-7.01 (m, 14H, ArH), 7.36 (t, 2H, *J* = 2 Hz, ArH); ^{13}C NMR (C_6D_6, 125 MHz) δ = 121.72, 123.34, 123.82, 124.97, 125.26, 125.87, 126.00, 129.74, 130.71, 143.00, 147.39, 149.71; MS *m/z* 568, 570, 572 (M$^+$-2, M$^+$, M$^+$+2). Found: C, 64.0; H, 3.9; N, 4.6%. Calcd for $C_{30}H_{22}Br_2N_2$: C, 63.2; H, 3.9; N, 4.9%.

N,N'-Bis(3-bromophenyl)-N,N'-bis(4-methoxyphenyl)-1,4-phenylenediamine 8. A toluene solution (12 ml) of N,N'-bis(4-methoxyphenyl)-1,4-phenylenediamine (0.37 g, 1.2 mmol) and 1,3-dibromobenzene (2.8 g, 12 mmol) was reacted at 110°C for 37 h in the presence of sodium *t*-butoxide (0.34 g, 3.5 mmol), palladium(II) acetate (11 mg, 0.049 mmol), and 1,1'-bis(diphenylphosphino)ferrocene (52 mg, 0.093 mmol). Yield 66%; mp 156°C; IR (KBr pellet): 1242, 1036 cm^{-1} (ν_{C-O-C}); ^{1}H NMR (C_6D_6, 500 MHz) δ = 3.25 (s, 6H, -OCH$_3$), 6.63 (dd, 4H, *J* = 3, 9 Hz, ArH), 6.69 (t, 2H, *J* = 8 Hz, ArH), 6.87 (dd, 2H, *J* = 2, 8 Hz, ArH), 6.89 (s, 4H, *p*-Ph), 6.91-6.96 (m, 6H, ArH), 7.39 (t, 2H, *J* = 2 Hz ArH); ^{13}C NMR (C_6D_6, 125 MHz) δ = 54.93, 115.38, 120.06, 123.43, 124.20, 124.37, 125.26, 127.96, 130.65, 140.12, 143.00, 150.32, 157.30; MS *m/z* 628, 630, 632 (M$^+$-2, M$^+$, M$^+$+2). Found: C, 61.8; H, 3.8; N, 4.0%. Calcd for $C_{32}H_{26}Br_2N_2O_2$: C, 61.0; H, 4.2; N, 4.4%.

N,N',N''-Tris[4-(phenylamino)phenyl]-N,N',N''-triphenyl-1,3,5-benzenetriamine 9. N,N'-Diphenyl-1,4-phenylenediamine (5.5 g, 21 mmol) and 1,3,5-tribromobenzene (0.74 g, 2.3 mmol) were dissolved in 23 ml of toluene. Sodium *t*-butoxide (1.0 g, 11 mmol), palladium(II) acetate (16 mg, 0.073 mmol), and tri-*t*-butylphospine (57 mg, 0.28 mmol) were added to the solution, and the reaction mixture

was stirred at 100°C for 22 h under nitrogen.   After cooling to room temperature, the resulting solution was quenched by adding aqueous ammonia (20 ml) and taken up in ether.   The organic phase was evaporated, and the crude product was washed with methanol (1000ml) and was purified by flash chromatography on silica gel (hexane/ethylacetate = 3/1) to yield 0.32 g of **9** as a milky-white solid.   Yield 16%; mp 88°C; IR (KBr pellet): 3393 (v_{N-H}), 1289 cm^{-1} (v_{C-N}); ^{1}H NMR (CDCl$_3$, 500 MHz) δ = 4.92 (br s, 3H, NH), 6.67-7.20 (m, 45H, ArH); ^{13}C NMR (CDCl$_3$, 125 MHz) δ = 111.86, 117.31, 119.95, 120.61, 122.33, 123.62, 127.05, 129.31, 129.52, 139.17, 141.28, 144.11, 148.11, 149.97; MS *m/z* 853 (M$^+$).   Found: C, 84.9; H, 6.1; N, 9.0%.   Calcd for C$_{60}$H$_{48}$N$_6$: C, 84.5; H, 5.7; N, 9.8%.

Polymerization.   A general procedure was as follows: In a 10 ml ampule tube, the aromatic di- or tri-*sec*-amine as a functional group, the aryl di- or trihalide, sodium *t*-butoxide (4.5 equiv. to *sec*-amine group), Pd catalyst (4 mol% Pd for *sec*-amine group), and phosphine ligand (12 mol% P for *sec*-amine group) were added, and toluene was then added to it in the desired concentration.   The tube was attached to a vacuum line, sealed off, and then heated to 100°C in an oil bath.   After cooling to room temperature, the resulting crude product was treated with 5 ml of aqueous ammonia and extracted with 50 ml of dichloromethane.   In the course of this workup, an insoluble fraction was filtered off and washed with methanol and water.   The residual organic phase was concentrated and precipitated into 50 ml of methanol to give a yellow macromolecule. Reprecipitation from dichloromethane or tetrahydrofuran into methanol was repeated until the monomer was removed.

1,3,5-Tribromobenzene **3** (0.227 g, 0.720 mmol) and 1,3,5-tris(anisylamino)benzene **4** (0.318 g, 0.720 mmol) in 1 ml of toluene were reacted for 10 min in the presence of sodium *t*-butoxide (0.311 g, 3.24 mmol), tris(dibenzylideneacetone)dipalladium (13.1 mg, 1.43×10^{-5} mol), and tri-*t*-butylphosphine (17.4 mg, 8.59×10^{-5} mol) to give a yellow gel (Table 6.1, run 3).   CP-MAS ^{13}C-NMR (100 MHz) δ = 55.1, 105.6, 111.8, 114.8, 126.5, 128.9, 136.0, 138.1, 140.3, 149.3, 156.3.

1,3,5-Tribromobenzene **3** (0.377 g, 1.20 mmol) and *N,N'*-diphenyl-1,4-phenylenediamine **5** (0.234 g, 0.899 mmol) in 3 ml of toluene were reacted for 24 h in the presence of sodium *t*-butoxide (0.261 g, 2.72 mmol), tris(dibenzylideneacetone)dipalladium (11.1 mg, 1.22×10^{-5} mol), and tri-*t*-

butylphosphine (14.6 mg, 7.22×10^{-5} mol) to give the dichloromethane soluble macromolecule **10** (9.8 mg) and its gel (0.389 g). ^{1}H NMR of the soluble fraction (C_6D_6, 600 MHz) δ = 6.82-7.89 (m, ArH); ^{13}C NMR of the soluble fraction (C_6D_6, 150 MHz) δ = 122.64 (overlapped), 123.34 (overlapped), 123.98 (overlapped), 125.09, 125.37, 126.09, 126.85, 143.12, 143.39, 146.78, 147.21, 147.82, 149.62, 150.11, 150.52; CP-MAS ^{13}C-NMR of the gel (100 MHz) δ = 124.9, 129.6, 143.3, 146.9; UV/vis λ_{max} = 319 nm; fluorescence Em_{max} = 412 nm.

1,3,5-Tribromobenzene **3** (0.377 g, 1.20 mmol) and *N*,*N'*-bis(4-methoxyphenyl)-1,4-phenylenediamine **6** (0.288 g, 0.899 mmol) were reacted in a similar manner to give the dichloromethane soluble macromolecule **11** (24.9 mg) and its gel (0.240 g). IR (KBr pellet): 1240, 1085 cm^{-1} (ν_{C-O-C}); ^{1}H NMR of the soluble fraction (C_6D_6, 500 MHz) δ = 3.22-3.33 (br m, -OCH$_3$), 6.34-7.25 (m, ArH); ^{13}C NMR of the soluble fraction (C_6D_6, 125 MHz) δ = 54.91, 114.96, 115.30 126.37, 126.74, 127.41 (two peaks overlapped), 133.04, 140.37, 141.04 (overlapped), 143.43 (overlapped), 150.53 (overlapped), 156.47 (overlapped); CP-MAS ^{13}C-NMR of the gel (100 MHz) δ = 56.3, 112.1, 114.9, 125.0, 129.3, 135.8, 141.2, 143.9, 149.9, 156.0; UV/vis λ_{max} = 317 nm; fluorescence Em_{max} = 429 nm.

1,3,5-Tris(anisylamino)benzene **4** (88.5 mg, 0.200 mmol) and *N*,*N'*-bis(3-bromophenyl)-*N*,*N'*-diphenyl-1,4-phenylenediamine **7** (0.339 g, 0.594 mmol) in 1 ml of toluene were reacted for 24 h in the presence of sodium *t*-butoxide (87.3 mg, 0.908 mmol), tris(dibenzylideneacetone)dipalladium (3.7 mg, 4.1×10^{-6} mol), and tri-*t*-butylphosphine (4.9 mg, 2.4×10^{-5} mol) to give the macromolecule **12** (56.0 mg). IR (KBr pellet): 1242, 1073 cm^{-1} (ν_{C-O-C}); ^{1}H NMR (C_6D_6, 500 MHz) δ = 3.20-3.36 (br m, 9H, -OCH$_3$), 6.55-7.35 (m, 53H, ArH); UV/vis λ_{max} = 310 nm; fluorescence Em_{max} = 423 nm.

1,3,5-Tris(anisylamino)benzene **4** (88.7 mg, 0.201 mmol) and *N*,*N'*-bis(3-bromophenyl)-*N*,*N'*-bis(4-methoxyphenyl)-1,4-phenylenediamine **8** (0.375 g, 0.595 mmol) were reacted in a similar manner to give the macromolecule **13** (0.256 g). IR (KBr pellet): 1241, 1037 cm^{-1} (ν_{C-O-C}); ^{1}H NMR (C_6D_6, 500 MHz) δ = 3.21-3.31 (br m, 21H, -OCH$_3$), 6.57-7.36 (m, 55H, ArH); UV/vis λ_{max} = 310 nm; fluorescence Em_{max} = 419 nm.

N,*N'*,*N''*-Tris[4-(phenylamino)phenyl]-*N*,*N'*,*N''*-triphenyl-1,3,5-benzenetriamine **9** (0.149 g, 0.175 mmol) and *N*,*N'*-bis(3-bromophenyl)-*N*,*N'*-diphenyl-1,4-

phenylenediamine **7** (0.298 g, 0.523 mmol) in 0.88 ml of toluene were reacted for 24 h in the presence of sodium *t*-butoxide (76.9 mg, 0.800 mmol), tris(dibenzylideneacetone)dipalladium (3.4 mg, 3.7×10^{-6} mol), and tri-*t*-butylphosphine (4.3 mg, 2.1×10^{-5} mol) to give the macromolecule **14** (0.156 g). ^{1}H NMR (C_6D_6, 500 MHz) δ = 6.67-7.38 (m, ArH); ^{13}C NMR (C_6D_6, 125 MHz) δ = 112.17, 117.74, 117.92, 117.97, 118.88, 119.13, 121.53, 122.91, 122.98, 123.17, 123.40, 123.66, 124.30 (overlapped), 124.59, 124.78, 125.08, 125.58, 125.75, 125.96, 126.05, 126.22, 126.30, 129.43, 129.53, 129.78, 130.36, 130.78, 142.27, 142.54 (w), 142.91, 142.98, 143.09 (w), 143.16, 143.26, 143.51 (w), 143.93, 147.60, 147.72, 147.88, 148.01, 148.14 (w), 148.31 (w), 148.41 (w), 149.06, 149.15, 149.19, 149.36 (w), 149.47 (w), 149.78, 149.94, 150.03 (w); UV/vis λ_{max} = 316 nm; fluorescence Em_{max} = 410 nm.

N,*N*',*N*''-Tris[4-(phenylamino)phenyl]-*N*,*N*',*N*''-triphenyl-1,3,5-benzenetriamine **9** (0.150 g, 0.176 mmol) and *N*,*N*'-bis(3-bromophenyl)-*N*,*N*'-bis(4-methoxyphenyl)-1,4-phenylenediamine **8** (0.330 g, 0.524 mmol) were reacted in a similar manner to give the macromolecule **15** (82.4 mg). IR (KBr pellet): 1241, 1036 cm^{-1} (ν_{C-O-C}); ^{1}H NMR (C_6D_6, 500 MHz) δ = 3.28, 3.29, 3.31 (s, 12H, -OCH$_3$), 6.64-7.37 (m, 85H, ArH); UV/vis λ_{max} = 317 nm; fluorescence Em_{max} = 414 nm.

Oxidation. A dichloromethane solution of NOPF$_6$ (22.9 mM) solubilized with a minimum amount of 18-crown-6 was added to a dichloromethane/trifluoroacetic acid/trifluoroacetic anhydride solution of the macromolecule (2.8 μmol/radical unit) under a nitrogen atmosphere at room temperature. The solution rapidly turned dark green but it was stirred for 5–10 minutes to complete the reaction. A small excess of the oxidant was used, of which the quantity (ca. 1.2 equiv.) was determined by the saturation of the ESR intensity. The final concentration was adjusted to 10 mM/radical unit. A small amount of trifluoroacetic acid (5–9 vol%) was added to stabilize the generated polyradicals, and a smaller amount of trifluoroacetic anhydride (0.25–0.45 vol%) was used for dehydration.

6.2.3 Measurements

For the ESR, IR, NMR, mass, and electrochemical and magnetic measurements, the details were described in Chapter 5. In the electrochemical measurements, a glassy carbon electrode was used as a working electrode when trifluoroacetic acid was added to the electrolyte solution. For the magnetic measurement using a SQUID
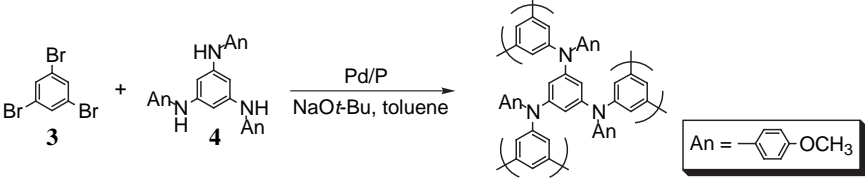
magnetometer, the polyradical solution was sealed off in a quartz tube immediately after oxidation and subjected to the measurement. The paramagnetic ^{1}H NMR spectrum of the polyradical was taken in CD_2Cl_2 containing 9 vol% trifluoroacetic acid, 0.45 vol% trifluoroacetic anhydride, and 1 vol% cyclohexane at 300 K. The chemical shift difference of the cyclohexane resonance was monitored to calculate the mass susceptibility. The ^{13}C solid state NMR spectrum was recorded on a JEOL CMX-400. The molecular weight of the macromolecules was estimated by GPC (polystyrene gel column, eluent THF, polystyrene calibration). The MALDI-TOF mass spectrum was measured with a Shimadzu/Karatos AXIMA-CFR using dithranol as a matrix. For **14**, a lower molecular weight fraction of the filtrate in the last reprecipitation operation was used to make the analysis easy.

The UV/vis spectra during the electrolytic oxidation of the macromolecules were recorded on a JASCO V-550 spectrometer at room temperature. In a special cell with 2 mm light-path length were placed an optically transparent thin-layer platinum working electrode, a commercial Ag/AgCl electrode as the reference, and a platinum wire as the counter. The dichloromethane solution of the macromolecule (8.3×10^{-5} M/radical unit) containing 0.1 M tetrabutylammonium tetrafluoroborate was put in the cell and the solution was kept under a nitrogen atomosphere. A potentiogalvanostat (Nikko Keisoku NPGS-301) was used for potential application.

The details of the AFM measurement have been shown in Chapter 2. A drop of dilute dichloromethane solution of the macromolecule (0.2 mg l^{-1}) was transferred onto mica surface, and the solvent was carefully blotted off by air-drying. Around 500 samples were collected in each macromolecule for the statistical analysis.

6.3 Polycondensation of amine monomers and bromobenzene derivatives

First, the appropriate combination of a catalyst and a ligand in the polymerization was explored through the polycondensation between 1,3,5-tribromobenzene **3** and 1,3,5-tris(anisylamino)benzene **4** (Table 6.1). The polymerization for the feed ratio of [*sec*-amine]/[bromide] = 1 with $Pd_2(dba)_3$ as the catalyst and BINAP ((S)-(−)-2,2'-bis(diphenylphosphino)-1,1'-binaphthyl) as the bulky ligand gave only an oligomer even

Table 6.1. Polycondensation results of 1,3,5-tribromobenzene **3** and
1,3,5-tris(anisylamino)benzene **4** using various catalysts[a]

Run	catalyst	ligand	time (h)	$M_w{}^b$	$M_w/M_n{}^b$
1	Pd$_2$(dba)$_3$	BINAP	72	1200	1.1
2	Pd$_2$(dba)$_3$	P(*o*-tolyl)$_3$	6	gel	-
3	Pd$_2$(dba)$_3$	P(*t*-Bu)$_3$	0.17	gel	-
4	Pd(OAc)$_2$	P(*t*-Bu)$_3$	1	gel	-

[a] Polymerizations were carried out in the presence of 4.5 eq NaO*t*Bu for **4**, 4 mol% Pd
for **4**, and phosphine ligand ([Pd]/[P] = 1/3) in toluene at 100°C; [**3**] = [**4**] = 0.72 M.
[b] Number- and weight-average molecular weight measured by GPC.

after 3 days.　　However, the use of P(*o*-tolyl)$_3$ and P(*t*-Bu)$_3$ in place of BINAP under the
same conditions afforded a yellow gel in 6 hours and 10 minutes, respectively.
Judging from the superiority of Pd$_2$(dba)$_3$ to Pd(OAc)$_2$, the combination of Pd$_2$(dba)$_3$ and
P(*t*-Bu)$_3$ was proven to be the most effective catalyst system in the present study.

　　　The attempted integration of *p*-phenylenediamine-based aminium cationic
radicals was tried into the macromolecule.　　It is well known that the stability of
aminium cationic radicals is improved by the lack of *sec*-amine groups, that is,
N,N,N',N'-tetraaryl-*p*-phenylenediamine structures are desired at the terminal or
peripheral positions of the macromolecule.　　The bifunctionalized monomer and the
trifunctionalized monomer were reacted in the feed ratio of [*sec*-amine]/[bromide] = 1/2
using the combination of Pd$_2$(dba)$_3$ and P(*t*-Bu)$_3$ in toluene at 100°C for 24 h (Scheme
6.1 and Table 6.2).　　According to Flory's theorem, the polycondensation of a
trifunctionalized monomer (3A) and bifunctionalized monomer (2B) with the feed ratio
[A]/[B] = 1/2 provides a macromolecule with an infinite molecular weight and terminal
B groups.[30]　　The reaction of *N,N'*-diaryl-*p*-phenylenediamine and 1,3,5-
tribromobenzene gave a yellow gel and trace amounts of a soluble fraction with a low
molecular weight, while that of the trifunctionalized amine monomer **4** or **9** and the aryl
dibromide **7** or **8** yielded solvent-soluble macromolecules with a high molecular weight.
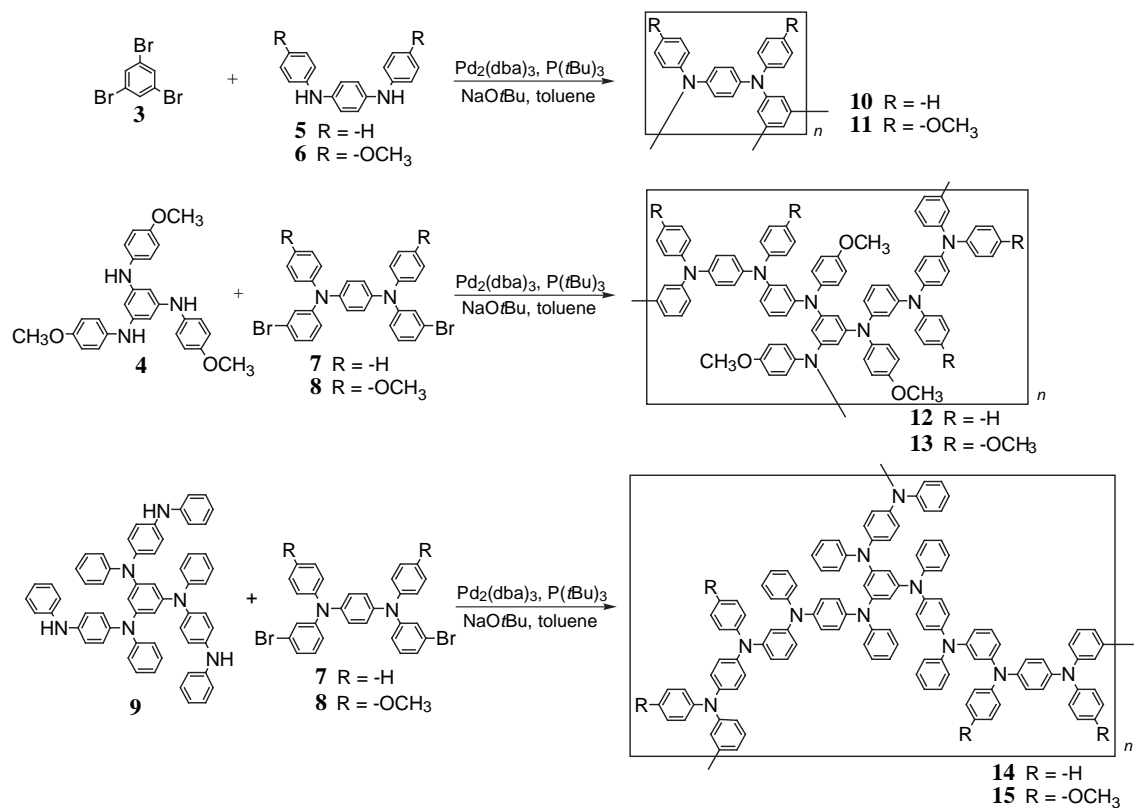
Scheme 6.1.

Table 6.2. Polycondensation results[a]

3A monomer	2B monomer	macromolecule	yield (%)	$M_n (10^3)^b$	$M_w/M_n{}^b$
3	**5**	**10**	2.6 (100)[c]	2.9	3.3
3	**6**	**11**	5.9 (84)[c]	3.0	2.7
4	**7**	**12**	21	7.7	2.6
4	**8**	**13**	75	5.0	3.0
9	**7**	**14**	51	16	4.9
9	**8**	**15**	25	6.5	1.5

[a] Polymerizations were carried out in toluene with 1.5 eq NaOtBu, 0.67% Pd$_2$(dba)$_3$, 4.0% P(t-Bu)$_3$ at 100°C for 24 h; [*sec*-amine] = 0.60 M. [b] Number- and weight-average molecular weights were measured by GPC. [c] Total yield with gel in it.

Use of the dibromide compound **7** brought about the higher molecular weight than that from the electron-donating dibromide **8**.   These results suggest that monomer geometry strongly influences the gelation or the amount of cyclization in the resulting macromolecule and that the reaction of the aryl bromide substituted with an electron donating group and aryl amine is difficult to complete in high yield.

The IR and ^{1}H NMR spectra of these soluble macromolecules indicated the disappearance of the secondary amines and all the terminal bromide groups.   For the ^{13}C NMR spectrum of **14**, very weak 9 absorptions ascribed to the terminal triarylamine moieties appeared besides the 15 well-defined ones in the region of the quaternary carbon adjacent to a nitrogen atom, which indicated the possibility of two conformations in the repeat unit (Fig. 6.1).   The MALDI-TOF mass spectrum of **14** provided further evidence of its structure (Fig. 6.2).   All signals corresponded to the proton adduct of the structure with all bromide terminal groups but not secondary amines, and some of them observed at m/z 2932.5, 3502.9, 4683.6, 5253.9, 6433.9, and
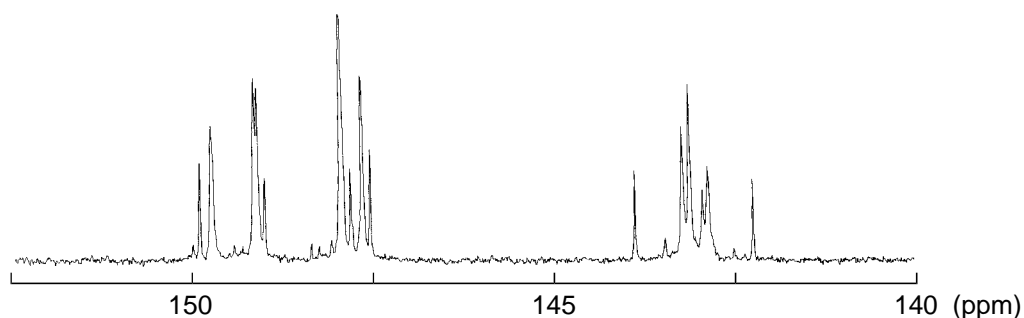
Fig. 6.1. ^{13}C-NMR spectrum of **14**, in the region of the quaternary carbon adjacent to a nitrogen atom.   Marked peaks correspond to the terminal triarylamine moieties.
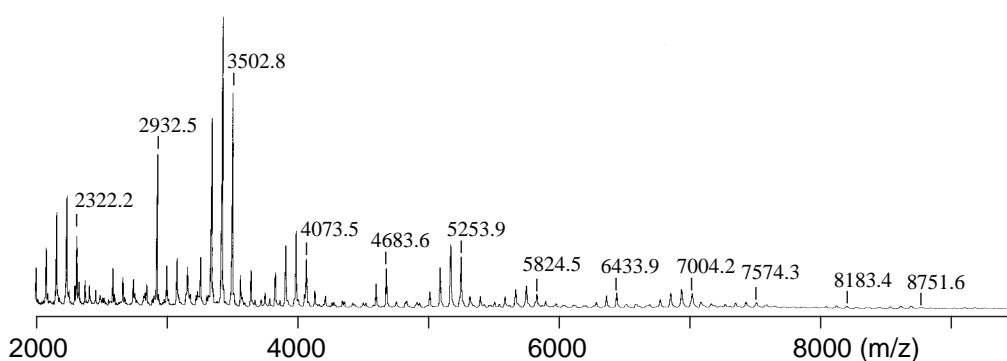

Fig. 6.2.   MALDI-TOF mass spectrum for the low molecular weight fraction of **14**.

79

7004.2 were consistent with the formation of cyclic products, which would lead to the restricted movement of the polymer chain. This result supported the idea of two conformations in the repeat unit, i.e., labile and limited ones, for the macromolecule.

6.4   Electrochemical behavior of poly(arylamine)s

The redox behaviors of the macromolecules and stability of the corresponding poly(aminium cationic radical)s were investigated before the chemical oxidation. These results are summarized in Table 6.3.   The potentials (vs. Ag/AgCl) $E^{o'}(1)$–$E^{o'}(3)$ correspond to a one-electron removal from the neutral amine to aminium cationic radical, and $E^{o'}(4)$ and $E^{o'}(5)$ represent the subsequent one from the cationic radical to the bication.

Cyclic voltammetry of the macromolecules **10**, **11**, **14**, and **15** in dichloromethane showed completely reversible oxidation and reduction waves at room temperature (Fig.
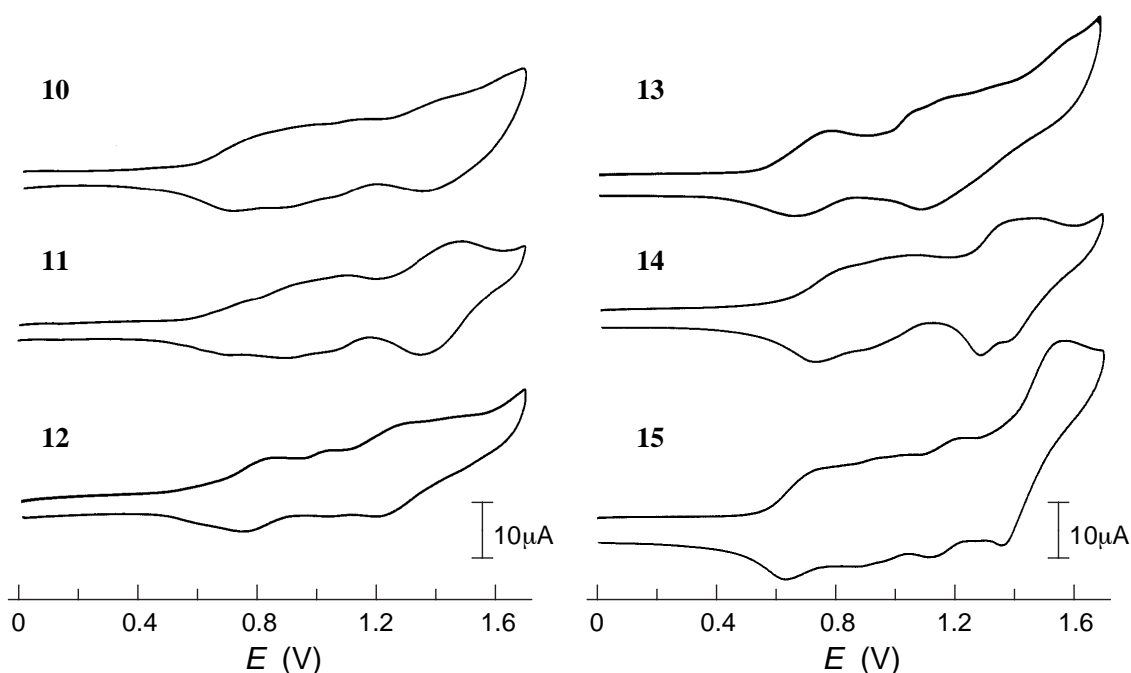
Fig. 6.3.   Cyclic voltammograms of the arylamine macromolecules (1 mM/radical unit) in CH$_2$Cl$_2$ with 0.1 M (C$_4$H$_9$)$_4$NBF$_4$ at room temprerature, at 100 mV s^{-1} scan rate.   Potential vs. Ag/AgCl.

Table 6.3. Redox potentials of the arylamine macromolecules[a]

macromolecule	$E^{o'}(1)$	$E^{o'}(2)$	$E^{o'}(3)$	$E^{o'}(4)$	$E^{o'}(5)$
10	0.75	0.91	1.09	1.38	
11	0.71	0.91	1.08	1.41	
12	0.79	1.03[b]		1.24	1.51[b]
13	0.72	1.00[b]		1.13	1.35[b]
14	0.78	0.93	1.03	1.33	1.42
15	0.69	0.92	1.01	1.16	1.45

[a] V vs Ag/AgCl, in CH_2Cl_2 with 0.1M $(C_4H_9)_4NBF_4$. Unresolved peaks are clarified by differential pulse voltammetry. $E^{o'}(1)$ $E^{o'}(3)$ correspond to one-electron removal from neutral amine to cationic radical, and $E^{o'}(4)$ and $E^{o'}(5)$ represent the subsequent one from the cationic radical to bication. [b] Irreversible waves.

6.3).   The generated cationic radicals were stable enough even in the macromolecular framework to be further oxidized one electron from each *p*-phenylenediamine site, as well as the corresponding oligomer **2**[28].   However, repeated sweeps up to 1.7 V resulted in the increasing current especially in the redox region from the cationic radical to bication, which indicated the adsorption of the macromolecule or poly(bication) on the electrode.   Differential pulse voltammetry of the macromolecules displayed unequivocal waves step by step.   For **14**, the potentials at 0.78, 0.93, and 1.03 V are ascribed to the redox from the amine to aminium cationic radical and their potential splitting reflects the strong interaction between adjacent radicals.   On the other hand, the cyclic voltammetry of **12** and **13** exhibited irreversible waves at the potentials $E^{o'}(2)$ and $E^{o'}(5)$, which are attributed to the 1,3,5-benzenetriamine moiety by considering the previous report on **1**[24] (Fig. 6.3).   This means that the other potentials, $E^{o'}(1)$ and $E^{o'}(4)$, are caused by the redox of the *p*-phenylenediamine moiety interposed between two *m*-phenylene couplers.

The exact assignment of the potentials for **14** and **15** was ascertained by another method.   Trifluoroacetic acid (TFA) is known to form a proton adduct with certain arylamines.   For example, it is reported that *N*,*N'*,*N''*-triphenyl-1,3,5-benzenetriamine and its derivatives undergo protonation at the central aromatic ring.[28,31,32]   For **14** or **15**,

the addition of 1 vol% TFA to the electrolyte solution resulted in the anodic shift of $E^{o'}(2)$ and $E^{o'}(3)$, while $E^{o'}(1)$ remained (Fig. 6.4(b)). The 1,3,5-benzenetriamine ring is supposed to be easily protonated over the 1,3-benzenediamine moiety because of many tautomeric intermediates and/or its high nucleophilicity. The redox potential adjacent to the protonated moiety would anodically shift due to an electrostatic repulsion. The addition of 5 vol% TFA brought about the anodic shift of $E^{o'}(1)$ and overall oxidation potentials, which suggests the protonation of 1,3-benzenediamine (Fig. 6.4(c)). Thus the first potential $E^{o'}(1)$ results from the *p*-phenylenediamine between two *m*-phenylene couplers and the second and third potentials, $E^{o'}(2)$ and $E^{o'}(3)$, are attributable to the stepwise redox of the *p*-phenylenediamines connected with 1,3,5-benzenetriamine. This result was supported by the knowledge that the overall potentials of **10** and **11**, which have 1,3,5-benzenetriyl couplers but not *m*-phenylene, anodically shifted with only 1 vol% TFA.
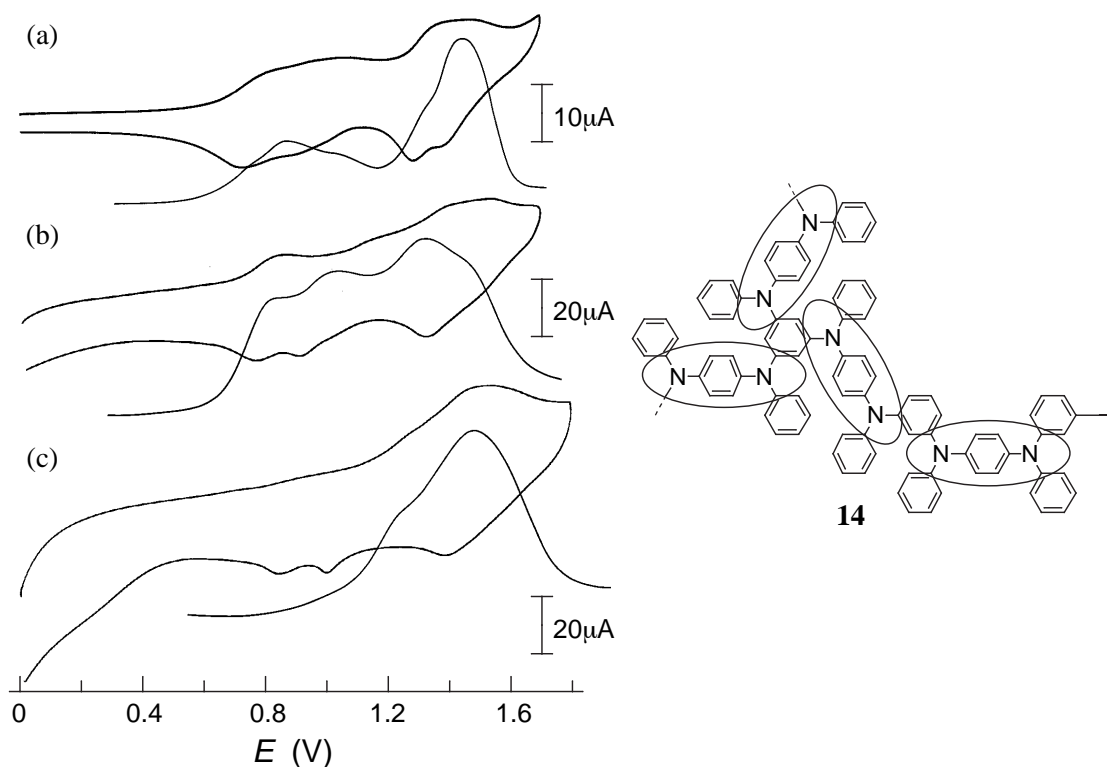
Fig. 6.4. Cyclic voltammograms and differential pulse voltammograms of **14** (1 mM/radical unit) in CH_2Cl_2 with 0.1 M $(C_4H_9)_4NBF_4$ at room temprerature, at 100 mV s^{-1} scan rate, (a) without TFA, (b) with 1 vol% TFA, and (c) with 5 vol% TFA. Potential vs. Ag/AgCl.

The UV/vis spectra during the electrolytic oxidation of the macromolecules **10**, **11**, **14**, and **15** were monitored. The application of 1.2 V to the dichloromethane solution of the macromolecules resulted in the gradual appearance of new absorptions at 401, 417, 412, and 431 nm for **10**, **11**, **14**, and **15**, respectively, and in the near IR region, which are ascribed to the aminium cationic radicals, and the concurrent decrease of the initial bands. The spectral change accompanies an isosbestic point, which indicates the generation of the corresponding poly(aminium cationic radical) without any side reaction under this condition. The difference in the absorption maxima could be explained by the electron-donating effect of the methoxy groups and π-coplanarity in the macromolecular framework. After saturating the growth of the absorptions, application of a higher potential, e.g., 1.5 V, to the electrolyte solution of the macromolecules **10**, **11**, and **14** provided the insoluble poly(bication)s on the electrode which lead to an overall decrease of their absorbance, that was consistent with the cyclic voltammetry results. In contrast, the spectrum for **15** under the same condition continued to change with an increase in the new absorption at 792 nm, still accompanying an isosbestic point (Fig. 6.5). The absorption was assignable to the bication derived from the *p*-phenylenediamine moiety between two *m*-phenylene couplers in **15**. The potential $E^{o'}(4)$ of **15** is low enough to be easily oxidized as compared to the other macromolecules, therefore, it should be necessary to carefully adjust the oxidation condition to achieve a higher spin concentration.
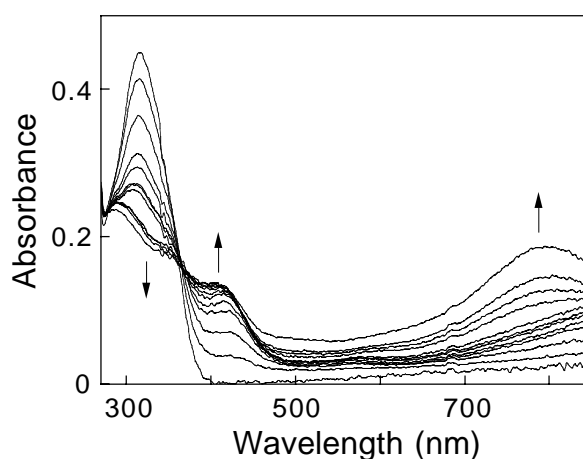

Fig. 6.5. UV/vis spectra during the electrolytic oxidation of **15** (8.3×10^{-5} M/radical unit) in CH_2Cl_2 with 0.1 M $(C_4H_9)_4NBF_4$.

6.5   Magnetic property of poly(aminium cationic radical)s

The chemical oxidation of **14** and **15** using $NOPF_6$ also gave the corresponding poly(aminium cationic radical)s.   The ESR spectra (10 mM/radical unit) at room temperature were composed of broad singlet lines at $g = 2.003$, which is characteristic of aminium cationic radicals.   The spectra still showed a single line without hyperfine splitting even at a low solution concentration (0.1 mM/radical unit) due to electron exchange between the unpaired electrons in the macromolecule.   The addition of a small amount of TFA to the dichloromethane solution dramatically improved the spin concentration and chemical stability of the polyradicals.   The oxidation of the macromolecules in dichloromethane often resulted in the production of a dark gel in a few minutes even if less than one equivalent of the oxidant was added, and the half-life of the polyradicals estimated by ESR at room temperature was not long (e.g., 3 h for the polyradical of **14**).   However, when the same reaction was carried out in the presence of 5 vol% TFA, the gelation never occurred and the half-life of the polyradical of **14** was prolonged to 1 week in solution under a nitrogen atmosphere.   This was probably because the position protonated by TFA was overlapped with the spin density distribution of the aminium cationic radical, which prevents the intramolecular or intermolecular dimerization of the radicals.

The ESR of the polyradicals in frozen media clearly showed a $\Delta M_s = \pm 2$ forbidden transition with a fine structure, which means the occurrence of multiplet states equal to or higher than a triplet (Fig. 6.6(a)).   The temperature dependence experiments of these signals were performed to obtain insight into the ground state of the polyradicals.   The signal plots versus the reciprocal of the absolute temperature displayed an upward deviation from Curie's law in the lower temperature region, indicating a ferromagnetic interaction between adjacent aminium cationic radicals and the multiplet ground state for the polyradicals (Fig. 6.6(b)).

The magnetization and static magnetic susceptibility of the polyradicals were measured using a SQUID magnetometer in order to evaluate the magnitude of the ferromagnetic interaction and the spin-alignment number in the macromolecule.   The magnetization normalized with saturated magnetization, M/M_s, plots of the polyradicals of **14** and **15** with a spin concentration of 0.66 and 0.75, respectively, were almost close to the theoretical Brillouin curve for $S = 10/2$ at low fields and lied on the curve for $S =$
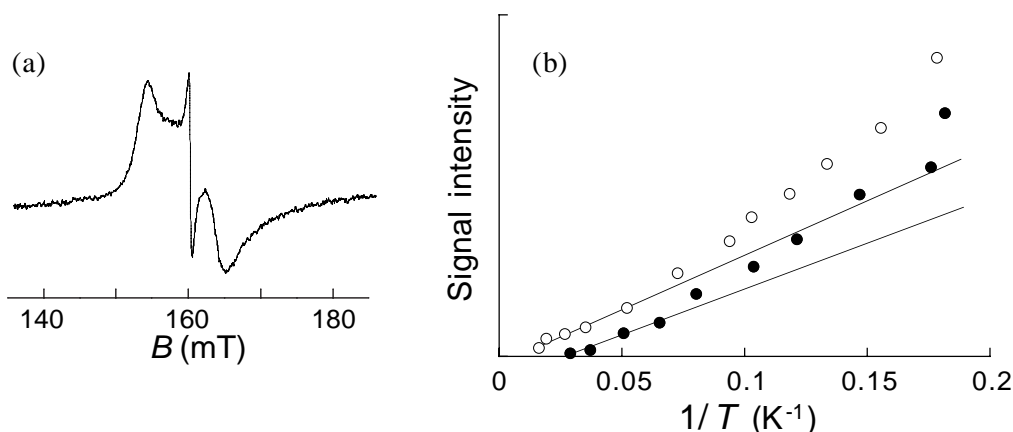
Fig. 6.6. (a) ESR $\Delta M_s = \pm 2$ spectrum for the polyradical of **15** at 5.6 K. (b) The temperature dependence of the $\Delta M_s = \pm 2$ signal intensity for the polyradical of **14** ( ) and **15** ( ).

7/2 at high fields (Figs. 6.7 and 6.8). The spin concentration was determined by the saturated magnetization of the weighed polyradical. The inset shows the product of unit molar magnetic susceptibility (χ_{mol}) and temperature (T) vs. T for these polyradicals. Both $\chi_{mol}T$ values were much higher than the theoretical value of 0.375 for $S = 1/2$ in the entire temperature range measured and increased below 100 K to reach 1.30 for $S = 8.4/2$ at 5 K. The decrease in the plots below 5 K was due to a weak intermolecular antiferromagneic interaction. This indicates a ferromagnetic coupling, on the average, between eight or nine unpaired electrons in the macromolecules at low temperature. However, the S value seems to be overestimated, taking into account the cross-conjugated structure of the polyradicals, the spin concentration, and the assignment of the redox potentials. Janssen et al. reported the specific behavior of the intervalence band during the oxidation of **2**, which presents the possibility that the tris(aminium cationic radical) of **2** is more stable than the monoradical of **2**. If this is also the case for the *N,N',N''*-tris[4-(diarylamino)phenyl]-*N,N',N''*-triphenyl-1,3,5-benzenetriamine moiety in the macromolecules, some local spin clusters will be formed in the polyradicals. In addition to this, the cyclic structure in the macromolecules would effectively act to compensate the radical defects with multiple pathways. These considerations will strongly support the observed S value for the polyradicals of **14** and **15**.
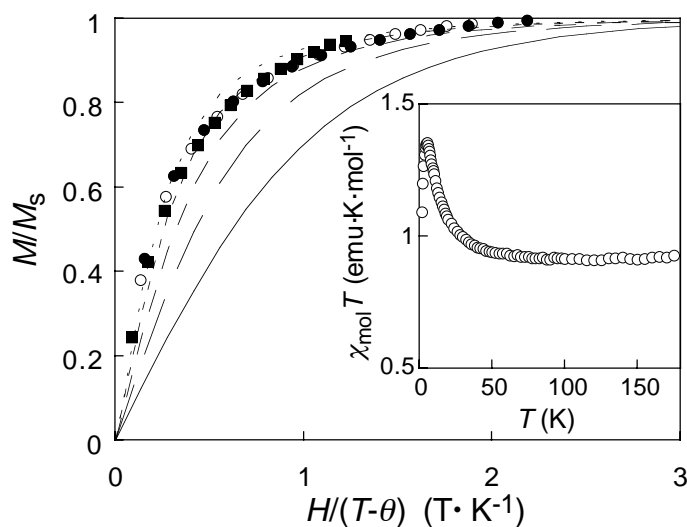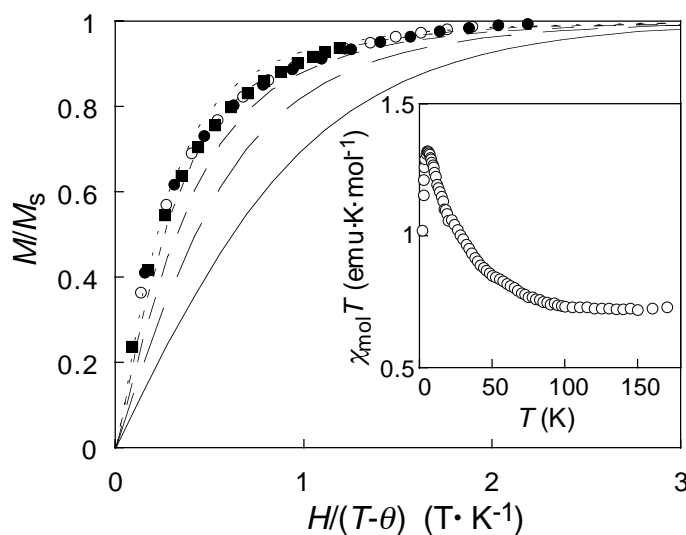
Fig. 6.7. Normalized plots of magnetization (M/M_s) vs. the ratio of magnetic field and temperature ($H/(T-\theta)$) for the polyradical of **14** with spin concentration of 0.66 in $CH_2Cl_2/CF_3COOH/(CF_3CO)_2O$ (91/8.5/0.5 vol%) at T = 2.5 ( ), 3 ( ), and 5 ( ) K and theoretical curves corresponding to the S = 2/2, 4/2, 6/2, 8/2, and 10/2 Brillouin functions. Inset: $\chi_{mol}T$ vs. T plots of the polyradical of **14**.

Fig. 6.8. Normalized plots of magnetization (M/M_s) vs. the ratio of magnetic field and temperature ($H/(T-\theta)$) for the polyradical of **15** with spin concentration of 0.75 in $CH_2Cl_2/CF_3COOH/(CF_3CO)_2O$ (91/8.5/0.5 vol%) at T = 2.5 ( ), 3 ( ), and 5 ( ) K and theoretical curves corresponding to the S = 2/2, 4/2, 6/2, 8/2, and 10/2 Brillouin functions. Inset: $\chi_{mol}T$ vs. T plots of the polyradical of **15**.

Atomic force microscopy (AFM) was used to study the difference in the molecular image between the macromolecules before and after oxidation. The molecular weight of **14** is sufficiently high ($M_n = 1.6×10^4$, $M_w = 7.7×10^4$) and suitable for this purpose. The dilute dichloromethane solution of **14** and the corresponding poly(aminium cationic radical) were transferred to a mica surface and subjected to AFM (Fig. 6.9). All images observed for the macromolecule and the polyradical were cylindrical. The horizontal and vertical distances of both samples were statistically analyzed. Multiple distributions emerged for **14**, some of which with a larger size being attributable to the aggregation. On the other hand, for the polyradical was observed only one distribution with the average horizontal distance of 17.4 nm and the average vertical distance of 0.83 nm, indicating that the aggregation was dispersed into single macromolecules by an electrostatic repulsion between the poly(aminium cationic radical)s. The average vertical distance observed for **14** with the single molecular size of 15–20 nm horizontal distance was 1.43 nm. The decrease in the vertical distance after oxidation suggests that the polyradical has a high coplanarity of π-conjugation, which would be essential for the intramolecular ferromagnetic interaction between radicals even at room temperature.
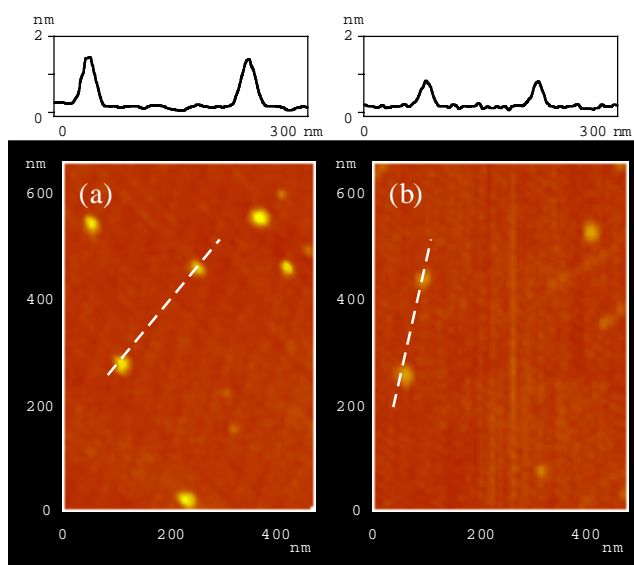

Fig. 6.9. AFM images of (a) the macromolecule **14** with a molecular weight of $M_n = 1.6×10^4$ ($M_w/M_n = 4.9$) and (b) the corresponding polyradical.

The solution magnetic susceptibility at 300 K was measured using the NMR Evans method to demonstrate the spin-alignment at room temperature. The $\chi_{mol}T$ value was 0.49 for the polyradical of **14**, which is higher than the theoretical value of 0.375 for S = 1/2 and almost coincides with the value of 0.5 for S = 2/2. This result is consistent with the molecular images detected by the AFM measurements. Thus, it was proved that high-spin species at least exist in the polyradical of **14** at room temperature.

References

1. J. B. Torrance, S. Oostra, and A. Nazzal, *Synth. Met*., **19**, 709 (1987).

2. A. Ito, K. Ota, K. Tanaka, T. Yamabe, and K. Yoshizawa, *Macromolecules*, **28**, 5618 (1995).

3. J. Louie and J. F. Hartwig, *J. Am. Chem. Soc*., **119**, 11695 (1997).

4. J. Louie and J. F. Hartwig, *Macromolecules*, **31**, 6737 (1998).

5. F. E. Goodson, S. I. Hauck, and J. F. Hartwig, *J. Am. Chem. Soc*., **121**, 7527 (1999).

6. T. Kanbara, K. Izumi, Y. Nakadani, T. Narise, and K. Hasegawa, *Chem. Lett*., **1997**, 1185.

7. N. Spetseris, R. E. Ward, and T. Y. Meyer, *Macromolecules*, **31**, 3158 (1998).

8. M. M. Wienk and R. A. J. Janssen, *J. Am. Chem. Soc*., **118**, 10626 (1996).

9. P. J. van Meurs and R. A. J. Janssen, *J. Org. Chem*., **65**, 5712 (2000).

10. T. D. Selby and S. C. Blackstock, *J. Am. Chem. Soc*., **121**, 7152 (1999).

11. T. D. Selby and S. C. Blackstock, *Org. Lett*., **1**, 2053 (1999).

12. T. D. Selby, K. R. Stickley, and S. C. Blackstock, *Org. Lett*., **2**, 171 (2000).

13. A. Ito, A. Taniguchi, T. Yamabe, and K. Tanaka, *Org. Lett*., **1**, 741 (1999).

14. A. Ito, Y. Ono, and K. Tanaka, *Angew. Chem. Int. Ed. Engl*., **39**, 1072 (2000).

15. S. I. Hauck, K. V. Lakshmi, and J. F. Hartwig, *Org. Lett*., **1**, 2057 (1999).

16. R. J. Bushby, D. R. McGill, K. M. Ng, and N. Taylor, *J. Mater. Chem*., **7**, 2343, (1997).

17. R. J. Bushby and D. Gooding, *J. Chem. Soc., Perkin Trans. 2*, **1998**, 1069.

18. R. J. Bushby, D. Gooding, and M. E. Vale, *Phil. Trans. R. Soc. Lond. A*, **357**, 2939 (1999).

19. A. Rajca, J. Wongsriratanakul, and S. Rajca, *Science*, **294**, 1503 (2001).

20. H. Nishide, T. Ozawa, M. Miyasaka, and E. Tsuchida, *J. Am. Chem. Soc.*, **123**, 5942 (2001).

21. T. D. Selby and S. C. Blackstock, *J. Am. Chem. Soc.*, **120**, 12155 (1998).

22. T. D. Selby, K.-Y. Kim, and S. C. Blackstock, *Chem. Mater.*, **14**, 1685 (2002).

23. K.-Y. Kim, J. D. Hassenzahl, T. D. Selby, G. J. Szulczewski, and S. C. Blackstock, *Chem. Mater.*, **14**, 1691 (2002).

24. K. R. Stickley and S. C. Blackstock, *J. Am. Chem. Soc.*, **116**, 11576 (1994).

25. K. Yoshizawa, M. Hatanaka, H. Ago, K. Tanaka, and T. Yamabe, *Bull. Chem. Soc. Jpn.*, **69**, 1417 (1996).

26. K. Sato, M. Yano, M. Furuichi, D. Shiomi, T. Takui, K. Abe, K. Itoh, A. Higuchi, K. Katsuma, and Y. Shirota, *J. Am. Chem. Soc.*, **119**, 6607 (1997).

27. K. R. Stickley, T. D. Selby, and S. C. Blackstock, *J. Org. Chem.*, **62**, 448 (1997).

28. M. M. Wienk and R. A. J. Janssen, *J. Am. Chem. Soc.*, **119**, 4492 (1997).

29. N. P. Buu-Hoï, *J. Chem. Soc.*, **1952**, 4346.

30. P. J. Flory, *J. Am. Chem. Soc.*, **63**, 3083 (1941).

31. D. T. Glatzhofer, D. Allen, and R. W. Taylor, *J. Org. Chem.*, **55**, 6229 (1990).

32. D. T. Glatzhofer and M. C. Morvant, *J. Phys. Org. Chem.*, **11**, 731 (1998).

Chapter 7

Conclusion and Future Prospects

7.1   Conclusion

In this thesis, a variety of magnetic macromolecules, which are persistent enough to be handled at room temperature, have been described.   The following concluding remarks can be derived from these studies.

1. For nanometer-sized macromolecular particles bearing 2,2,6,6-tetramethylpiperidine-1-oxyl radicals, magnetic force microscopy (MFM) is an effective tool to detect the very weak magnetic signal of the radical macromolecules.   A nm-sized polyradical particle is a new material of molecular-based magnetic dots potentially applicable to multiple representations by tuning the spin concentration.

2. The number of unpaired electrons in unit weight of the polyradical can be essentially enhanced by molecular design besides attempts to achieve a high yield for the polymer reaction.

3. Macromolecular nanoparticles complexed with gadolinium ions can also express MFM images in different ways.   The intensity of the MFM image is influenced not only by the spin concentration but also by the spin quantum number of the spin source employed in the magnetic macromolecule.

4. Bis(aminium cationic radical)s connected with 3,4'-stilbene are classified as a nondisjointed biradical molecule and their nonbonding molecular orbitals effectively overlap each other on the stilbene framework, which can realize both the efficient exchange interaction between two radicals and the stability of the biradical.

5. Poly(aminium cationic radical)s extended two-dimensionally in a non-Kekulé and nondisjoint fashion are new organic macromolecules that show both high-spin states and chemical stability even at room temperature.   In addition, it is possible to apply a series of scanning probe microscopy (SPM) techniques including MFM to the polyradicals because they possess their single molecular size on a nanometer scale.

In this manner, π-conjugated polyradicals are supposed to be the most promising as a new class of materials for MFM imaging.   They can potentially adjust the magnetic information with both the spin concentration and the spin quantum number and their molecular size is the smallest in the magnetic macromolecules mentioned in this thesis. These features will be primary factors to realize the fine processing and large data capacity needed for future information technology.

7.2   Future prospects

Since the present electronic technologies using semiconductors and inorganic materials are about to reach their fundamental limits, much research has focused on the development of quite new data storage systems.[1]

Organic macromolecules with a nanometer scale are expected to be some of the most promising candidates to this end.   In particular, π-conjugated macromolecules are attractive materials due to their high functionalities.   Taking arylamine macromolecules as an example, poly(*p*-aniline) is classified as a typical conducting macromolecule, while poly(*m*-aniline) is a ferromagnetic macromolecule.   Doping or an oxidation reaction leads to a significant change in their electronic properties.   The facility of doping of the macromolecule can be altered by molecular design.   The oxidation potential or the HOMO level of the arylamine and stability of the resulting aminium cationic radical are varied over a wide range by the extension of π-conjugated system and selection of the *o*- and *p*-substituents.[2,3]   The presence of a long conjugated system and the substitution of electron-donating groups lower the oxidation potential of the arylamine and increase the stability of the corresponding radical.   This knowledge should be considered when a specific property is built into the arylamine macromolecules.   For example, the accumulation of arylamine systems with different oxidation potentials makes it possible to construct a redox-gradient macromolecule, in which the direction of the electron transfer can be controlled to be applicable as single molecular data storage.[4]   For magnetic macromolecules described in Chapter 6, if the oxidation potential of the arylamine moiety connected with 1,3,5-benzenetriamine is much higher than that of the arylamine between *m*-phenylene couplers, the potential of the former redox site from amine to aminium cationic radical is in competition with the potential of the latter site from the aminium cationic radical to bication.   The intramolecular redox and incidentally the magnetic property of the macromolecule as ferromagnetic, paramagnetic, and diamagnetic may be tuned by external stimuli such as pH, temperature, and light (Fig. 7.1).   The electron transfer process via hopping or superexchange would then also be the primary subject from the viewpoint of spin electronics applications.[5-8]

In order to realize the practical use of the π-conjugated macromolecules as a single molecular information device, further advancements in the SPM techniques are
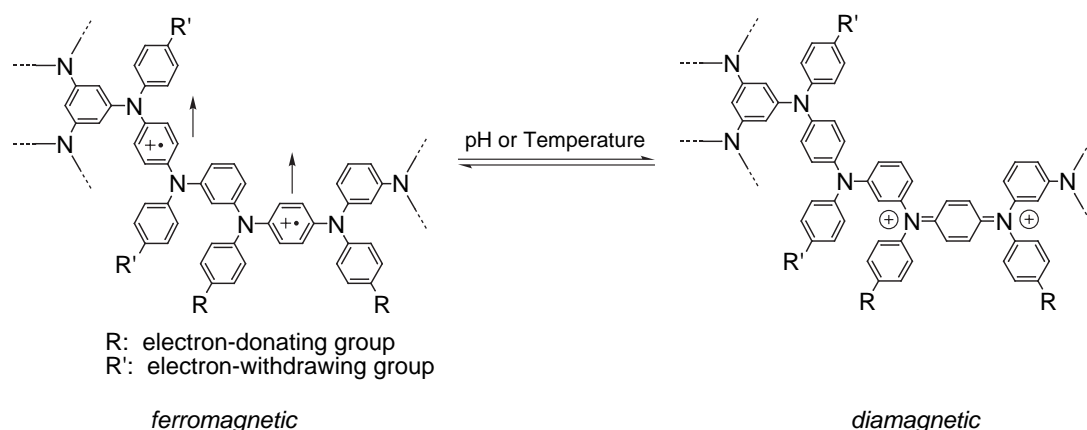
Fig. 7.1.   Proposed intramolecular redox reaction in arylamine macromolecule caused by external stimuli.

required.   Among the several kinds of magnetic detecting techniques, MFM is the most commonly used, however, its spatial resolution is limited to about 10 nm scales.   An improvement can be achieved by the application of a metal-capped carbon nanotube to an MFM probe.[9]   Carbon nanotube seems to be the most suitable for the probe because of its small size, the shape with high aspect ratio, and the mechanical rigidity.   The establishment of a fabrication process of the probe will support the feasibility of using it as a conventional probe.   Additionally, the characteristic electronic properties of carbon nanotubes might provide the possibility of other applications.   On the other hand, the advantage of scanning tunneling microscopy (STM) was utilized for the magnetic structure to achieve the ultimate resolution on an atomic scale.   The spin-polarized scanning tunneling microscopy (SP-STM) has been studied to reveal the correlation between the local electronic and magnetic properties on an atomic scale by combining the spectroscopy technique.   It has recently been shown that SP-STM can resolve the superstructure down to the atomic scale and that the disturbing influence of the probe on the sample disappears by using the antiferromagnetic probe.[10,11]   The technique can also measure the local magnetic susceptibility in soft magnetic materials when an appropriate combination of probe and sample is carefully selected.[12]   These advantages will be applicable to the nanometer-sized magnetic macromolecules in the future.

Other SPM techniques can also potentially be applied to detect the various properties of the π-conjugated macromolecules. Electric force microscopy (EFM) is suitable for the imaging of charged macromolecules.[13] Surface modified macromolecules would be detected with chemical force microscopy (CFM).[14] Light emission from single macromolecules and other optical properties can be observed with scanning near-field optical microscopy (SNOM), which is expected to be a read/write system with a fast access speed.[15,16] Since π-conjugated macromolecules often simultaneously possess many of these features, the combination of these SPM techniques could tremendously raise the data capacity. Although there are now many unresolved problems such as easy access to a single molecule and manipulation of the molecule on the specific place, the next decade will see further developments of the single macromolecular device in combination with the SPM versatility.

References

1. Y. Wada, *Proc. IEEE*, **89**, 1147 (2001).

2. S. Dapperheld, E. Steckhan, K.-H. G. Brinkhaus, and T. Esch, *Chem. Ber.*, **124**, 2557 (1991).

3. T. P. Bender, J. F. Graham, and J. M. Duff, *Chem. Mater.*, **13**, 4105 (2001).

4. T. D. Selby and S. C. Blackstock, *J. Am. Chem. Soc.*, **120**, 12155 (1998).

5. C. Lambert and G. Nöll, *Angew. Chem. Int. Ed. Engl.*, **37**, 2107 (1998).

6. C. Lambert and G. Nöll, *J. Am. Chem. Soc.*, **121**, 8434 (1999).

7. C. Lambert, and G. Nöll, *Chem. Eur. J.*, **8**, 3467 (2002).

8. C. Lambert, G. Nöll, and J. Schelter, *Nature Mater.*, **1**, 69 (2002).

9. T. Arie, H. Nishijima, S. Akita, and Y. Nakayama, *J. Vac. Sci. Technol. B*, **18**, 104 (2000).

10. S. Heinze, M. Bode, A. Kubetzka, O. Pietzsch, X. Nie, S. Blügel, and R. Wiesendanger, *Science*, **288**, 1805 (2000).

11. A. Kubetzka, M. Bode, O. Pietzsch, and R. Wiesendanger, *Phys. Rev. Lett.*, **88**, 057201 (2002).

12. W. Wulfhekel, H. F. Ding, and J. Kirschner, *J. Appl. Phys.*, **87**, 6475 (2000).

13. H. Takano and M. C. Porter, *J. Am. Chem. Soc.*, **123**, 8412 (2001).

14. C. D. Frisbie, L. F. Rozsnyai, A. Noy, M. S. Wrighton, and C. M. Lieber, *Science*, **265**, 2071 (1994).

15. E. Betzig and R. J. Chichester, *Science*, **262**, 1422 (1993).

16. J. W. P. Hsu, *Mater. Sci. Eng.*, **33**, 1 (2001).

List of publications

1. <u>Tsuyoshi Michinobu</u>, Jun Inui, Hiroyuki Nishide, "Magnetic Force Microscopic Images of Nanometer-Sized Polyradical Particles", *Polymer Journal*, **35**, 71-75 (2003).

2. <u>Tsuyoshi Michinobu</u>, Eishun Tsuchida, Hiroyuki Nishide, "5,4'-Bis[bis(methoxyphenyl)amino]-2-methoxystilbene and its Cationic Biradical", *Polyhedron*, **20**, 1147-1150 (2001).

3. <u>Tsuyoshi Michinobu</u>, Eishun Tsuchida, Hiroyuki Nishide, "3,4'-Bis[bis(*t*-butyl- and methoxy-phenyl)amino]stilbene Bis(cation radical)s and Their Electrochemical and Magnetic Properties", *Bulletin of the Chemical Society of Japan*, **73**, 1021-1027 (2000).

4. <u>Tsuyoshi Michinobu</u>, Masahiro Takahashi, Eishun Tsuchida, Hiroyuki Nishide, "Robust Triplet Molecule: Cationic Diradical of 3,4'-Bis(diphenylamino)stilbene", *Chemistry of Materials*, **11**, 1969-1971 (1999).

Acknowledgement

December 2002

Tsuyoshi Michinobu